Full Scale Numerical Simulation of Girder Bridges to Determine the Influential Factors Causing Transverse Cracking in RC Deck Slabs

RC床版のひび割れの影響要因を特定するための橋梁上部工の全橋シミュレーション

by

ARIFA IFFAT ZERIN

A dissertation submitted to
Yokohama National University
In partial fulfillment of the requirements for the degree of

Doctor of Philosophy in Engineering

Supervised by

AKIRA HOSODA

Professor, Faculty of Urban Innovation

Graduate School of Urban Innovation, Yokohama National University
Yokohama, Japan, August 2018

CONTENTS

ABSTRACT

A large number of reinforced concrete structures in Japan constructed during the last 50 years are undergoing severe deterioration due to environmental and loading actions. Particularly, transportation infrastructures in cold and snowy regions appear to be highly susceptible to sever deterioration due to the combined actions of freezing and thawing, chloride attack from deicing agent, alkali silica reaction (ASR), cracking, fatigue, and so on. Additionally, the occurrence of early age thermal and shrinkage cracks in RC deck slabs restrained by girders provide rapid routes for harmful agents leading to severe damages. For such road structures, it is indispensable to assure durability performance in design considering conceivable cold and aggressive environmental conditions and loading actions during their service lives.

In November 2011, the Japanese government resolved to build the "Reconstruction Roads" in Tohoku region to accelerate recovery from the Great East Japan Earthquake that occurred in March 2011. Since Tohoku region experiences cold and snowy weather in the winter, complex degradation involving multiple factors for deterioration as formerly described are anticipated. Thus, in order to ensure the high durability performance of the transportation infrastructures, specifically for RC deck slabs on bridges along the Reconstruction Roads, a durable concrete design accounting multiple countermeasures against deterioration has been formulated incorporating low water-to-cement ratio in the concrete mix, mineral admixtures such as blast furnace slag and/or fly ash, expansive additive and lime stone aggregates, anti-corrosion rebar and 6% entrained air for frost damage. Application of multiple protection counter measures for deck slab was proved effective without any signs of early age thermal and shrinkage cracks in case of several short span bridges particularly for single span bridges such as single span steel girder Mukai-sada-nai Bridge and single span PC composite girder Hikohei Bridge. However, minor transverse early age cracks were observed in different segments of the RC deck slab of the multiple span box girder Shinkesen Ohashi Bridge (length=438 m). In general, it is assumed that the potentials for the early age transverse cracks in RC deck slab are increased in case of multiple span continuous steel girder bridges due to its higher structural restraints against volumetric changes and tensile stresses in hardened slab because of stepping constructions. Since, the construction of multiple span steel girder bridges such as Kosano viaduct in Iwate prefecture, Koori Viaduct in Fukushima prefecture etc. are followed after construction of Shinkesen Ohashi bridge with multiple protection durable concrete, it is important to define the influential factors for the occurrence of such early age cracks in RC deck slabs especially for multiple span deck girder bridges to prevent deterioration.

The principal objectives of the present research are (1) to Evaluate the potential risk of early age cracking in RC decks slab due to structural restraints establishing a 'Systematic Analytical Scheme' for FEM full scale real structural simulation of girder bridges and (2) to identify the significant influencing factors generating early age thermal and shrinkage cracks to provide fundamental information for improving guidelines ensuring durable RC bridge slabs for cold and coastal regions

Methodology of the present research involves establishing FEM numerical simulation system based on thermal and structural stress analysis for RC deck slab bridges considering differential structural restraints applying appropriate thermal and structural boundary conditions to simulate the volumetric changes caused by thermal, shrinkage and creep in early age. First, laboratory investigations were conducted to measure free autogenous shrinkage, chemical expansion and compressive strength development for the regarding concrete. Second, the obtained material properties were utilized in member level numerical models to simulate volume changes which were successfully verified by experimental results. Some important input parameters such as autogenous shrinkage, chemical expansion energy and creep coefficients were calibrated through this verification process. Third, a numerical model has been developed for 'Shinkesen Ohashi' RC slab with restraining steel girders confirming rational thermal and structural boundary conditions. The time dependent thermal behavior of the bridge model was satisfactorily verified with the monitored slab and girder temperature. Thermal analysis was followed by time dependent stress analysis where calibrated material properties were given as inputs. The analytically obtained concrete and steel strain for RC slab shows sufficiently good agreement with the measured data. The maximum tensile stress generated due to the volume changes in the RC slab obtained from the analysis indicates the possibility of the occurrence of early age cracks in few segments of the slab where the initially accumulated tensile stress due to the placing of concrete is comparatively high.

It is to be noted that the highly durable concrete was also applied in RC deck slab construction of single span PC composite girder Hikohei post tensioned bridge where no cracks were generated. In this respect the study includes the numerical simulation of single span Hikohei bridge FEM model to confirm the thermal and volumetric changes in Hikohei bridge RC slab following the established systematic FEM simulation scheme applied in the simulation of Shinkesen Ohashi Bridge RC slab. The followed FEM numerical analysis approach has accurately simulated the early age volume changes of Hikohei bridge slab proving the low risk of cracking in RC deck slab for such single span PC composite girder bridge.

Furthermore, extensive parametric studies were conducted utilizing the established FEM full-scale bridge models to evaluate the effect of concrete material behavior such as coefficient of thermal expansion of concrete, autogenous shrinkage, chemical expansion and initial concrete temperature, along with different structural systems of bridges upon the occurrence of early age cracks due to the tensile stresses generated by restrained volume changes of RC deck slabs.

Through experimental investigations in material levels and systematic numerical simulations in several member levels as well as in full-scale real structural levels along with extensive parametric studies on structural restraint and restraint volumetric changes, factors affecting the generation and propagation of early age cracks are identified.

1

INTRODUCTION

1.1 GENERAL

A large number of reinforced concrete structures in Japan constructed during the last 50 years are undergoing severe deterioration due to environmental and loading actions [1]. Particularly, transportation infrastructures in cold and snowy regions appear to be highly susceptible to sever deterioration due to the combined actions of freezing and thawing, chloride attack from deicing agent, alkali silica reaction (ASR), cracking, fatigue, and so on. Additionally, the occurrence of early age thermal and shrinkage cracks in RC deck slabs restrained by girders provide rapid routes for harmful agents leading to severe damages. For such road structures, it is indispensable to assure durability performance in design considering conceivable cold and aggressive environmental conditions and loading actions during their service lives.

In November 2011, the Japanese government resolved to build the "Revival roads" in Tohoku region to accelerate recovery from the Great East Japan Earthquake that occurred in March 2011. Since Tohoku region experiences cold and snowy weather in the winter, complex degradation involving multiple factors for deterioration as formerly described are anticipated. Thus, in order to ensure the high durability performance of the transportation infrastructures, specifically for RC deck slabs on bridges along Revival roads, a durable concrete design accounting multiple countermeasures against deterioration has been formulated incorporating low water-to-cement ratio in the concrete mix, mineral admixtures such as blast furnace slag and/or fly ash to mitigate the risks of chloride attack and ASR, expansive additive and lime stone aggregates to compensate autogenous and drying shrinkage preventing cracks, anti-corrosion rebar and 6% entrained air for frost damage[2]. It should be noted here that such a highly durable concrete specification may conversely increase the risk of early age cracking caused by thermal and volumetric stresses generated due to the influence of large amount of cement incorporating mineral admixtures [1].

In this context, the present study focuses on numerical simulation of early age thermal and volumetric stresses to determine the influential factors on the occurrence of early age cracks in RC bridge slabs followed by a three levelled systematic full scale 3D FEM analysis scheme. First, laboratory investigations were conducted to confirm the material properties such as time dependent compressive strength and Young's modulus development, free autogenous shrinkage, restrained expansion along with setting time of the highly durable concrete applied in the constructions of RC deck slabs for road bridges in Tohoku region [3]. Second, the experimentally obtained concrete material properties were utilized as the inputs in the small scale specimen FEM models and the simulation system was verified in several member levels for early age volume changes [3]. Third, the simulation scheme was further validated in structural level utilizing the full scale FEM models for real RC slab deck girder bridges constructed along Revival roads. Furthermore, extensive parametric studies were conducted utilizing the established FEM full scale bridge models to evaluate the effect of concrete material behaviour, initial concrete

temperature, ambient temperature, and concrete placement seasons along with different structural systems of bridges upon the occurrence of early age cracks due to the tensile stresses generated by restrained volume changes of RC deck slabs. Through experimental investigations in material levels and systematic numerical simulations in several member levels as well as in full-scale real structural levels, factors affecting the generation and propagation of early age cracks are identified.

1.2 BACKGROUND AND IMPORTANCE OF THE RESEARCH

1.2.1 Revival Roads and Bridges in Tohoku Region

Recovery from the Great East Japan Earthquake was delayed because of the obstructions in national rout since dozens of national road bridges were washed away by the devastating tsunami in March 2011. In that circumstance, the Japanese government undertook the project for the "Revival roads" located along the Sanriku Coast (Fig. 1.1) to accelerate the recovery process from the devastations of the earthquake and consequent tsunami (Fig. 1.2). The elevation of all the new bridges along Revival roads were planned to be higher than the predicted Tsunami inundation height. The total length of the Revival roads is 359 km including 148 km of new sections. Reconstruction assistance roads connecting major cities with the Sanriku region were also considered as a leading project of the construction plan in Tohoku region. Hence, the total length of new sections become 224 km where approximately 250 bridges are planned to be constructed by around 10 years after the disaster in 2011 which are progressing in a tremendously fast speed. Since these bridges are located in the severely cold and quite aggressive environment, ensuring high durability performance is an utmost importance [2].

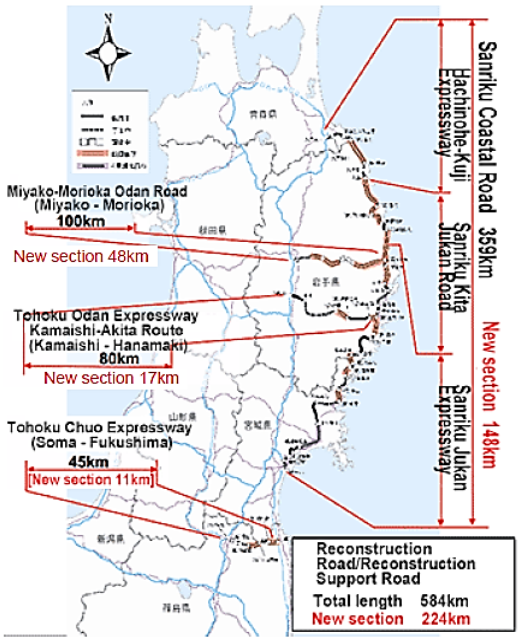

Fig. 1.1 The Revival roads along Sanriku Coast in Tohoku Region[4]

Fig. 1.2 Devastation of Road Infrastructures by Tsunami in 2011[5]

1.2.2 Deterioration of RC Deck Bridges in Cold and Coastal Regions of Japan

In Tohoku region, where Revival roads are under constructions, highway bridges are reported to be highly susceptible to severe deterioration due to the complex effect of extremely cold and coastal environment and load actions (Fig. 1.3 to Fig. 1.8). Figure 1.3 represents the typical damage observed on the asphalt pavement on RC deck slabs owing to the coupling effect of frost damage, cyclic wheel load, and so on. Even, aggregation of concrete is often observed where substantial amount of deicing salt has been used in areas of low traffic volume. A total of 10-30 t/km of salt is sprayed every year on the national routes in this region [4]. Hence, many old bridges are found to be deteriorated with severe rebar corrosion due to chloride attacks initiated by deicing salt. Large amount of deicing salt accelerates not only the rebar corrosion, but also frost damage and ASR which leads to severe deterioration of RC deck slabs in cold region.

Fig. 1.3 Damages in RC deck slab due to fatigue caused by repeated loading (traffic=12000 vehicles/day)[4]

Fig. 1.4 RC bridge deck deteriorated (Exposed rebar and aggregation) due to the action of ASR[5]

Fig. 1.5 Combined deterioration due to ASR, de-icing salt, repeated load, water migration etc. [5]

Fig. 1.6 RC bridge in coastal zone attacked by sea waves in winter[5]

Fig. 1.7 RC bridge with severe rebar corrosion in coastal region (Itoigawa, Niigata) [5]

Fig. 1.8 Large amount of deicing salt accelerates rebar corrosion in bridge RC slabs[5]

1.2.3 Occurrence of Cracks in RC Deck Slab due to External Restraints

Early age cracks can be generated in bridge decks initiated by the volume changes in slab concrete restrained by RC deck slab steel girder composite action (Fig. 1.9 to Fig. 1.12). In design, RC slabs are assumed to be simply supported on the steel girders and can shrink/expand freely without any external restraint. In reality, RC slabs are connected with the steel girders by anchors and metallic connectors preventing free movement of the slab. Therefore, tensile stress is generated in the concrete caused by the restraint volume changes of the RC deck slab particularly for hydration heat generation, autogenous and drying shrinkage, ambient temperature variations etc. Consequently early age cracks can be generated when the tensile stress in the restrained RC slab exceeds the tensile strength of the slab concrete. Early age cracks provide a rapid route for harmful agents (moisture, deicing salt, O_2, C_{l2}, CO_2 etc.) to reach the reinforcement initiating to

rebar corrosion which may lead to severe deterioration of the bridge deck in cold regions ultimately causeing loss of serviceability and increased maintenance cost.

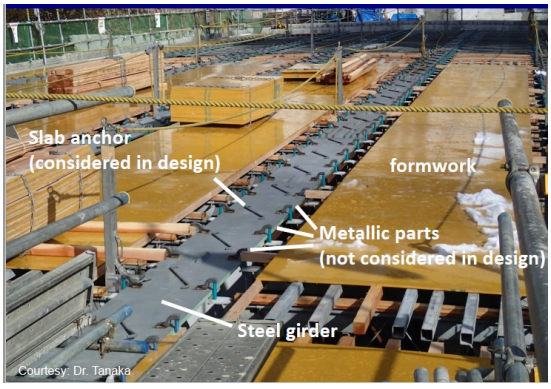

Fig. 1.9 Metallic connectors and slab anchors provide external restraints against RC deck slab[5]

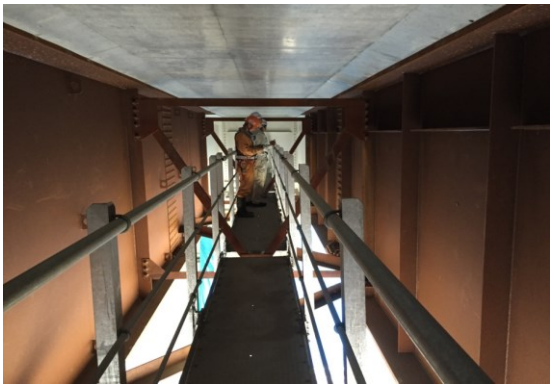

Fig. 1.10 Structural restraints due to undeneath steel girdes (Mukai-Sadanai bridge, Kamaishi)

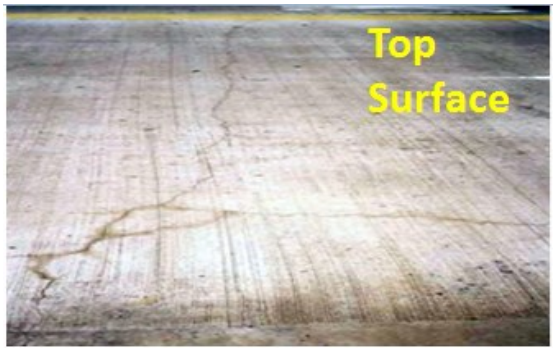

Fig. 1.11 Early age transverse cracks initiated by thermal stress and shrinkage externally restraint by steel girders[5]

Fig. 1.12 Efflorescence along the penetrating transverse crack in RC slab[5]

1.2.4 Visual Inspection Grades for Bridges in Tohoku Region

The visual inspection grade explained in Table 1.1 for prestressed concrete (PC) and steel girder bridges were constructed within the last 20 years in Tohoku region were summarized in Table 1.2 in transition probability matrix by comparing the previous (5 years) and present visual inspection grades [4]. Moreover, the transition of visual inspection grade with time was predicted by Markov chain as shown in Figure 1.13 and Figure 1.14 where grades S and M are replaced to grade A, B, C or E. Fifteen years after construction, half of the bridges are classified as C or E, which require repair because of deterioration regardless of bridge type [4]. This degradation speed is substantially high in Tohoku region compared to the average in the whole country as reported in a previous research [6]. Therefore, it has been confirmed that the durability design should be improved for the design and construction of RC and PC deck slabs in constructing Revival roads. Otherwise, the bridges would suffer from early age deterioration in several decades.

Table 1.1 Visual Inspection Grade for Bridges in Tohoku Region [4]

A	No defect
B	Repair is not required
C	Repair is required within five years
E	Urgent repair is required
S	Urgent inspection is required
M	Repaired is schedule

Table 1.2 Transition probability matrix of visual inspection grade (constructed in 1987-2014)[4]

	PC Bridge (Present) (%)								Steel Girder Bridge (Present) (%)							
PC Bridge (5 years ago) (%)		A	B	C	E	S	M	Steel Girder Bridge (5 years(%) ago)		A	B	C	E	S	M
	A	22	67	0	0	0	11		A	50	25	0	0	0	25
	B	0	57	26	0	9	8		B	0	56	27	1	9	8
	C	1	21	65	1	9	4		C	3	30	55	0	6	6
	E	0	57	29	14	0	0		E	-	-	-	-	-	-
	S	0	28	54	0	16	1		S	0	37	37	0	26	0
	M	0	64	20	0	0	16		M	0	25	25	0	13	38

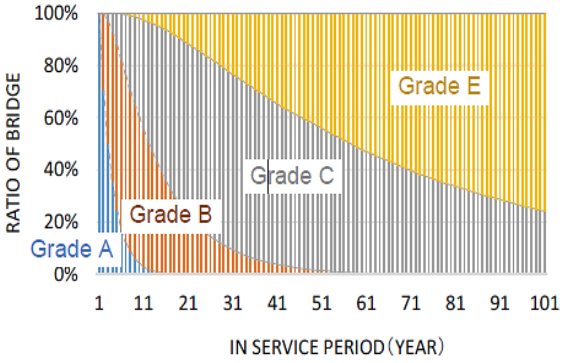

Fig. 1.13 Transition probability of visual inspection grade for PC composite bridge (constructed in 1987-2014) [4]

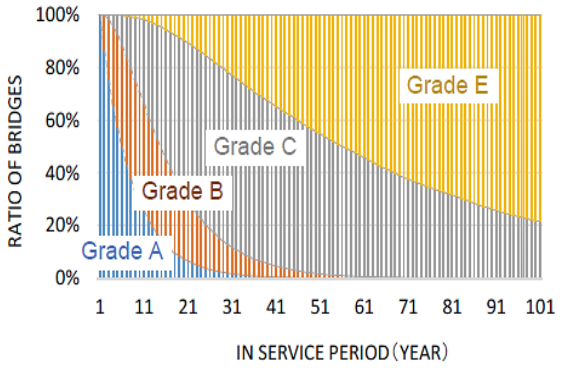

Fig. 1.14 Transition probability of visual inspection grade for steel girder bridge (constructed in 1987-2014) [4]

1.2.5 Multiple Protection Concrete Design Preventing Deterioration in RC Bridge Slabs and its Applications

In general, the same standard specification is followed in durability design of RC structures although there are various climatic conditions in Japanese territory. However, the present Japanese standard does not sufficiently cover the effects of severe environments such as complex actions of frost and salt damage. Considering the severely cold and harsh environment of Tohoku region, a new initiative has been undertaken by the academics collaborating with government authorities and construction companies to secure highly durable bridge deck construction ensuring multiple countermeasures against deterioration [2][3] as illustrated in Fig. 1.15 and Fig. 1.16.

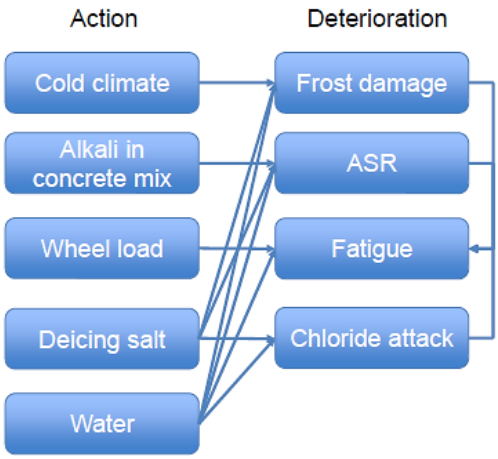

Fig. 1.15 Relationship between action and deterioration assumed in multiple protection concrete design[2]

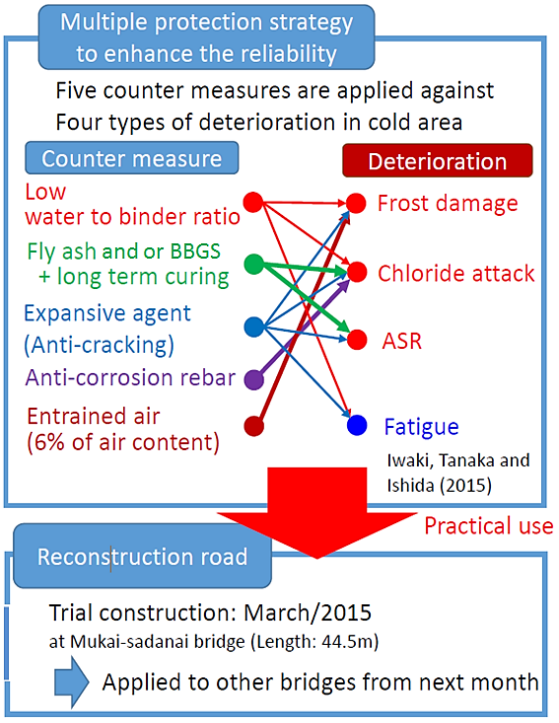

Fig. 1.16 Multiple protection counter measures to prevent deterioration in RC bridge slab[2]

Fig. 1.17 Concrete casting at single span Mukai-sada-nai Bridge (Length=43.7m constructed in March 2015) (First trial contraction of durable RC slab) [2]

Fig. 1.18 Application of multiple protection concrete design in RC slab construction of single span Hikohei Bridge in Fukushima (Length=43.7m concrete placement in July,2017) [7]

Fig. 1.19 Multiple span Kosano Viaduct, another application of multiple protection durable RC slab in Kamaishi (Length=260m, concrete placement started in March,2018)

In the proposed highly durable concrete design for RC deck slabs, the application of fly ash and/or blast furnace slag cement with low water-binder ratio was the key counter measure against frost damage, salt damage and ASR resistance. Expansive additive was applied to prevent cracks by compensating autogenous and drying shrinkage along with fatigue. Also limestone aggregate was used to reduce drying shrinkage for its low shrinkage properties. Air content was

set as 6% to achieve anti-frost performance. 28 days wet curing was considered applying three layers of special curing mats to control thermal changes and prevent evaporation. Moreover, epoxy coated reinforcing bars were applied for the protection against corrosion [3].

The trial construction for the proposed multiple protection concrete design was carried out at the Mukai-sada-nai Bridge in March 2015 (Fig. 1.17), which was a single span steel girder bridge with an RC slab exhibiting satisfactory performances without showing any early age cracks and deterioration[2]. Since the first trial was successful, several highly durable RC deck slabs applying multiple protection concrete design were constructed on along Revival road such as Fudo-sawa Bridge (in August 2015), Ohsawa-dai3 Bridge (in April 2016), Nami-ita Bridge (in April 2016), Shinkesen Bridge (in June 2016), Hikohei Bridge (in July 2017) and Kosano Viaduct (in March 2018) (Fig. 1.18, Fig. 1.19, and Fig. 1.20).

Fig. 1.20 Several durable RC slabs on bridges along Revival Roads adopting multiple protections concrete design [2]

1.2.6 Early Age Cracks in RC Deck Slab on Shinkesen Ohashi Multiple Span Continuous Steel Girder Bridge

The new cross linking site of 438 m long Shinkesen Ohashi seven continuous span deck girder bridge (Fig. 1.21) along Reconstruction Roads in Tohoku region is about 3 km from the estuary of the mountainous Kesengawa River in Iwate Prefecture. The height of the bridge is around 30 m from the ground surface considered to be highly vulnerable to deterioration due the effect of freezing and thawing, chloride attack and ASR caused by deicing salt. Early age cracks were also anticipated to initiate in the RC slabs restrained by underneath steel girders due to slab anchors (Fig. 1.22). Hence, the multiple protection durable RC slab concrete was applied in the construction of Shinkesen Ohashi Bridge deck (Fig. 1.23).

Fig. 1.21 Shinkesen Ohashi Bridge in Kamaishi (June 2016)

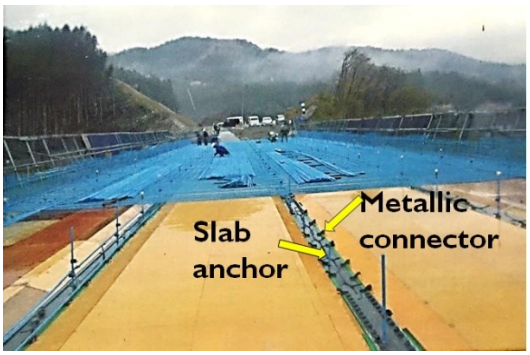

Fig. 1.22 Slab anchors and metallic connectors

Fig.1.23 Multiple protection highly durable concrete placement

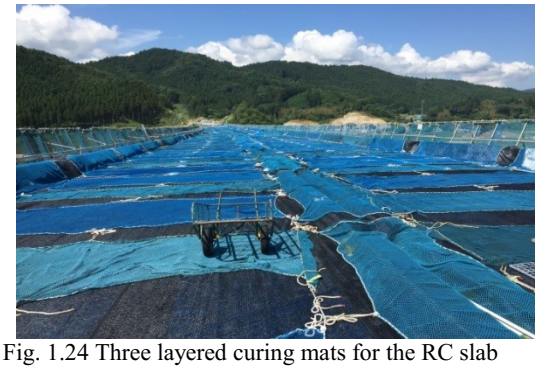

Fig. 1.24 Three layered curing mats for the RC slab

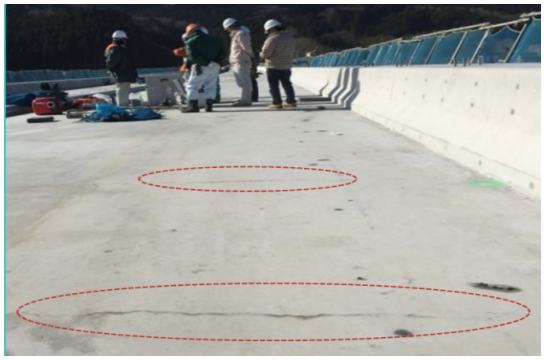

Fig. 1.25 Transverse cracks in Shinkesen Ohashi RC slab

Fig. 1.26 Efflorescence in penetrating transverse cracks (Photo Courtesy: Yokogawa Bridge Holdings Corp.)

(1) Construction Methods adopted for Shinkesen Ohashi RC Slab

The concrete placement of Shinkesen Ohashi Bridge slab was performed between June to July in 2016 adopting special construction and curing methods such as appropriate concrete placement steps considering setting time of concrete and around 22 days wet curing followed by initial 7 days sealed curing applying three layers of special curing mats to control thermal changes and prevent evaporation (Fig.1.174). Stepwise concrete placement was adopted in the construction of the RC slab segmented into thirteen placement lots to minimize the structural stresses. Embedded strain gauges with thermocouples were installed to monitor concrete strain and temperature in longitudinal (X), transverse (Y) and vertical (Z) directions in the deck slab concrete placement Lot-8 upon Pier-3 at two locations of slab under different restraining conditions such as in the RC slab directly connected with the steel girder and in the RC slab away from the steel girder.

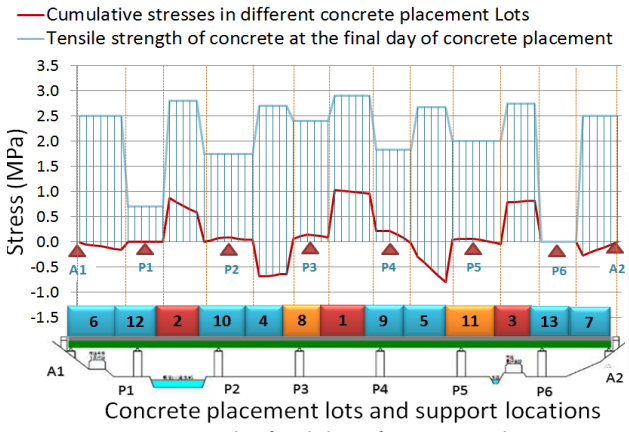

Fig.1.27 Cumulative structural stress and tensile strength along different lots at the day of Lot13 concrete placement (29th day of Lot1 placement)

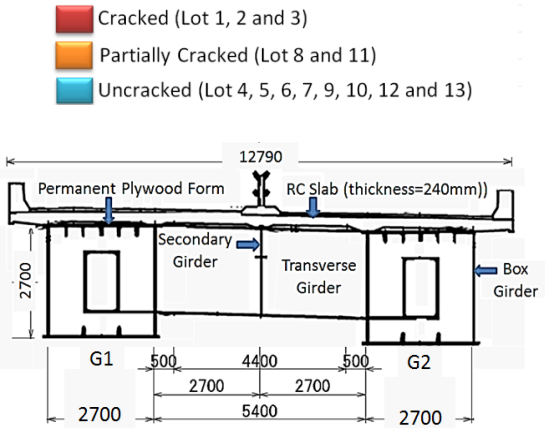

Fig.1.28 Cross section of Shinkesen Ohashi deck girder bridge

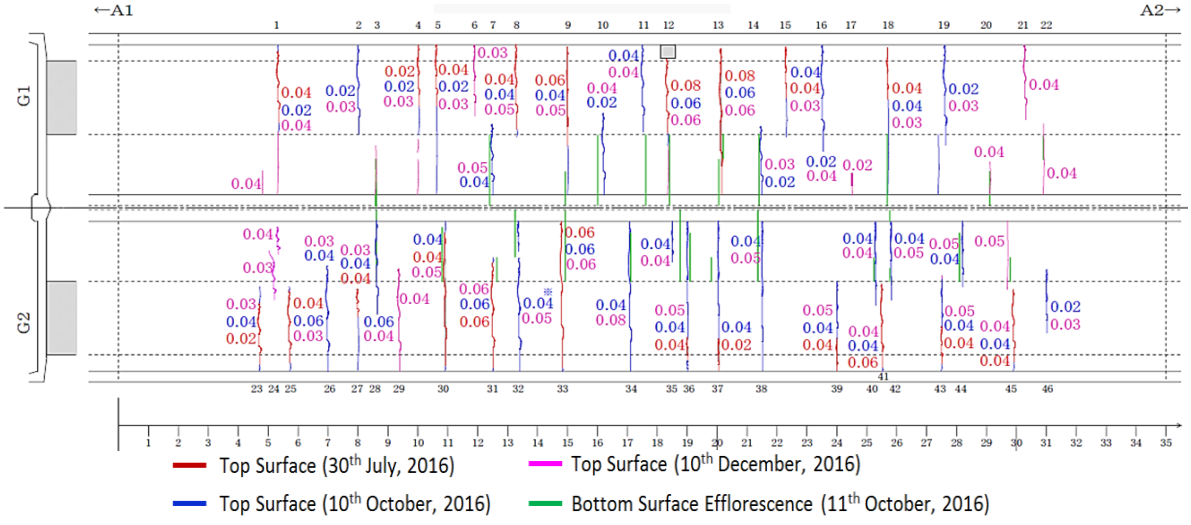

Fig.1.29 Distribution of cracks in concrete placement Lot 1 according to the date of observation

(2) Cracking Scenario in Shinkesen Ohashi RC Slab

Although the multiple protection highly durable concrete was applied following systematic stepping construction and three layered special curing methods, minor transvers cracks were generated and identified (Fig.1.25 to Fig.1.29) in Lot 1, Lot 2, Lot 3, Lot 8 and Lot 11 after removing the curing mats after 28th days of special wet curing. The maximum crack width was 0.08 mm in Lot 1. Fig.1.27 shows the tensile strength of each lot at the day of Lot 13 concrete placement and reveals that the cumulative tensile stresses in concrete are comparatively large in Lot 1, Lot 2 and Lot 3 due to the stepping construction. Initially, primary cracks were generated in the concrete placed upon the permanent plywood forms (Fig.1.28 and Fig.1.29) and propagated towards the central axis of the slab. Effloresce observed in the bottom surface of the slab confirmed that some cracks were penetrating (Fig.1.26). However, recent inverstigation has confirmed that the crack width in Shinekesen RC slab has increased up to 0.2 mm exceeding the allowable limit of crack width (0.0035c where c=cover thickness) in highly corrosive zone[8].

1.3 MOTIVATIONS OF THE RESEARCH

Application of multiple protection counter measures for highly durable concrete for deck slab was proved effective without any signs of early age thermal and shrinkage cracks in case of several short span bridges particularly for single span bridges such as single span steel girder Mukai-sada-nai Bridge (length=45 m) and single span PC composite girder Hikohei Bridge (length=43.7 m). However, some minor transverse early age cracks were observed in different segments of the RC deck slab of the multiple span continuous box girder Shinkesen Ohashi Bridge (length=438 m). In general, it is assumed that the potentials for the early age transverse cracks in RC deck slabs are increased in case of multiple span continuous steel girder bridges due to its higher structural restraints against volumetric changes and tensile stresses in hardened slab due to stepping constructions. Since, the construction of multiple span steel girder bridges such as Kosano viaduct in Iwate prefecture, Koori Viaduct in Fukushima prefecture etc. are followed after construction of Shinkesen Ohashi bridge, it is important to define the influential factors for the occurrence of such early age cracks in RC deck slabs especially for multiple span continuous girder bridges to prevent deterioration which can be aggravated by early age cracks added with loss of serviceability of the structures and huge maintenance costs.

1.4 OBJECTIVES

The principal objectives of the present research are demonstrated as below:

- To Evaluate the potential risk of early age cracking in RC decks slab due to structural restraints establishing a 'Systematic Analytical Scheme' for FEM full scale real structural simulation of girder bridges

- To identify the significant influencing factors generating early age thermal and shrinkage cracks to provide fundamental information for improving guidelines ensuring durable RC bridge slabs for cold and coastal regions

1.5 METHODOLOGY OF THE RESEARCH

Methodology of the present research involves establishing FEM numerical simulation system based on thermal and structural stress analysis for RC deck slab bridges considering differential structural restraints applying appropriate thermal and structural boundary conditions to simulate the volumetric changes caused by thermal, shrinkage and creep in early age. The methodology follows three levelled systematic analysis scheme for FEM full scale structural simulation of deck girder bridges. Two different structural bridge types i.e., Type I: Multiple span steel box girder bridge (Shinkesen Ohashi Bridge and Kosano Viaduct in Iwate Prefecture) and Type II: Single span PC composite girder bridge (Hikohei Bridge in Fukushima Prefecture) were considered in this analysis scheme to confirm the distinctive attributes of thermal stresses in RC deck slab with respect to differential structural restraints for multi-span and single span bridges. The established FEM RC slab bridge models for multi-span steel girder bridge and single span PC composite girder bridge have been utilized for extensive parametric studies to determine the influential factors for the risk of early age thermal and shrinkage cracks under different restraint conditions.

The schematic diagram of the systematic analytical scheme for FEM full scale structural simulation of deck girder bridges is illustrated in Fig.1.30 as follows.

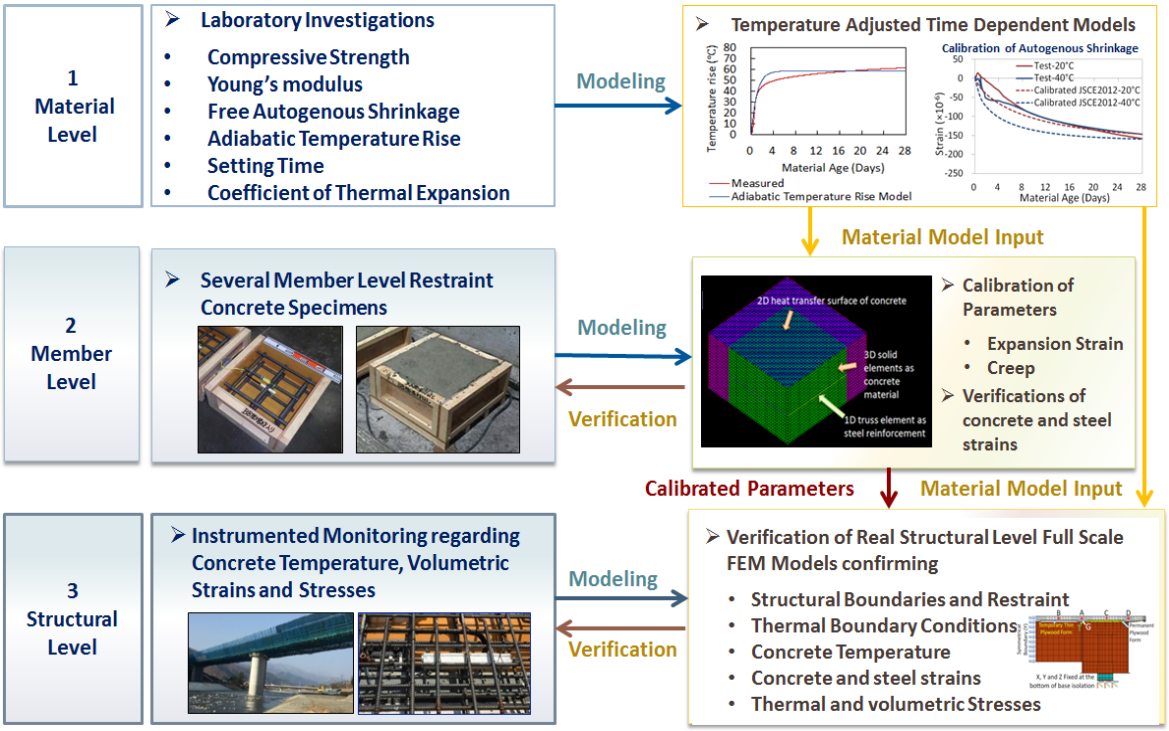

Fig.1.30 The schematic diagram of the systematic analytical scheme for FEM full scale structural simulation of deck girder bridges

The established three levelled systematic analysis scheme in the present research is illustrated as below:

Level-1: Material Level

The Level-1 in the analysis scheme involves laboratory investigations to confirm the mechanical properties for the highly durable concrete considering multiple counter measures applied in several RC deck slabs bridges. The determined material properties include adiabatic temperature rise, time dependent compressive strength and Young's modulus development, setting time, thermal expansion, restraint chemical expansion, free autogenous shrinkage and drying shrinkage.

Level-2: Member Level

In Level-2, FEM numerical simulation procedure was established and verified utilizing the member level FEM numerical models for restrained specimens such as restrained expansion strain specimen, small scale RC beam specimen and small scale RC slab specimen by inputing the material properties obtained from the laboratory investigations in Level-1.

Level-3: Structural Level

In Level-3, the real structural level FEM bridge models were established inputting material properties obtained from the material (Level-1) and calibrated parameters confirmed from member level (Level-2) investigations and finally validated comparing the simulation results with the monitored data for temperature and strains (expansion and shrinkage) recorded in the real bridge slabs.

1.6 ORGANIZATION OF THE THESIS

Chapter 1: Introduction

Chapter 2: Literature Reviews

Chapter 3: A systematic analytical scheme for FEM full scale structural simulation of deck girder bridges

Chapter 4: Numerical modeling and simulation of thermal stresses in RC bridge deck slabs

Chapter 5: Effects of structural restraints on the occurrence of thermal stresses in RC bridge deck slabs

Chapter 6: Influential factors causing early age thermal and shrinkage cracks in RC deck slabs

Chapter 7: Conclusions

References

[1] T. Ishida and I. Iwaki, "Multi-scale and Multi-chemo-physical Modeling of Cementitious Composite and Its Application to Early Age Crack Assessment of Reinforced Concrete Slab Decks," in 2nd RILEM/COST Conference on Early Age Cracking and Serviceability in Cement-based Materials and Structures-EAC2, Brussels,2017.

[2] Y. Tanaka, T. Ishida, I. Iwaki and K. Sato, "Multiple Protection Design for Durable Concrete Bridge Deck in Cold Regions," Journal of JSCE, vol. 5, pp. 68-77, 2017.

[3] A. Zerin, A., Hosoda and S. Komatsu,"Numerical simulation of early age expansion and autogenous shrinkage behavior of blast furnace slag concrete with expansive additive," Journal of Structural Engineering, JSCE, vol. 64A, pp. 666-674,2018.

[4] Earthquake Memorial Museum, Tohoku Regional Bureau, http://infra-archive311.jp/en/s-fukkoudouro.html.

[5] T. Ishida, Multi-scale and multi-chemo-physics modeling of structural concrete-toward a sustainable society through durable concrete structures, JCI 50thAnniversary Workshop on Multi-scale Modelling, Toshi Center Hotel, 13th July, 2015, www.jci-net.or.jp/~multi-scale/Ishida.pdf.

[6] T.Tamakoshi, Y.Yokoi and M.Ishino, "Degradation characteristics of concrete members of Japanese highway bridges based on periodic inspection data", *Concrete Research and Technology*, Vol.25, pp.167-180, 2014.

[7] A. Zerin, A., Hosoda and S. Komatsu and Nobuyuki NAGATA," Numerical simulation of thermal stress in highly durable Rc slab on pc composite girder bridge," Journal of Structural Engineering, Proceedings of JCI Annual convention 2018 (In press).

[8] Japan Society of Civil Engineering, Standard Specifications for Design of Concrete Structures, JSCE, 2007.

2

LITERATURE REVIEWS

2.1 SYNOPSIS

Chapter 2 presents a comprehensive literature review of the influential factors for transverse cracking in bridge deck slab especially in steel girders RC deck bridges which covers survey investigations on the effects of different design factors and concrete properties on RC deck slab cracking. Efforts were made to include all the aspects indispensable to visualize the causes and mechanism of transverse crack generation in RC deck slab restrained by steel girders. Additionally the limit values of crack widths and methods of controlling thermal cracks indicated in guidelines are demonstrated. Moreover, previous researches incorporating field investigations, structural monitoring and corresponding numerical simulation to uncover the causes and mechanism of transverse deck cracking were also explained. Finally the requirements of conducting the present research are briefly discussed in context of the literature survey as well as the present needs.

2.2 FACTORS INFLUENCING EARLY AGE CRACKING IN BRIDGE DECKS

Concrete utilized in the bridge deck slab construction is vulnerable at its early stages. Although construction phases normally proceed with great caution and preparation, some defects cannot be avoided [1-3]. Early-age cracking is caused primarily by volumetric changes of the RC deck slab restrained by the structural elements of the bridge. Thus, the amount of volume change and the degree of restraint present in a bridge have a direct and interrelated effect on the amount of cracking that may develop in the deck slab. The types of loads associated with early age concrete are numerous and can be classified in two categories. The first category entails the effects of internal stresses due to differential volume changes such as heat of hydration and shrinkage. Whereas the second category includes external stresses associated with external restraints and loads due to construction practices [4].

2.2.1 Internal Stresses due to Volume Changes

Internal restraint exists in members with non-uniform volume changes on a cross section occurring within deck slabs with interior temperatures larger than surface temperatures or with differential drying shrinkage[5]. Cracks in concrete may generate with the change in volume of a restrained mass. The amount of volume change in concrete depends on the properties of its constituents and their proportions, as well as environmental conditions such as ambient temperature changes and humidity. Volume change in the concrete bridge deck, as influenced by the properties of concrete, is caused by Hydration heat, drying shrinkage, autogenous shrinkage, plastic shrinkage, and creep [6, 7].

(1) Heat of Hydration and Thermal Stress

Heat of hydration causes thermal stresses resulting concrete cracking in mass concrete. High heat of hydration is also accompanied by high early strength and modulus of elasticity enhances the risk of early age cracking. Since concrete is very weak in tension, a small temperature difference can possibly result in thermal cracking in large concrete structures [8]. Thermal cracking in concrete structures develops due to combine effects of type of structure, boundary condition, materials, mix proportions, construction method, construction condition, weather conditions, and so on [9].

(2) Shrinkage of Concrete

Due to differential shrinkage of the concrete as a result of stepping construction, cracks generate at the construction joints. ACI 209 [2] defines the three types of shrinkage as drying, autogenous, and carbonation. Another type of shrinkage is plastic shrinkage. Plastic shrinkage and autogenous shrinkage occur at an early age of the concrete, while drying shrinkage continues over a long period of time [10].

(a) Drying Shrinkage

Drying shrinkage is considered for the main reasons of bridge deck shrinkage cracking associated with loss of water in the hardened concrete capillary stress, disjoining pressure and surface tension. In general, bridge decks experience relative humidity from 45% to 90%, when the capillary stress mechanism plays the significant role. Paste volume, water-cement ratio, aggregates type, environment conditions and curing methods directly influence the drying shrinkage of concrete, of all these factors, paste volume is the most important since drying shrinkage reduces intensively if the paste volume is decreased [8, 11-14].

(b) Autogenous Shrinkage

Autogenous shrinkage is caused by the self-desiccation of concrete during hydration due to lack of water in concrete with low water-cement ratio. Although, autogenous shrinkage is usually small, it may become an important factor leading to shrinkage cracking for concrete including high-range-water-reducing admixture, fine materials such as silica fume, and blast furnace slag, [15, 16].

(c) Carbonation Shrinkage

Carbonation shrinkage results from a reaction between hydrated cement and carbon dioxide in the atmosphere [17].

(d) Plastic Shrinkage

Plastic shrinkage is caused by a rapid loss of water on the concrete surface before the concrete hardens. This loss of water can be caused by evaporation or suction by a dry sub-base. When significant amount of water rapidly evaporates from the newly placed concrete, the water that remains in the concrete will not be sufficient, and voids occur leading to plastic shrinkage cracking. Environmental conditions, such as wind and temperature, have great influence on plastic shrinkage cracking of concrete. Therefore, when there are high wind speeds, concrete casting should be avoided, or wind breaks and fogging should be used to prevent water loss. Since water evaporation happens only at the surface, plastic shrinkage cracking occurs at the surface, and it is usually small [1, 18].

(3) Properties of Concrete and Influencing Factors

(a) Modulus of Elasticity and Strength Development

The modulus of elasticity of concrete has a significant effect on the tensile stresses generation in deck slab due to thermal and shrinkage strains. The volume changes due to shrinkage and thermal effects create tensile stresses proportional to the modulus of elasticity of concrete related to the strength of concrete. In general, with the increase of compressive strength, creep decreases in a faster rate than the increase of tensile strength. [8]. Therefore, the concrete mix designs should satisfy the strength development requirement not only at one fixed time but in a certain time period satisfying the trend of low early strength and high later strength [19, 20].

(b) Creep

The material age of concrete and its time dependent strength when the load is applied to concrete influence the magnitude of the creep strains. Creep of concrete has a positive effect on early age concrete deck cracking. Creep of concrete reduces tensile stresses caused by restrained drying shrinkage and thermal changes, and thereby, reduces the risk of cracking. Like shrinkage of concrete, creep of concrete occurs only in cement paste matrix in concrete (i.e., aggregate does not creep). Hence, more cement paste in a concrete mix contributes to higher creep and higher shrinkage. Increasing the paste content and selecting the aggregates that have low modulus of elasticity can increase the creep of concrete. Reversely, high cement content increases autogenous shrinkage and drying shrinkage. Therefore, a proper balance between concrete strength, shrinkage, creep, and other long-term properties are needed to be determined carefully [8, 21].

(d) Cement Content and Water-to-cement Ratio

Cement content is a very important factor affecting the shrinkage of bridge decks which leads to volume changes in concrete. Reducing paste content results in a decrease in free shrinkage. Increasing water content increases the shrinkage of concrete and increases creep which helps reducing shrinkage. Decreasing the water-to-cement ratio can decrease drying shrinkage but increases autogenous shrinkage. Again, a low water-to-cement ratio may influence early-age cracking due to increased autogenous shrinkage [8, 22-24].

(e) Cement Type

Cement type plays an important role in bridge deck cracking, as the drying shrinkage of concrete is affected by the cement fineness. Finer cement particles generate greater heat of hydration and require a greater amount of water during the hydration process, which may lead to the increased risk of cracking in the concrete [25].

(f) Aggregates Size and Type

In contrast to the cement paste, aggregates have much low shrinkage and creep. Aggregates provide restraint to shrink. It is generally believed that larger size aggregates decrease the cracking tendency of bridge decks. The properties of aggregates determine the amount of restraint that will be applied to cement paste. Limestone aggregate has higher resistance to cracking than other types of aggregates. The ratio of elastic moduli of aggregate and cement is important on the shrinkage of concrete: the concrete has lower shrinkage potential if the ratio is higher [26].

2.2.2 External Stresses

Various factors related to external stresses which influence the deck cracking are explained below.

(1) External Restraints due to Supporting Girders and Steel Reinforcement

Composite behavior between RC deck and girders is the primary source of restraint in bridge decks [27]. The practice of designing decks fully composite with the girders to decrease the size of the girders is common. Nevertheless, removal of this restraint is not economical, and the current trend in design has been to develop greater composite action through larger amount of shear connectors installed on the girders. Because of the strong composite action between the concrete bridge deck and supporting girders, the girders apply strong restraint to the concrete bridge deck, which constrains the thermal and shrinkage deformation of the deck. At the same time, the internal reinforcement of the concrete deck also restrains the volume changes of the concrete and therefore the concrete deck experiences high tensile stress, which may lead to its cracking.

The length of the span, type of girders, skew of the deck, amount of reinforcement, type of abutments, and spacing of the girders all influence the restraint in the deck and thus, the degree of cracking [27-29]as pointed out below:

- Bridge decks on simply-supported pre-stressed girders showed significantly less cracking than decks on continuous steel girders.
- Decks supported by steel girders usually had higher risks of transverse deck cracking and higher tensile stresses than the ones with concrete girders. This is because the steel girders have different coefficient of thermal expansion (CTE) from that of concrete deck, which leads to large volumetric differentials upon temperature fluctuations.
- Larger girder and closer spacing tend to be more prone to cracking. Thus, using smaller girder and wider spacing will reduce the cracking tendency.
- Girder end conditions also affect deck cracking, restrained girder ends can lead to severe deck cracking.
- In regions over the bridge piers, the bottom of overhangs in bridge decks should have the same quantity of longitudinal reinforcement as the top to avoid severe shrinkage cracks that may develop.

(2) Degree of Restraint

The degree of restraint K is defined as $K=1-\varepsilon_{meas}/\ \varepsilon_{free}$, where ε_{meas} is the strain developed in concrete under restraint, ε_{free} is the strain in concrete without restraint due to heat of hydration and autogenous shrinkage. For the cases of complete and no restraint, the dgrees of restraint are 1.0 and 0, respectively [9].

According to ACI Committee 207 report [5], numerically, the restrained strain is equal to the product of the degree of restraint and the change in unit length which would occur if the concrete were not restrained. All concrete elements are restrained to some degree by volume because there is always some restraint provided either by the supporting members or by different parts of the member itself. Restrained volume change can induce tensile, compressive, or flexural stresses in the members, depending on the type of restraint and whether the change in volume is an increase or decrease. Present discussion is primarily concerned with restraint conditions which induce tensile stresses in concrete which can lead to cracking. In the following discussion, the continuous and discontinuous external restraints are discussed [5].

(a) Continuous External Restraint

Continuous restraint exists along the contact surface of concrete and any material against which the concrete has been cast. The degree of restraint depends primarily on the relative dimensions, strength, and modulus of elasticity of the concrete and restraining material.

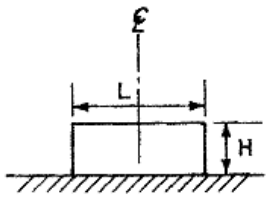

Fig. 2.1 Continuous Base Restraint[5]

Stress distribution

By definition, the stress at any point in an uncracked concrete member is proportional to the strain in the concrete. The horizontal stress in a member continuously restrained at its base and subject to an otherwise uniform horizontal length change varies from point to point in accordance with the variation in degree of restraint throughout the member. The distribution of restraint varies with the length-to-height ratio (L/H) of the member. For *L/H* equal to or greater than 2.5, restraint K_R at any point at a height *h* above the base may be approximated by

$$K_R = [(L/H-2)/(L/H+1)]^{h/H} \qquad \text{Eq.2.1}$$

For *L/H* less than 2.5, restraint K_R at any point may be approximated by

$$K_R = [(L/H-1)/(L/H+1.0)]^{h/H} \qquad \text{Eq.2.2}$$

Using the degree of restraint *KR*, from Fig. 2.1 or calculated from Eq. 2.1 or 2.2, the tensile stress at any point on the centerline due to a decrease in length can be calculated from

$$f_t = K_R \Delta_c E_c \qquad \text{Eq.2.3}$$

Where, K_R = degree of restraint expressed as a ratio with 1.0 = 100 percent, Δc = contraction if there were no restraint and *Ec* = sustained modulus of elasticity of the concrete at the time when Δc occurred and for the duration involved.

The stresses in concrete due to restraint decrease in direct proportion to the decrease in stiffness of the restraining material. The multiplier to be used in determining K_R from Fig. 2.1 is given by

$$\text{Multiplier} = \frac{1}{1+\dfrac{A_g E_c}{A_F E_F}} \qquad \text{Eq.2.4}$$

Where, *Ag* = gross area of concrete cross section, A_F = area of foundation or other element restraining shortening of element, generally taken as a plane surface at contact and E_F = modulus of elasticity of foundation or restraining element. For mass concrete on rock, the maximum effective restraining mass area A_F can be assumed at $2.5A_g$ and the values of the multipliers are then shown in the following Table 2.1.

Table 2.1 Multipliers for the foundation/restraining body rigidity

$\frac{E_F}{E_c}$	Multipliers
∞	1.0
2	0.83
1	0.71
0.5	0.56
0.2	0.33
0.1	0.20

Cracking pattern

When stress in the concrete due to restrained volume change reaches the tensile strength of the concrete, a crack will form. If a concrete member is subject to a uniform reduction in volume but is restrained at its base or at an edge, cracking will initiate at the base or restrained edge where the restraint is greatest and progress upward or outward until a point is reached where the stress is insufficient to continue the crack. After initial cracking, the tension caused by restraint in the region of the crack is transferred to the uncracked portion of the member, thereby increasing the tensile stresses above the crack. For *L/H* greater than about 2.5, Fig. 2.1 indicates that if there is enough tensile stress to initiate a crack, it should propagate to the full block height because of the stress-raising feature just mentioned. It has also been found from many tests that once begun, a crack will extend with less tensile stress than required to initiate it [1].

(b) Discontinuous external or end restraint

When the contact surface of the concrete element under restraint and the supporting element is discontinuous, restraint to volume change remains concentrated at fixed locations. This is typical of all concrete elements spanning between supports.

Stress distribution of members spanning between supports

A member that is not vertically supported throughout its length is subject to flexural stress as well as stress due to length change. When a decrease in volume or length occurs in conjunction with flexural members spanning between supports, additional rotation of the cross sections must occur. If the supports themselves are also flexural members, a deflection will occur at the top of the supports and this deflection will induce moments at the ends of the member undergoing volume change. These flexural stresses will be in addition to the tensile stresses induced by the shear in the deflected supports. The end moments thus induced will increase tensile stresses in the bottom face and decrease tensile stresses in the top face of the member undergoing volume change. The magnitude of induced stress depends on the relative stiffnesses of the concrete element under restraint and the supporting members and may be determined when the degree of restraint *KR* has been determined for the support system. For members spanning two supports, the degree of restraint can be approximated by

$$K_R = \frac{1}{1 + \frac{A_B h^3}{4L I_c}} \qquad \text{Eq.2.5}$$

Where, L and A_B = the length and area, respectively, of the member undergoing volume change, and I_c and h = the average moment of inertia and height respectively of the two supporting end members.
The change in bottom face steel stress for members spanning flexural supports can be approximated by

$$\Delta f_s = \frac{K_R C_T T_E E_S}{2pnj}\left[\frac{h}{d}\left(\frac{K_f}{K_f + K_c}\right) + 4pnj\right] \qquad \text{Eq.2.6}$$

Where,
C_T = linear thermal coefficient as defined in Section 3.6
T_E = design temperature change including shrinkage effects
E_S = elastic modulus of steel
K_f = stiffness of beam or floor system undergoing volume change
K_c = average stiffness of vertical restraining elements subject to deflection by volume change

If the supporting members are very stiff relative to the member undergoing volume change, the deflection at the top of the supporting members will be essentially a shear deflection and no end moments will be induced in the member. Under these conditions the change in steel stress throughout the member will simply be

$$\Delta f_s = 2K_R C_T T_E E_S \qquad \text{Eq.2.7}$$

(3) External Stress due to Construction Practices

When volume changes in concrete and restraint are generally independent of one another, design detailing, formwork, and construction practices influence both the volume change and restraint occurring in bridge decks [8].

(a) Stepping Construction

Construction method may have a very large influence on the early-age cracking of RC bridge decks. In stepping construction when two adjoining cantilevers are made continuous, stress redistribution takes place. This redistribution is not only the effect of the step sequence of construction but also of time dependent effects that are recurring in the concrete long after construction ends. It is suggested that placing positive moment regions successively on one day and then placing of negative moment regions after three days may minimize cracking [2, 3].

Fig. 2.2 (a) SIP Forms

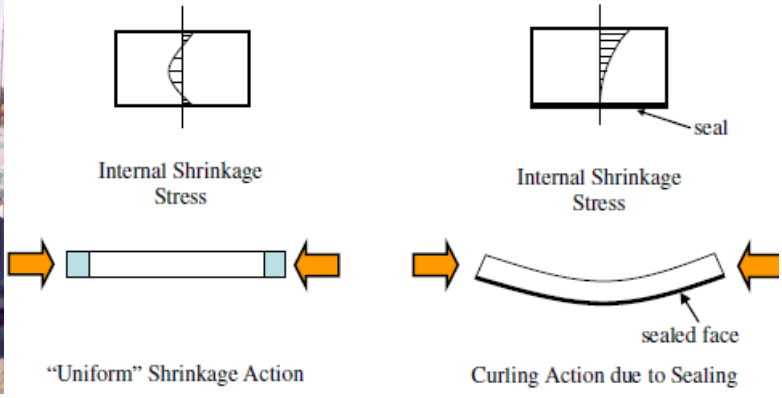

Fig. 2.2 (b) Shrinkage in Bridge Deck

(b) Types of formwork

The type of formwork used during construction affects how shrinkage varies through the depth of the deck. Drying shrinkage in a bridge deck is not uniform because the concrete near the surface will dry more quickly than concrete in the middle of the deck [30]. When both faces of a bridge deck are exposed, the deck will shrink relatively uniformly as illustrated in Fig.2.2(a) and Fig.2.2(b). Decks constructed with stay-in-place (SIP) formwork will have shrinkage at the exposed surface and virtually none at the sealed surface. Internal equilibrium is maintained by the deck curling as shown in Fig.2.2(a). Thus, bridge decks constructed with SIP forms must not only resist internal axial tension but also an internal moment due to shrinkage. Furthermore, the use of SIP steel forms provides a small amount of additional restraint to the bridge deck at the bottom surface of the deck [31].

(c) Concrete Placement Time and Ambient Temperature

The magnitude of deck cracking is greatly affected by concrete placement time. Late morning or early afternoon concrete placement in warm summer days should be avoided because it increases the temperature in concrete, especially during hydration. The ambient temperature directly affects the maximum temperature drop of placed concrete as shown in Fig. 2.3. One of the ways to suppress the maximum temperature and temperature drop is to produce and place concrete during nighttime or early in the morning [9].

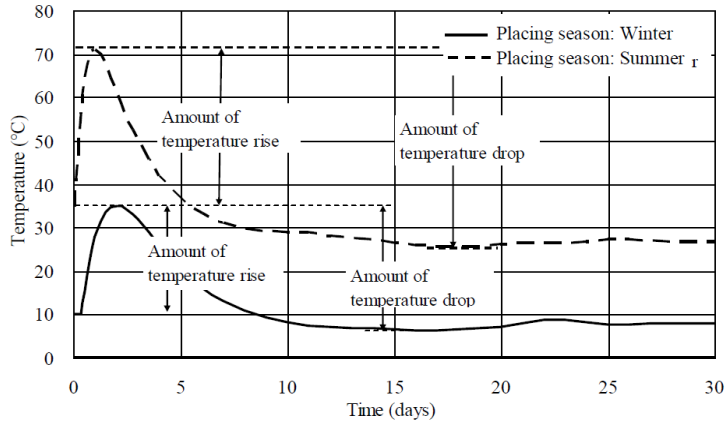

(a) Concrete temperature

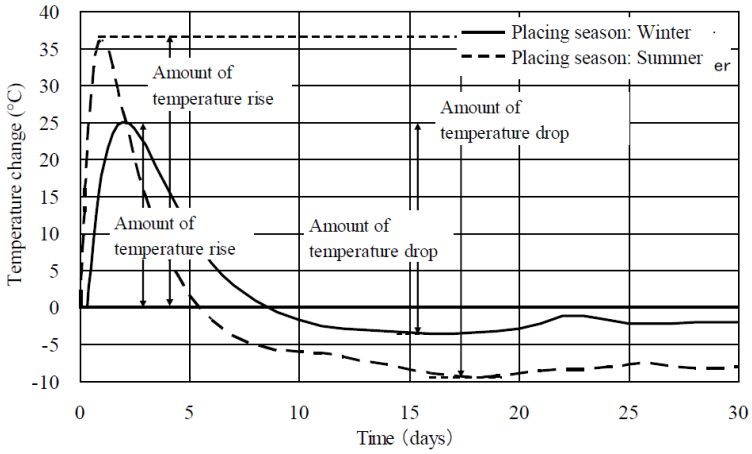

(b) Amount of temperature change

Fig. 2.3 Schematic diagram of transient temperature in mass concrete [9]

(d) Vibration, Finishing and Curing of Concrete:

The literature study indicates that inadequate vibration is a major cause of cracking. Proper vibration methods will improve all the important properties of concrete in bridge decks [8]. Delayed finishing can make concrete prone to cracks. Surface finishing and texturing should be completed as soon as possible to allow the final cure of the deck. Furthermore, early finishing can reduce the number and width of cracks which develop in concrete [32]. Curing is an important factor that influences early-age bridge deck shrinkage cracking. Ineffective curing was the most common reason suggested by the transportation agencies for excessive deck cracking. Immediately after finishing, use of wet curing should be applied. Concrete with high cement content and low water-to-cement ratio is more sensitive to curing conditions than that with low cement content and high water-to-cement ratio. For concrete with silica fume and/or fly ash/blast furnace slag, a 7-day continuous moist curing is recommended to reduce early age cracking. By employing construction procedures, such as wet curing, concrete shrinkage can be reduced and delayed until the concrete develops sufficient tensile strength [27].

2.3 LIMIT VALUES FOR CONTROLLING CRACK WIDTHS

2.3.1 Guidelines for Control of Cracking of Mass Concrete, JCI 2016 [9]

According to the guidelines for Control of Cracking of Mass Concrete by Japan Concrete Institute (2016) limit values for controlling thermal crack widths are demonstrated below:

(1) Limit values of thermal cracks widths should be defined to provide satisfactory in terms of structural performances related to serviceability, durability, appearance, sense of anxiety, etc. Since, environmental conditions substantially affect corrosion, limit values of crack widths should be determined in accordance to the environmental conditions in which the structures are constructed. A lower reinforcement ratio may result in a region with extremely large thermal crack widths. A temperature drop after occurrence of thermal cracks causes further contraction deformation, which widen crack widths unless new thermal cracks appear. Thermal cracks may also widen due to the effect of design loads applied to completed structures, drying shrinkage in concrete, etc. [33].

(2) The limit values of crack widths at the surface can be determined based on the value of crack width for preventing steel corrosion, that is 0.005c (c: concrete cover) specified in the 'Standard Specifications for Concrete Structures, Design' [34] or the limit values in Table 2.2 given in the 'Recommendations for Practice of Crack Control in Reinforced Concrete Buildings (Design and Construction)' [35]. Again, According to the JSCE standard 2007, the limit value of crack width for concrete in a severely corrosive environment is 0.0035c, where c refers to the concrete cover [36].

(3) The limit values of crack widths should be established with consideration for the allowable amount of leakage. Table 3 lists the limit values of crack widths with respect to water tightness given in the 'Standard Specifications for Concrete Structures, Design 2012' [34]. The limit values in the table are different according to the types of predominant section forces. In the case when external restraint is a major influential factor, it is recommended to adopt the limit values of crack widths assigned to the case for predominant axial tensile force. Further, according to Table 3, since the whole section should be under compressive stress to realize high water tightness, the above case should not be considered to fall under the requirements for control of cracking specified in the Guidelines.

(4) In the Design Part of the JSCE Specifications [34] a general value of 0.3 mm is recommended to maintain for satisfactory appearance.

Table 2.2 Limit values of crack widths for control of shrinkage cracks (mm) [35]

Purpose	Limit values of crack widths
Prevention of leakage	0.15
Measures against deterioration under normal environmental condition	0.5 (indoors) 0.3 (outdoors)

Note: 'Limit value of crack width' in the above table is presented as 'allowable value of crack width' or allowable crack width' in reference (AIJ).

Table 2.3 Reference limit values of crack widths for water tightness (mm) [34]

Required level of water tightness		High	Normal
Predominant section forces	Axial tensile force	----------1)	0.1
	Flexural moment 2)	0.1	0.2

[1)] Stress in concrete due to section forces should be compressive all through the section with the minimum stress of 0.5N/mm2 and over unless a detailed analysis is conducted to specify otherwise.

[2)] When the structures are subjected to reversible loads, the provision for the case of predominant tensile forces is applied.

2.3.2 Control of Cracking in Concrete Structures according to ACI 224R-08

In ACI 207 [5], for water-retention elements, very narrow, just-visible cracks 0.002 inch (0.05 mm) will probably leak, at least initially; however, nonmoving cracks up to 0.005 inch (0.127 mm) may heal in the presence of excess moisture and therefore would not be expected to leak continually.

2.4 PREVIOUS RESEARCH ON TRANSVERSE DECK SLAB CRACKING

2.4.1 Field Survey Investigations

Several studies have been conducted in the past regarding transverse bridge deck cracking and its effect on the durability of concrete bridge decks are summarized below:

(1) Portland Cement Association (PCA1970) [37]

The objectives of the study were to determine the types and extent of concrete bridge deck durability problems, causes of the various types of deterioration, methods for obtaining improved durability, and methods for retarding existing deterioration. Important factors affecting the development of transverse cracking were found to be:

- Transverse cracking was the most common cracking type
- Temperature variations in the deck are larger than in the rest of a bridge structure and restraint of the resulting volume changes induce cracking in the concrete deck.
- Older decks and longer spans typically displaying more transverse cracking due to the restraint from the girders on the early and long term shrinkage of the deck;

- The type of superstructure affected the occurrence of transverse cracks. Continuous span bridges and steel girders seemed to exacerbate transverse cracking, while simply supported spans and reinforced concrete girders alleviated transverse cracking.
- Influence of top slab reinforcement as a source of internal restraint in the concrete; and internal restraint of the concrete due to differential drying shrinkage.
- Live load stresses appeared to play a minor role in transverse cracking on steel girders

(2) Cady et al. (1971) [38]

Cady et al. [38] surveyed total 249 numbers four year old bridge decks in Pennsylvania to investigate the extent and causes of deterioration in concrete bridge decks. Transverse cracks were found to be the most prevalent type of cracking observed. The study found that transverse cracks occurred in 60% of all spans and in 71% of all bridges. In addition, the study determined:

- Decks constructed with stay-in-place (SIP) forms exhibited much less cracking than those built with removable forms.
- The transverse crack intensity increased as the span length increased.
- Superstructure type had a significant effect on the amount of cracking observed.
- Steel bridges had more cracking than prestressed concrete bridges.
- Continuous span bridges showed more cracking than simply supported span bridges.
- Construction practices were the single most influential variable in the extent of cracking observed in bridge decks.

(3) Purvis et al. (1995) [39]

Purvis et al. in 1995 [39] performed 99 field surveys and 12 in-depth surveys of different bridges in Pennsylvania to assess the causes of transverse cracking in bridge decks. The in-depth surveys included crack mapping, crack width measurement, rebar location and depth surveys, and concrete coring. Background design and construction records were also reviewed. The researchers found that transverse cracks intersected coarse aggregate particles indicating that transverse cracking was occurring in hardened concrete and was likely caused by drying and thermal shrinkage. Transverse cracks occurred through the plane of the transverse reinforcement due to planes of weakness caused by settlement-induced strains occurring while the concrete was still plastic. The researchers also performed a laboratory shrinkage study to investigate the effects of aggregate types on shrinkage of concrete, the effects of cement source and type on drying and thermal shrinkage, and the effect of fly-ash on shrinkage. The researchers recommended that the maximum differential deck/beam temperature be limited to 22° F (12° C) for 24 hours after the deck is placed. The study also recommended limiting the 4-month concrete drying shrinkage to 700 micro strains.

(4) Krauss and Rogalla (1996) [27]

Krauss and Rogalla in 1996 [27] surveyed 52 transportation agencies in the United States and Canada to evaluate the extent of early age transverse cracking. The researchers found that over 100,000 bridges in the United States developed early transverse cracks. The survey respondents indicated that stiffer decks and larger amounts of reinforcement is the effective. The respondents also recommended a minimum clear cover of 1.5 inches (38 mm) over the reinforcement and a maximum clear cover of 3 inches (75 mm). Additionally, the minimum recommended thickness of the deck should be between 8 and 9 in (200 mm and 225mm).

(5) Eppers, French, and Hajjar (1998) [40]

Eppers et al. (1998) surveyed 72 bridge decks in Minnesota and found the following influential factors:

- Dominant design factors impacting transverse cracking were identified as longitudinal restraint, deck thickness, and top transverse bar size.
- Material related parameters most affecting transverse cracking were found to be cement content, aggregate type and quantity, and air content.
- Decks constructed on simply supported prestressed girder bridges were in good condition relative to those constructed on continuous steel girder bridges.
- Diaphragms caused stress concentrations, and staggered diaphragms with closer spacing resulted in more tightly spaced cracks, which indicated smaller crack widths.

Based on the field study, the researchers recommended the following:

- Reduce restraint by using bridge expansion joints, simply supported spans, increasing girder spacing, and providing fewer shear connectors.
- Use #5 top transverse bars in concrete bridge decks on steel girders.
- Reduce the paste volume of the mix designs being used, use lower water-cement ratios, select minimum air content between 5.5% and 6.0%, maximize the coarse and fine aggregate content, and improve curing in the field.

(6) Le, French, and Hajjar (1998) [41]

Le et al. in 1998 performed a shrinkage study for two Minnesota Department of Transportation mix designs and a parametric study to assess the effects of individual parameters on transverse cracking in bridge decks. The parametric study considered bridges with steel and prestressed concrete girders.

The variables considered for the steel girder bridges included: end conditions; girder stiffness; locations of cross frames, girder splices, and supplemental reinforcing bars; shrinkage properties; concrete modulus; and temperature differential due to heat of hydration.

The variables for the prestressed girder bridge included the times casting relative to the times of both strand release and deck casting, and shrinkage properties of the both the deck and the girders.

The parametric study determined the following:

- Prestressed girder bridges with typical construction timelines did not exhibit transverse cracking due to lack of restraint at the end supports and the ability of concrete girders to shrink with the deck over time.
- Prestressed girder bridges where strand release was delayed resulted in higher tensile stresses in the deck.
- Decks placed on aged, prestressed girders developed high tensile stresses as a result of differential shrinkage between the girder and the deck.
- Steel girder bridges exhibited cracking in both the positive and negative moment regions of the bridge deck.
- Differential shrinkage between the deck and the girders was cited as the main cause of cracking.

- Ultimate shrinkage did not significantly affect the tensile stresses in the deck due to mitigation of stress through creep of the concrete.
- End conditions significantly affected the amount of transverse cracking. Cracking was most extensive in the fixed-fixed case and not observed in the simply supported case.
- Girder stiffness, cross frames, and splices dictated crack locations.

The parametric study recommended

- Reducing longitudinal restraint of the concrete deck by reducing the continuity of the deck over interior supports through the use of expansion joints on continuous girders,
- Minimizing girder restraint through increased girder spacing and minimizing shear connector restraint by using fewer rows of studs, and constructing with shorter, smaller diameter studs.

Nevertheless, the researchers concede that reducing restraint in the deck may significantly affect bridge performance (larger girders and greater deflections) and must be implemented with consideration given to other aspects of bridge performance.

2.4.2 Material Design, Field Monitoring and Numerical Simulation

(1) Krauss and Rogalla in 1996 [27]

The analytical studies were performed by Krauss and Rogalla [27] using both theoretical and finite element analysis techniques to evaluate the influence of various parameters on transverse cracking. These factors included drying shrinkage, creep, hydration temperatures and other thermal effects, position and amount of reinforcing steel, girder size and spacing, single- and two-span conditions, and age. The parametric study included bridge decks constructed on steel girders, reinforced concrete girders, precast-prestressed concrete girders, and cast-in-place post-tensioned girders.

From the parametric study, the researchers determined that the design factors which most significantly affected cracking were span type, concrete strength, and girder type. The researchers also observed that the amount of restraint, the amount of drying shrinkage, thermal movements of the deck and girders, and effective modulus of elasticity of the concrete affect the stresses and risk of transverse cracking in a bridge deck. The material properties of the concrete such as cement content, cement composition, early-age elastic modulus, creep, aggregate type, heat of hydration, and drying shrinkage also influenced cracking.

(2) Frosch and Bice in 2006 [4]

The objective of the research under taken by the Joint Transportation Research Program in cooperation with the Indiana Department of Transportation, USA was to evaluate the influence of design parameters on the performance of bridge decks with respect to cracking and to develop simple design tools that are appropriate for both steel and nonmetallic reinforcement. That research was conducted in two phases. The first phase consisted of a field investigation of four bridges which incorporated different design elements to determine the in-service performance of bridge decks. Bridges were instrumented, monitored, and crack mapped. In the second phase of the research, a simple, finite element model was developed and calibrated against data from the field investigation and laboratory studies conducted by others. A parametric study was then conducted using this method to evaluate the effects of a range of design variables on the resistance to crack formation and the width of cracks that subsequently formed. Based on the results of the parametric study, it was determined that the amount and spacing of reinforcement in

the deck directly influenced the extent of cracking that developed. It is recommended that the amount of reinforcement provided be sufficient to prevent localized yielding at cracks in the case of steel reinforcement and to prevent fatigue failure when FRP reinforcement is considered. Simple design equations are provided for the amount and spacing of reinforcement for both steel and FRP reinforcement to control cracking in bridge decks

(3) Tanaka et al. in 2017 [42]

In Tohoku region of Japan, 'Revival Roads' are constructed to accelerate recovery from the Great East Japan earthquake that occurred in 2011. The Revival Roads includes more than 250 bridges which are anticipated to be vulnerable to sever deterioration due to freezing and thawing, ASR, chloride attack and so on. Additionally, the occurrence of early age thermal and shrinkage cracks in RC deck slabs restrained by girders provide can rapid routes for harmful agents leading to severe damages. In this context, Tanaka et. al. designed the concrete and reinforcing materials to be durable for such RC deck slab. A multiple defense was a key phrase in their durability design where, expansive agent was used to reduce shrinkage cracks whereas; use of fly ash was the core counter measures because of its effectiveness against ASR and chloride attack. Air content was designed at 6% to achieve anti-frost performance. Epoxy-coated reinforcing bars were used to resist corrosion. Wet curing continued for three months to obtain a pozzolanic reaction. The quality of the hardened concrete was checked by element test and nondestructive tests. The multiple protection counter measures for durable concrete was applied in the construction of the RC deck slab for the Mukai-sada-nai bridge which is a steel girder single span bridge. For the post-evaluation, several strain sensors were embedded in the RC slab. The outside temperature and relative humidity (RH) were also measured to be used in the post evaluation. Strain changes in the RC slab were simulated by multi-scale finite element analysis [44, 45]. The DU-COM-COM3 program was used for simulating the moisture transport, thermal stress, hydration and non-linear structural responses. The simulation predicted that a few small cracks would occur after two years owing to drying shrinkage. The cracking strain is too small to cause corrosion.

(4) Ishida et al. in 2018 [46] [47]

Corresponding research by Ishida et.al.(2018) presents a numerical simulation of early age deformation and cracking of RC bridge decks with full 3D multiscale and multi-chemo-physical integrated analysis[44, 45].The subject of this analysis was Shinkesen Bridge in Iwate prefecture, Tohoku region, Japan which is amongst the 250 bridges that are scheduled to be constructed to accelerate the infrastructural recovery from the Great East Japan Earthquake. The Shinkesen Bridge was selected for the introduction of blast furnace slag (BFS) concrete for durable concrete design. With the use of a low water-to-binder ratio and BFS in the mix proportion, early-age cracking is anticipated to occur due to low creep and high autogenous shrinkage of BFS concrete allowing deleterious ions to deteriorate the concrete structures. Ishida et al conducted study comprising both experiments and multiscale thermodynamic integrated analysis from a laboratory scale up to a structural scale, followed by assessment and evaluation of the bridge deck via analytical results. With the aim to assess the early age thermal and shrinkage-induced cracks on real bridge deck, the study began with model validations by applying the multiscale and multi-physical integrated analysis system to small specimens, mock-up RC bridge deck specimens, preliminary analysis of Shikesen RC deck and post construction verification of on-site measurement (Fig. 2.4).The analytical strain was considered from the start of the 19th day for verification process in this study. Then, through the application of the computational system [44, 45], factors that affect the generation and propagation of thermal and shrinkage-induced

cracks are predicted via experimental validation and full-scale numerical simulation on real RC slab decks.

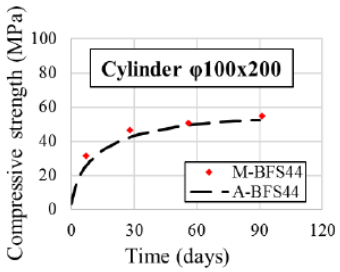

(a) Determination of Compressive strength[46]

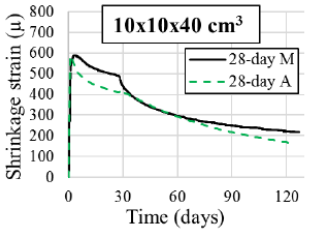

(b) Evaluating free volumetric change[46]

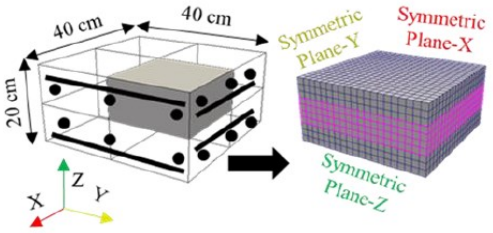

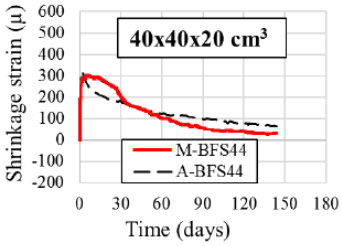

(c) Evaluating restrained volumetric change[46]

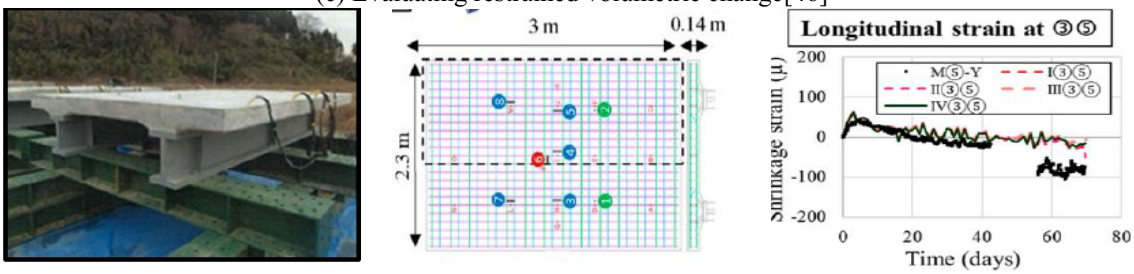

(d) Application of the Analytical Model on a Mock-Up Slab Specimen[46]

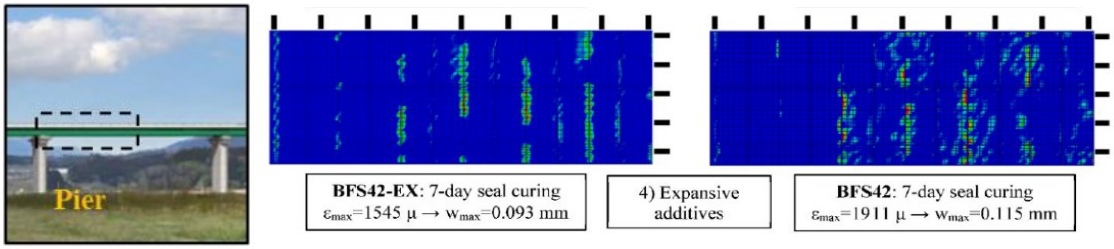

(e) Preliminary Analysis on Concrete Deck Slab of Shinkesen Bridge to Evaluate the Occurrence of Cracks[46]

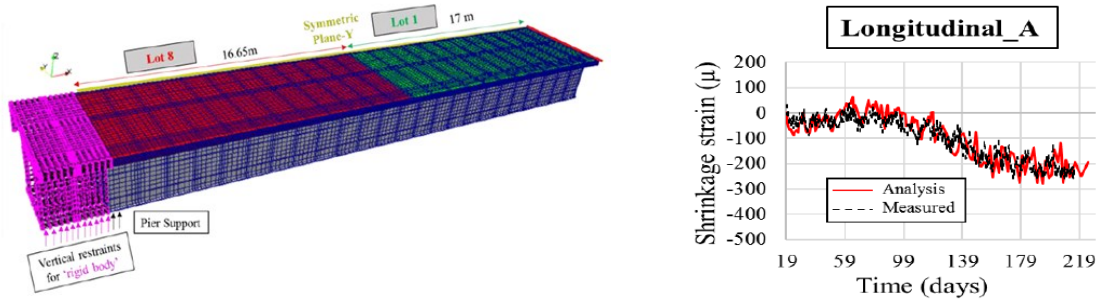

(f) Post-Construction Analysis on Concrete Deck of Shinkesen Bridge: Verification with on-Site Measurement[46]

Fig. 2.4 Schematic Experimental Numerical Analysis Scheme followed bt Ishida et al.[46]

(5) Guidelines for Control of Cracking of Mass Concrete (2008) and (2016)

The Guidelines for Control of Cracking of Mass Concrete (2008 and 2016) [48][9] recommends to verify thermal cracking probabilities utilizing a three-dimensional finite element analysis for thermal and stress simulation to consider a wide range of structures and geometric shapes. The analysis scheme incorporates equations for adiabatic temperature rise using parameters to shape the function as necessary to fit a multi-component model for heat of hydration proposed by Maekawa et. al.[45].

A Multi-Component Model for Hydration Heat[45] [47][9]

In the temperature analysis of concrete, the thermal conductivity equation (Eq.2.8) is solved by FEM in terms of time and space.

$$c\rho \frac{\partial T}{\partial t} = K\nabla^2 T + H \qquad \text{Eq.2.8}$$

$$H = \sum p_i H_i \qquad \text{Eq.2.9}$$

$$H_i = \gamma_i \beta_i \lambda_i \mu_i H_{i,To}(Q_i) exp[-\frac{E_i}{R}(\frac{1}{T_i} - \frac{1}{T_o})] \qquad \text{Eq.2.10}$$

The heat generation rate per unit mass of cementitious material H in Eq.2.8 is modeled by the multi-component model for heat of hydration [45]. The heat rate of the entire cementitious material including mineral admixtures is calculated as the summation of the heat rate of all reactions as shown in Eq.2.9. The individual component heat generation rates are functions of the reference heat generation rate ($H_{i,To}(Q_i)$), thermal activity ($-E_i/R$) and Temperature (T_i) of the component considering the interdependency of the reaction. Thus, temperature analysis utilizing multi-component model is a non-linear analysis which is considered as an accurate approach.

The reference heat generation rate ($H_{i,To}(Q_i)$) is dependent upon the mineral components and their fineness. The reference heat generation rate is shown in Fig.2.5. The heat generation rate at an arbitrary temperature is calculated step by step using Eq.2.10 taking into consideration the influence of temperature according Arrhenius' Law. The thermal activity $-E_i/R$ is assumed to be constant independent of the accumulated heat Q_i. The thermal activity of alite (C_3S) is -6977K, belite (C_2S) is -5814K, ground granulated blast-furnace slag is -5220K and flyash is -13920K. Eq.2.10 considers various factors including the delaying effect of chemical admixture in the initial hydration exothermic process (γ), the reduction in heat generation due to the reduced availability of free water (β), the change of the heat generation rate of mineral admixtures due to the lack of calcium hydroxide in the liquid phase (λ), and the change of heat generation rate with respect to the difference of mineral composition of Portland cement (μ).

In multi-component model, fineness and mineral composition of Portland cements are assumed as presented in Table 2.4. For class B blast-furnace slag cement, 40% of ordinary Portland cement is replaced by ground granulated blast furnace slag with fineness of 4200 cm^2/g, and for fly ash cement class B, 18% of ordinary Portland cement is replaced by fly ash with fineness of 3400 cm^2/g.

Table 2.4 Fineness and mineral compositions of Portland cement for calculating multi-component model for hydration heat [9]

Type of cement	Fineness modulus (cm^2/g)	Mineral composition (%)			
		C_3S	C_2S	C_3A	C_4AF
Ordinary	3300	55	19	8	10
Moderate heat	3400	40	39	4	11
Low heat	3400	25	56	3	10
High early strength	4200	63	12	9	8

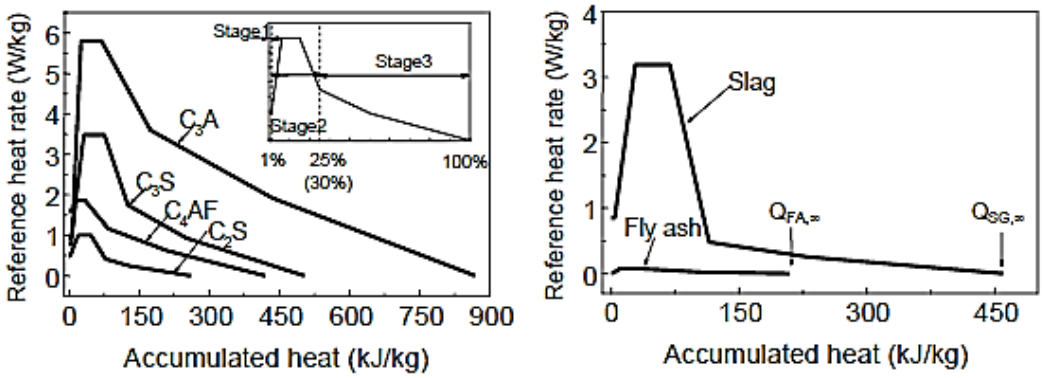

Fig. 2.5 Reference heat rate for each reaction. [45]

Adiabatic Temperature Rise Equation Based on the Multi-component Hydration Heat Model [9] [45] [48] [49]

The input data for the multi-component model are density, specific surface area, quantity of sulfur trioxide and quantity of mineral composition in cement. The thermal conductivity (K) is assumed to be a constant 2.7 W/m°C. Further, the initial temperature in the analysis is set as the placing temperature. Since, the multi-component adiabatic temperature rise equation (Eq.2.10) provides a sufficiently accurate prediction (Fig.2.5(a)), the estimated adiabatic temperature rise was regresses by Eq.2.11 and the parameters of the aforesaid equation were formulated as functions of unit cement content and placing temperature to conduct the non-linear analysis conveniently.

$$Q(t) = Q_\infty \left[1 - exp\left\{ -r_{AT} \left(t - t_{0,Q} \right)^{s_{AT}} \right\} \right] \qquad \text{Eq.2.11}$$

where, t : age (day)
$Q(t)$: adiabatic temperature rise at age of t days (°C)
Q_∞: ultimate adiabatic temperature rise (°C)
r_{AT}, s_{AT} : parameters representing rate of adiabatic temperature rise
$t_{0,Q}$: age at starting of temperature rise (day)

Fig. 2.5(a),(b) and (c) prove the accuracy of estimated adiabatic temperature rise by Eq.2.11 in case of different unit cement content, different placing temperature and different types of cement respectively [48]. Since, the estimated adiabatic temperature rise based upon the multi-component model was appeared sufficiently accurate in comparison to experimental data, the adiabatic temperature rise equation (Eq.2.11) along with the corresponding parameters were adopted in the JCI Guidelines for Control of Cracking of Mass Concrete 2008 and 2016.

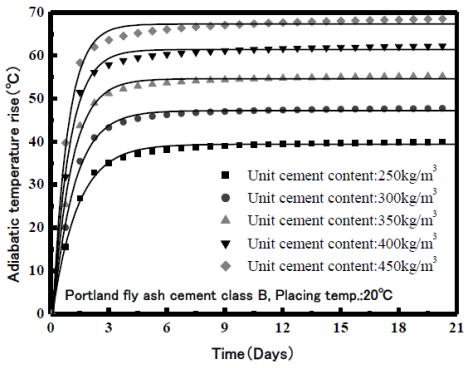

Fig. 2.6(a) Accuracy of estimated adiabatic temperature rise based on the multi-component model [47]

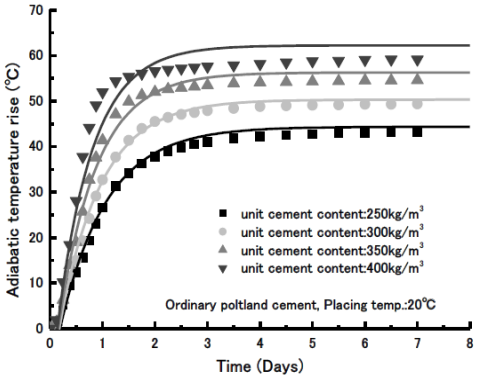

Fig. 2.6(b) Accuracy of estimated adiabatic temperature rise by Eq.2.11 in case of different unit cement contents [47]

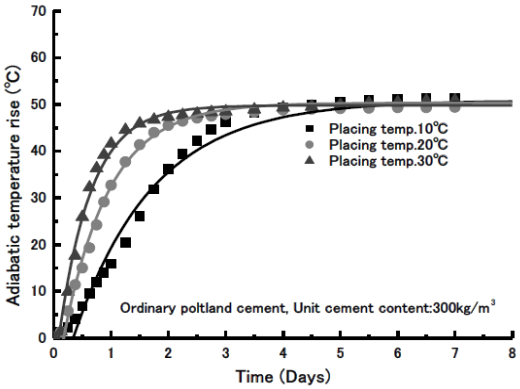

Fig. 2.6(c) Accuracy of estimated adiabatic temperature rise by Eq.2.11 in case of different placing temperature [47]

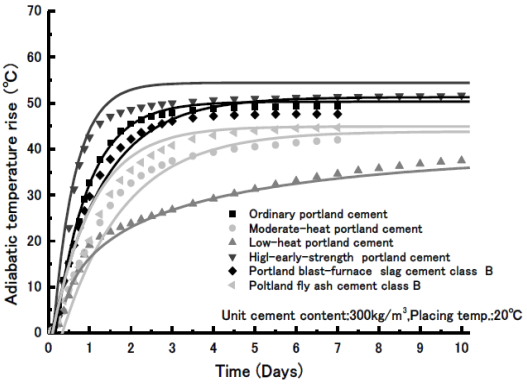

Fig. 2.6(d) Accuracy of estimated adiabatic temperature rise by Eq.2.11 in case of different types of cement [47]

Heat Transfer Coefficient of Concrete [9]

The Guidelines for Control of Cracking of Mass Concrete (2008 and 2016) [48][9] recommends to determine the heat transfer coefficient of different surfaces of concrete structures depending on formwork type, form removal time, curing method, curing duration, ambient temperature, wind velocity and ambient moisture conditions for simple but accurate thermal and structural stress analyses without direct application of the multi-scale modeling of moisture transport, micro-pore structure development and thermo-dynamic equilibrium in concrete[45].

Effective Young's Modulus Considering the Influence of Creep and Pickett effect

The Guidelines for Control of Cracking of Mass Concrete (2008 and 2016) [47][9] recommends to consider the influence of basic creep, drying creep or Pickett effect due to micro-cracking[50] and stress induced shrinkage by calculating the effective modulus of elasticity, which is the product of the modulus of elasticity of concrete and a reduction factor as shown in Eq.2.12.

$$E_e(t_e) = \varphi(t_e) \times E_c(t_e) \qquad \text{Eq.2.12}$$

Where,

$E_c(t_e)$: Modulus of elasticity (Young's modulus) of concrete at t_e （N/mm2）

$\varphi(t_e)$： Reduction factor for modulus of elasticity because creep is large in hardening process.

Until the temperature adjusted effective material age when temperature rise becomes the maximum:

$$\varphi(t_e)=0.42$$

Again, after one day in temperature adjusted effective material age as from the age at the maximum temperature:

$$\varphi(t_e)=0.65$$

$\varphi(t_e)$ is linearly interpolated between the above both temperature adjusted effective material age.

It is to be noted that although the compressive strength development is same for JSCE2007 and JCI2016 time dependent equations, JSCE2007 intentionally underestimates the Young's modulus development of concrete compared to that of JCI2016 and the test results for the cylindrical specimens under wet curing to compensate the effect of micro-cracking or Pickett effect in structures which may reduce the stiffness of the concrete members. On the other hand, the reduction factors for the Young's modulus to consider the creep effect are higher for JSCE2007 compared to those of JCI2016. For example, JSCE2017 consider φ(t) = 0.73 for temperature rising period (until 3 days of concrete material age) and φ(t) =1.00 for temperature decreasing period (from 5 days of concrete material age) whereas, JCI2016 has specified $\varphi(t_e)$ =0.42 until the temperature adjusted effective material age when temperature rise becomes the maximum and $\varphi(t_e)$=0.65 after one day in temperature adjusted effective material age as from the age at the maximum temperature to take into account the reduction of stiffness of concrete members due to basic creep, drying creep or Pickett effect and stress induced shrinkage.

2.5 REQUIREMENT OF CONDUCTING PRESENT RESEARCH

Most of the previous studies demonstrated here contributed in determining the influential factors for transverse cracking of RC deck slab corresponded to survey investigations of various bridges and emphasizing on the effect of long term restraint volume changes. Although Ishida et al.(2018) conducted multiscale and multi-chemo-physical integrated analysis to predict the factors affecting the generation and propagation of thermal and shrinkage-induced cracks via experimental validations and full-scale numerical simulation on real Shinkesen Ohashi RC slab decks in Tohoku region of Japan, the analytical strain was considered from the start of the 19th day for verification process in their study where early age thermal stresses due to the generation of hydration heat was not taken into account. However, crack investigation of the Shinkesen RC slab has revealed the occurrence of early age cracks (crack width=0.8 mm) in several casting lots of Shinkesen RC slab observed after removing the curing sheets after 28th days of wet curing. Moreover, recent investigations after two years of the construction of Shinkesen RC slab uncovered that the crack width has increased up to 0.2 mm exceeding the allowable crack width (0.0035c where c is cover thickness) [36] in highly corrosive regions such as Tohoku region in Japan. Therefore, it can be inferred that enough work has not been done on the simulation and

structural level monitoring and verification of the very early age thermal behavior of deck concrete which could be one of the most significant factors for early age cracking even after taking multiple protection counter measures. Therefore, the importance of further studies on numerical simulation of early age thermal and volumetric stresses to determine the influential factors on the occurrence of early age cracks in RC bridge slabs followed by a material-member-structure level systematic full scale 3D FEM analysis scheme have never been lost.

However, JCI Guidelines for Control of Cracking of Mass Concrete 2016 follows the estimated adiabatic temperature rise based upon the multi-component model considering parameters as the functions of cement contents, water to binder ratio and concrete temperature as placement which was proved to be sufficiently accurate in temperature analysis. Moreover, the physical properties of concrete depending on materials, mix proportion, temperature at placement, temperature history can be defined in the three-dimensional finite element analysis for thermal and stress simulation considering a wide range of structures, geometric shapes and environmental condition. In addition, the application of reduction factors can successfully calculate the effective Young's modulus of concrete evaluating creep and micro-cracking in reducing the stiffness of concrete structures. Nevertheless, the provision of heat transfer coefficients for different components of concrete structures depending on formwork type, form removal time, curing method, curing duration, ambient temperature, wind velocity and ambient moisture conditions for thermal stress analyses without direct application of the multi-scale modeling of moisture transport, micro-pore structure development and thermo-dynamic equilibrium in concrete has simplified the FEM thermal and structural stress analysis procedure to utilize in extensive parametric studies which can be said to be rational to exploit in the present research to identify the significant influential factors for early age thermal and shrinkage cracks in RC deck slabs.

References

[1] ACI Committee 224. (2008). ―Control of Cracking in Concrete Structures (ACI 224R-08), Manual of Concrete Practice,Part2, American Concrete Institute, Farmington Hills, MI,46 pp.

[2] ACI Committee 209. (2008). ―Prediction of Creep, Shrinkage and Temperature Effects in Concrete Structures‖ (ACI 209R-08), Manual of Concrete Practice, Part 2, American Concrete Institute, Farmington Hills, MI, 47 pp.

[3] ACI 331R-10 (2010) ―Report on Early-Age Cracking: Causes, Measurement, and Mitigation,‖ American Concrete Institute, Farmington Hills, MI.

[4] R.J. Frosch and J. K. Bice (2006) ―Report on Design Methods for the Control of Restrained Shrinkage Cracking, Purdue University, West Lafayette, Indiana 47907, 2006.

[5] American Concrete Institute, ACI Committee 207, Effect of Restraint, Volume Change, and Reinforcement on Cracking of Mass Concrete, ACI 207.2R-95, 2002.

[6] Lawler, J., Connolly, J.D., Krauss P.D., Tracy, S.L. Ankenman, B.E. (2007) ―Guidelines for Concrete Mixtures Containing Supplementary Cementitious Materials to Enhance Durability of Bridge Decks‖, NCHRP Report 566, Transportation Research Board.

[7] Li, H., Wee, T. H. and Wong, S. F. (2002). Early-age Creep and Shrinkage of Blended Cement Concrete,‖ ACI Materials Journal, Vol. 99, No. 1, Jan-Feb., pp. 3-10.

[8] V. Khatri, P.K.Singh and P.R.Maiti, "Shrinkage Effect and Transverse Cracking in Steel-Concrete Composite Bridge Deck," International Journal of Emerging Technology and Advanced Engineering, vol.2, Issue 11, November 2012.

[9] Japan Concrete Institute, JCI Guidelines for Control of Cracking of Mass Concrete, Tokyo, 2016.

[10] Yabe, J. (2004) Present Situation and Considering Point of Steel-Concrete Composite Slab, Proc. of the 7th Symp. on Steel Structures and Bridges, JSCE, pp.49-60, in Japanese.

[11] Tia, M., Subramanian, R., Brown, D., Broward, C. (2005) "Evaluation of Shrinkage Cracking Potential of Concrete Used in Bridge Decks in Florida," Research Report, University of Florida, Sep., 129 pages.

[12] Tritsch, N., Darwin, D. and Browning J. (2005) Evaluating Shrinkage and Cracking Behavior of Concrete Using Restrained Ring and Free Shrinkage Tests‖, The Transportation Pooled Fund Program Project No. TPF-5(051), Structural Engineering and Engineering Materials SM Report No.77, The University of Kansas Center for Research, Inc. at Kansas.

[13] Turcry, P., Loukili, A., Laurent, B., Casabonne, J., Can the maturity concept be used to separate the autogenous shrinkage and thermal deformation of a cement paste at early age?,Cement and Concrete Research, 2002.

[14] Viviani, M., (2005). Monitoring and Modeling of Construction Materials During Hardening,‖ Doctoral Thesis, Swiss Federal Institute of Technology, Lausanne, Switzerland, 172 pp.

[15] Weiss, W.J., and Shah, S. P. (2002), Restrained Shrinkage Cracking: The Role of Shrinkage Reducing Admixtures and Specimen Geometry‖ Materials and Structures, March, VOL. 35 - NO 246, pp. 85-91.

[16] Whigham, J., ―Evaluation of Restraint Stresses and Cracking in Early-Age Concrete with the Rigid Cracking Frame,‖ Master's Thesis, Auburn University, 2005.

[17] Mindness, S., Young, J. F., and Darwin, D., 2003, Concrete, 2nd ed., Prentice Hall, Upper Saddle River, NJ, pp. 417-476.

[18] Bisonnette B., J. Marchand, C. Martel, M. Pigeon, Influence of Superplasticizer on the Volume Stability of Hydrating Cement Pastes at an Early Age‖, Concrete: Material Science to Application, A Tribute to Surendra P. Shah, ACI SP-206, 2002, pp. 167-176.

[19] Al-Manaseer and Jian-Ping Lam, Statistical Evaluation of Shrinkage and Creep Models, ACI Materials Journal, V. 102, No. 3, May-June 2005.

[20] Nagai M., Okui Y., Ohta T., Nakamura H., Inomoto M., Nishio K., Ohgak K., Yamamoto A. (2000) Time dependent stress variation of a composite two-I-girder bridge-Chidorinosawagawa Bridges, Bridge Management 4, Thomas Telford, London.

[21] Weiss, W. J., and Berke, N. S. (2003), Admixtures for Reduction of Shrinkage and cracking‖, Early Age Cracking In Cementitious Systems, Chapter 7.5, RILEM Report 25, A. Bentur, ed., Bagneux, France, pp. 323-338.

[22] Lindquist, W., Darwin, D., Browning, J., (2005).Cracking and Chloride Contents in Reinforced Concrete Bridge Decks, SM Report No. 78, University of Kansas Center for Research, Inc., Lawrence, Kansas, 453 pp.

[23] Lura, P., Jensen, O.M., and van Breugel, K., Autogenous shrinkage in high-performance cement paste: An evaluation of basic mechanisms, Cement and Concrete Research, Volume 33, Issue 2, Pages 223-232, 2003.

[24] Mazloom, M., Ramezanianpour, A.A., and Brooks, J.J. (2004) Effect of silica fume on mechanical properties of high-strength concrete‖, Cement and Concrete Composites, Vol. 26, pp. 347–357.

[25] Delatte, N., Mack, E., and Cleary, J. (2007) ―Evaluation of High Absorptive Materials to Improve Internal Curing of Low Permeability Concrete‖, State Job Number 134227, Final Report, Cleveland State University, Cleveland, OH.

[26] Chariton, T. and Weiss, W. J., ―Using Acoustic Emission to Monitor Damage Development in Mortars Restrained from Volumetric Changes‖, Concrete: Material Science to Application, A Tribute to Surendra P. Shah, ACI SP-206, 2002, pp. 205-218.

[27] Krauss, P. D. and Rogalla, E. A., 1996, NCHRP Report 380: Transverse Cracking in Newly Constructed Bridge Decks, Transportation Research Board, Washington, D.C.

[28] Blackman, D., 2002, Evaluation of Design Methods for the Control of Early Age Bridge Deck Cracking, Masters Thesis, Purdue University, West Lafayette, IN.

[29] Larson, M., ―Thermal Crack Estimation in Early Age Concrete— Models and Methods for Practical Application,‖ doctoral thesis, Luleå University of Technology, Division of Structural Engineering, 2003, 190 pp.

[30] Carlson, R. W., 1937, "Drying Shrinkage of Large Concrete Members, "Journal of the American Concrete Institute, V. 8, No. 3, American Concrete Institute, pp. 327-338.

[31] Radabaugh, R. D., 2001, Investigation of Early Age Bridge Deck Cracking, Master's Thesis, Purdue University, West Lafayette, IN.

[32] Rogalla, E. A., Krauss, P. D., and McDonald, D. B., 1995, "Reducing Transverse Cracking in New Concrete Bridge Decks," Concrete Construction, Hanley Wood, LLC, September 1995, pp. 735-738.

[33] R.Sato,I.Ujike, M.Kimura and H.Ito: Behaviours of Reinforcement Stress and Cracking in Reinforced Concrete Members with Thermal Cracking, Proceedings of the Japan Concrete Institute, Vol.14, No.1, pp.1137-1142, July 1992 (In Japanese).

[34] Japan Society of Civil Engineering, JSCE Standard Specifications for Concrete Structures, 2012.

[35] Architectural Institute of Japan: Recommendations for Practice of Crack Control in Reinforced Concrete Buildings (Design and Construction), pp.39-45, February 2006 (in Japanese).

[36] Standard Specification for Concrete Structures—2007; JSCE: Tokyo, Japan, 2010; ISBN 978-4-8106-0752-9.

[37] Portland Cement Association, 1970, Final Report—Durability of Concrete Bridge Decks, Portland Cement Association, Skokie, IL, 34 pp.

[38] Cady, P. D.; Carrier, R. E.; Bakr, T. A.; and Theisen, J. C., 1971, Final Report on the Durability of Bridge Deck Concrete, Pennsylvania Department of Transportation, Harrisburg, PA, 153 pp.

[39] Purvis, R.; Babei, K.; Udani, N.; Qanbari, A.; and Williams, W., 1995, "Premature Cracking of Concrete Bridge Decks: Causes and Methods of Prevention," Proceedings of the 4th International Bridge Engineering Conference, Washington, D.C.

[40] Eppers, L. J.; French, C. E.; and Hajjar, J., 1998, "Transverse Cracking in Bridge Decks: Field Study," Summary Report 1999-05, Minnesota Department of Transportation, St. Paul, MN, 103 pp.

[41] Le, Q. T.; French, C. E.; and Hajjar, J., 1998, "Transverse Cracking in Bridge Decks: Parametric Study," Summary Report 1999-05, Minnesota Department of Transportation, St. Paul, MN.

[42] Y. Tanaka, T. Ishida, I. Iwaki and K. Sato, "Multiple Protection Design for Durable Concrete Bridge Deck in Cold Regions," Journal of JSCE, vol. 5, pp. 68-77, 2017.

[43] Specifications for Highway Bridges: Part III Concrete Bridges, Japan Road Association, 2012.

[44] Maekawa, K., Pimanmas, A. and Okamura, H.: Nonlinear Mechanics of Reinforced Concrete, Spon Press, 2003.

[45] Maekawa,K., Ishida, T. and Kishi, T. :Multi-Scale Modeling of Structural Concrete, Taylor and Francis, 2008.

[46] T. Ishida and I. Iwaki, "Multi-scale and Multi-chemo-physical Modeling of Cementitious Composite and Its Application to Early Age Crack Assessment of Reinforced Concrete Slab

Decks," in 2nd RILEM/COST Conference on Early Age Cracking and Serviceability in Cement-based Materials and Structures-EAC2, Brussels,2017.

[47] T. Ishida, K. Pen, Y. Tanaka, K. Kashimura and I. Iwaki, "Numerical Simulation of Early Age Cracking of Reinforced Concrete Bridge Decks with a Full-3D Multiscale and Multi-Chemo-Physical Integrated Analysis," Appl. Sci. 2018, 8, 394.

[48] Japan Concrete Institute, JCI Guidelines for Control of Cracking of Mass Concrete, Tokyo, 2008.

[49] Shima, T., Suzuki,Y., Otabe, Y. and Kishi, T., "Proposal of Standard Values of Adiabatic Temperature Rise and Development of Strength", Proceedings of the JCI, Vol.29, No.2, pp.181-186,2007.

[50] Pickett, G., "The effect of Change in Moisture Content on the Creep of Concrete under Sustained Load", J.ACI, 38, 333-355.

3

A SYSTEMATIC ANALYTICAL SCHEME FOR FEM FULL SCALE STRUCTURAL SIMULATION OF GIRDER BRIDGES

3.1 PHILOSOPHY OF THE PRESENT RESEARCH

Philosophy of the present research was preceded with the aim of establishing an FEM numerical simulation system based on thermal and structural stress analysis of RC deck bridges considering different structural restraints and applying appropriate thermal and structural boundary conditions to simulate the volumetric changes of the RC deck slab in early age. The methodology of the numerical procedure follows three leveled systematic analytical scheme for FEM full scale structural simulation of girder bridges (Fig.3.1). Two different structural bridge types i.e., Multiple span steel box girder bridge and Single span PC composite girder bridge were considered in this analysis scheme to confirm the distinctive attributes of thermal stresses in RC deck slab with respect to different structural restraints. The established FEM RC slab bridge models for multi-span steel girder bridge and single span PC composite girder bridge were utilized for parametric studies to determine the influential factors for the risk of early age thermal and shrinkage cracks.

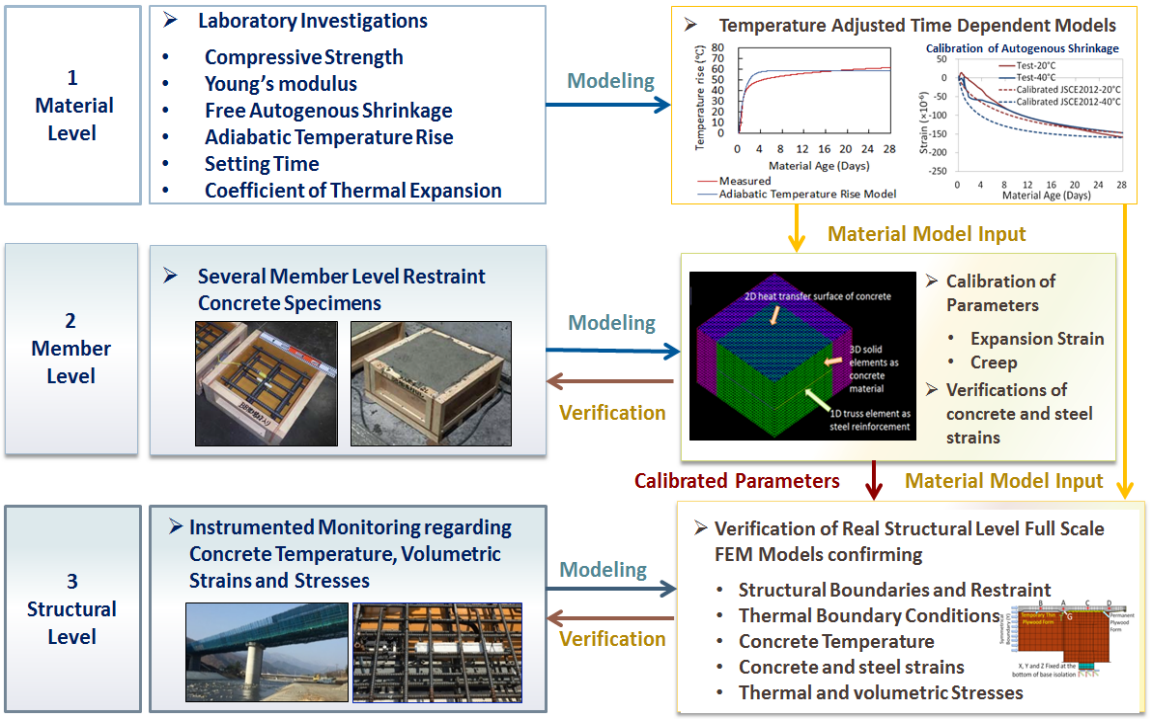

Fig.3.1 The schematic diagram of the systematic analytical scheme for FEM full scale structural simulation of deck girder bridges

The established three leveled systematic analysis scheme in the present research is briefly demonstrated in the following sub-sections:

3.1.1 Level-1: Laboratory Investigations to Determining Concrete Material Properties to Establish Appropriate Material Models

The Level-1 in the analysis scheme involves laboratory investigations to confirm the mechanical properties for the highly durable concrete considering multiple counter measures applied in RC deck slab. The determined material properties include adiabatic temperature rise, time dependent compressive strength and Young's modulus development, setting time, coefficient of thermal expansion and free autogenous shrinkage (Fig. 3.2).

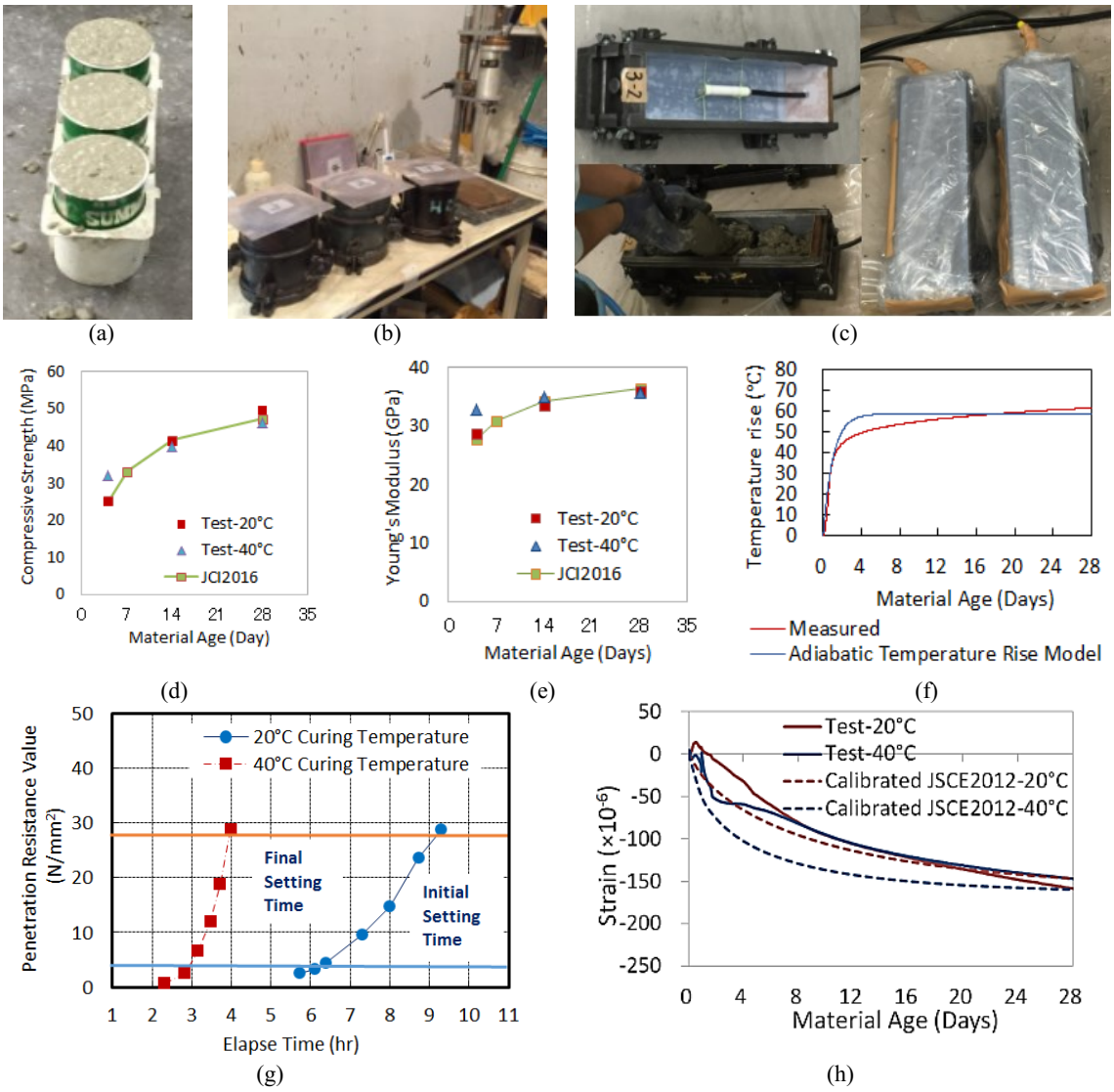

Fig. 3.2 Laboratory investigations and fundamental concrete material models established in Level 1: (a) JIS A 1108 specimens for compressive strength and Young's modulus development, (b) JIS A 6204 ssetting time test specimens, (c) Free autogenous shrinkage specimens with embedded type strain gauges, (d) Calibrated JCI2016 model for compressive strength development of concrete, (e) Calibrated JCI2016 model for Young's modulus development of concrete, (f) Calibrated adiabatic temperature rise model, (g) Defined setting time of concrete and (h) Calibrated JSCE2012/JCI2016 autogenous shrinkage model.

The obtained properties such as setting time, time dependent compressive strength development and Young's modulus development, free autogenous shrinkage were measured to establish material model as inputs in restrained member level and real structural level FEM numerical models respectively in Level-2 and Level-3 in the three leveled systematic analysis scheme.

3.1.2 Level-2: FEM Simulation of Restrained Specimens in Member Level

In Level-2, an FEM numerical simulation procedure was established and validated by configuring three different FEM numerical models in member level concrete specimens under different restrained conditions (Fig.3.3) as illustrated below:

1) JCI-S-009-2012 cylindrical thin walled tinplated steel mold expansion strain specimen,

2) JCI-SAS3-2 autogenous shrinkage strain beam type restrained specimen, and

3) Small size RC slab restrained specimen

Fig.3.3 (a) JCI-S-009-2012 specimen

Fig.3.3 (b) JCI-SAS3-2 specimen

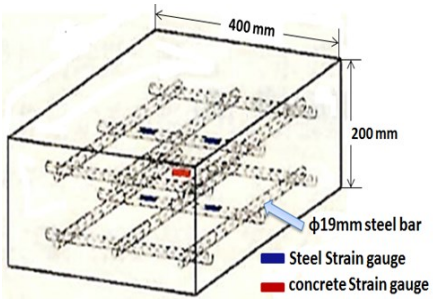

Fig.3.3 (c) Small size RC slab specimen

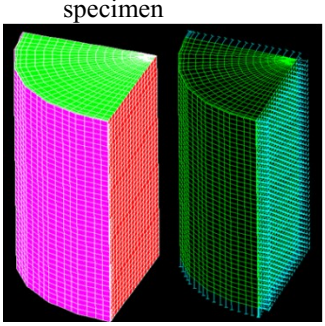

Fig.3.3 (e) JCI-S-009-2012 FEM models

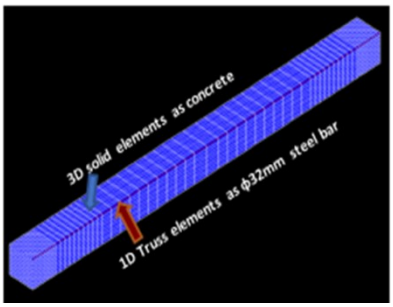

Fig.3.3 (f) JCI-SAS3-2 FEM models

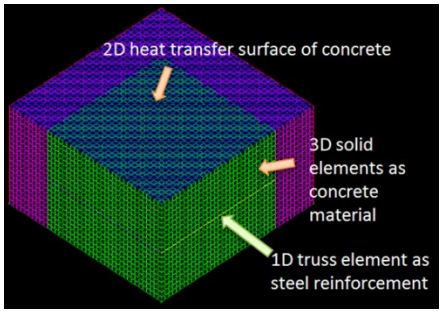

Fig.3.3 (g) Small size RC slab model

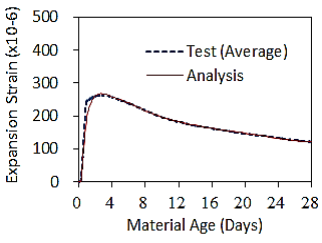

Fig.3.3 (h) Simulation of expansion strain utilizing JCI-S-009-2012 FEM model

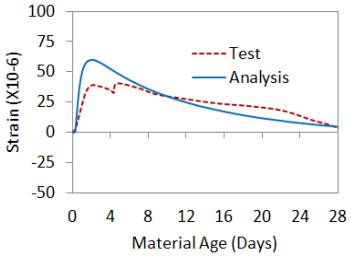

Fig.3.3 (i) Simulation of steel strain utilizing JCI-SAS3-2 FEM models

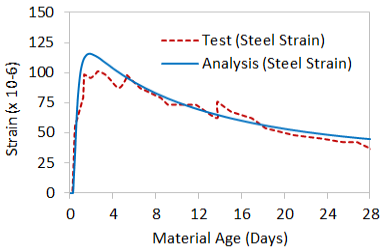

Fig.3.3 (j) Simulation of steel strain utilizing small size RC slab model

First, in the aforementioned FEM specimen models, the fundamental material property models calibrated for material inputs considering effective material age to take into account the temperature history of the corresponding concrete for adiabatic temperature rise, setting time, time dependent strength and Young's modulus development and free autogenous shrinkage acquired from the laboratory investigations in Level 1 were given inputs for structural stress analysis.

Moreover, some material parameters significant for structural stress analysis such as expansion strain parameters for the concrete including expansive additive and reduction factors for Young's modulus development to consider temperature dependent creep in concrete are calibrated utilizing the aforesaid three FEM models for member level specimens under different restrained conditions. Thus the FEM numerical simulation scheme was established for structural stress analysis and validated in member levels.

3.1.3 Level-3: Real Structural Level Simulation of RC Deck Girder Bridge Models

In Level-3, the real structural level FEM bridge models were established considering appropriate thermal and structural boundary conditions inputting material properties such as strength and Young's modulus development, setting time, free autogenous shrinkage and coefficient of thermal expansion acquired from the laboratory investigation results in Level 1.

Fig.3.3 (a) Multiple span steel girder Shinkesen Ohashi bridge

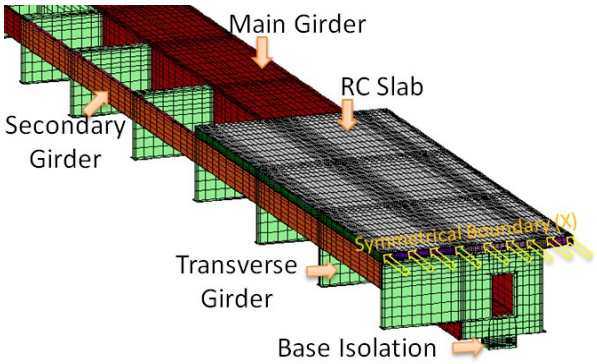

Fig.3.3 (b) Shinkesen Ohashi Bridge FEM model

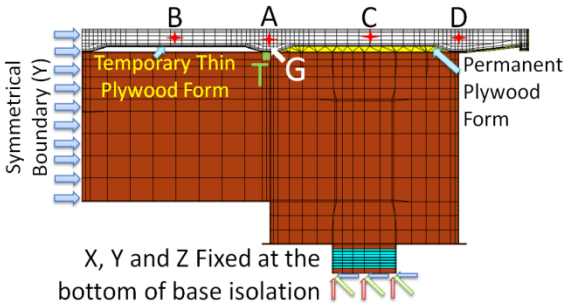

Fig.3.4(a) Locations of measurement in Shinkesen Ohashi bridge deck

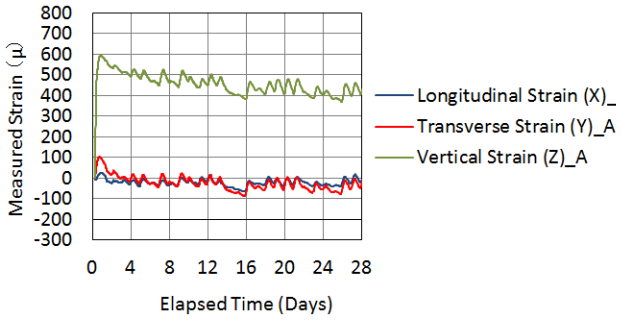

Fig.3.4(b) Longitudinal, transverse and vertical strains Shinkesen Ohashi RC slab at location A

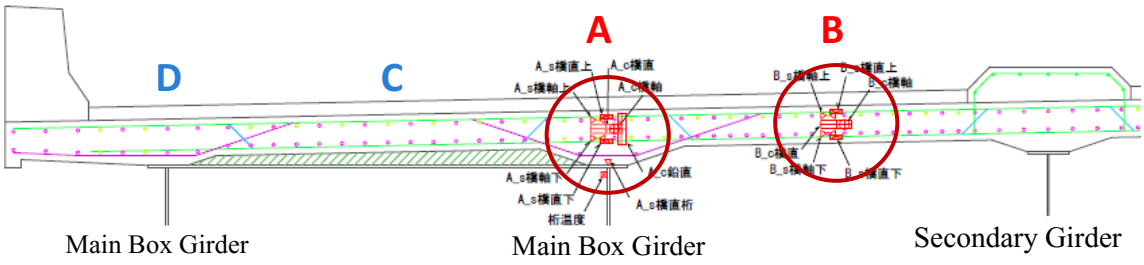

Fig.3.4(c) Locations of measurement (A: directly connected with main girder and B: in flexural part of RC slab) in the Shinkesen Ohashi Bridge deck RC slab

The expansion strain parameters for the concrete with expansive additive and the reduction factors for Young's modulus development to consider creep in concrete which were calibrated utilizing member level specimen FEM models in three different restrained conditions in Level 2 were given as inputs in the real structural level FEM bridge models.

The thermal behavior corresponding to concrete temperature in the RC deck slab concrete was calibrated following JCI2016 [1] adiabatic temperature rise model and the monitored temperature data in the real bridge slab in the site. Finally the three directional simulated thermal and volumetric strains (longitudinal strain along bridge axis (X), along transverse direction to the bridge axis (Y) and in vertical (thickness) direction to the bridge slab (Z)) in RC slab concrete were verified utilizing the recoded strains in the real bridge slabs (Fig.3.4 (b)). In real structural level verification of RC deck bridge models, three directional concrete strains which are considered to be under different restraint conditions were taken into account.

Since there was no steel reinforcement in vertical direction, restraints in vertical direction was negligible which can be the key measure for verification of chemical expansion and autogenous shrinkage under negligible restraints. Moreover, hardening point of concrete was also determined from the vertical strain history with respect to temperature rise due to the hydration heat generation of concrete.

In reverse, transverse strain in RC slab is governed by the transverse reinforcement, non-uniform shape of the RC slab, the stay-in-place (SIP) plywood forms and the supporting girders. Therefore, some modeling assumptions such as modeling of SIP plywood forms were conveniently verified utilizing monitored transverse strain data (Fig. 3.4 (a),(b) and (c)).

Most importantly, measured longitudinal strain in RC slab was observed under the highest external restraints due to the continuous composite connections of the main girders and RC slab at location A and flexural part of RC slab at location B. It should be noted that the development of tensile stress due to the external restraint against volumetric changes of concrete along the longitudinal direction is the key factor for generation of transverse cracks in RC deck slab. This is why; recorded longitudinal strains were efficiently utilized to validate the model corresponding to the restrained longitudinal strain along bridge axis at locations A and B (Fig. 3.4 (a),(b) and (c)).

3.1.4 Parametric Studies

The validated real structural level models for Shinkesen Ohashi multi-span steel girder bridge and Hikohei Single span PC composite girder bridges were successfully utilized in extensive parametric studies to determine the influential factors related to external stress and internal stress in early age.

(1) Influential Factors Related to External Stress

Influential factors corresponding to external stress due to the external restraint conditions were identified by the comparative analytical studies based on multiple span continuous steel girder Shinkesen Ohashi Bridge FEM model and single span simply supported Hikohei Bridge FEM models.

(2) Influential Factors Related to Internal Stress

Influential factors related to internal stress (volume changes due to the non-uniform expansion and contraction of concrete) such as initial temperature of concrete, ambient temperature, winter and summer seasons, coefficient of thermal expansion (CTE), effect of cement types, effect of pozzolanic admixtures, support condition, effect of autogenous shrinkage etc. in RC slabs were confirmed from parametric studies done utilizing the both types of real structural level FEM bridge models.

3.1.5 Proposing Performance Base Strategies to Minimize the Transverse Cracking of RC Bridge Deck

The final goal of the present research is to establish performance strategies for future guidelines for mitigating thermal and shrinkage cracks in RC slab deck girder bridges base on the extensive parametric utilizing the established FEM models for RC deck girder bridges as well as the knowledge obtained from corresponding structural monitoring.

3.2 FEM MODELING FOR THERMAL STRESS ANALYSIS OF REAL STRUCTURES

Temperature stress generated during the construction process of concrete structures has been required to be extremely accurate with remarkable advancement in FEM analysis techniques based on long history of research results from the early 1980s. It became apparent that it is extremely difficult to prevent thermal cracking by merely taking measures at the construction stage, depending on materials used and design. The current calculation methods for temperature and stresses to control cracking in mass concrete in JSCE and JCI guidelines were supported by the numerous laboratory and field investigation results and solutions from numerical the analyses contributing to the improvement of the quality of concrete structures. As described above, in the problem of control of the temperature stress of concrete, it is recognized that the progress and dissemination of numerical analysis technology have made a major contribution. In the present study, FEM analysis tool JCMAC3 has been utilized for realistic evaluation of thermal and volumetric stresses in RC deck slab with the aim of reflecting the analysis results in the specifications and guidelines.

3.2.1 Finite Element Modelling Utilizing JCMAC3[1]

In the present research, a series of material, member and structural level numerical simulations have been conducted to simulate the early age restraint expansion and shrinkage of concrete applied in Shinkesen Ohashi Bridge RC slab and Hikohei Bridge RC slab utilizing commercial finite element software (JCMAC3) designed for thermal and structural stress analysis of concrete structures incorporating JCI Guidelines for Control of Cracking of Mass Concrete (2008/2016), 'Standard Specifications for Design of Concrete Structures', JSCE (2007/2012), and AIJ guidelines [2-6]. The thermal analysis is followed by the structural stress analysis. Three dimensional linear hexahedral isoparametric heat generating and non-heat generating solid elements were considered for material models. Two dimensional heat elements were pasted upon

the heat transfer surfaces of the 3D solid material models to apply heat transfer boundary conditions. Moreover, reinforcing bars were modelled with one dimensional truss elements [1].

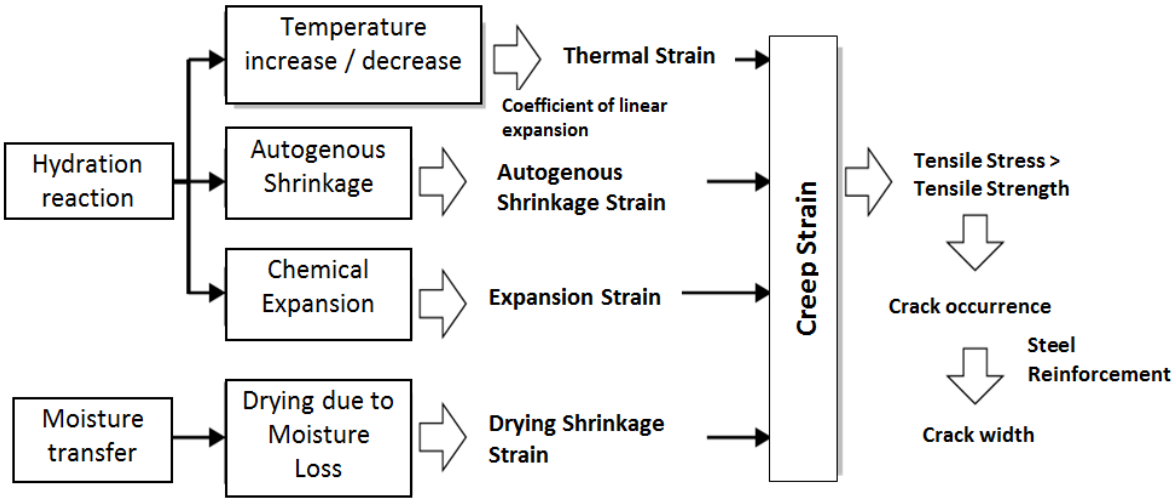

Fig.3.5 Flow of crack generation due to restrained volume changes [1]

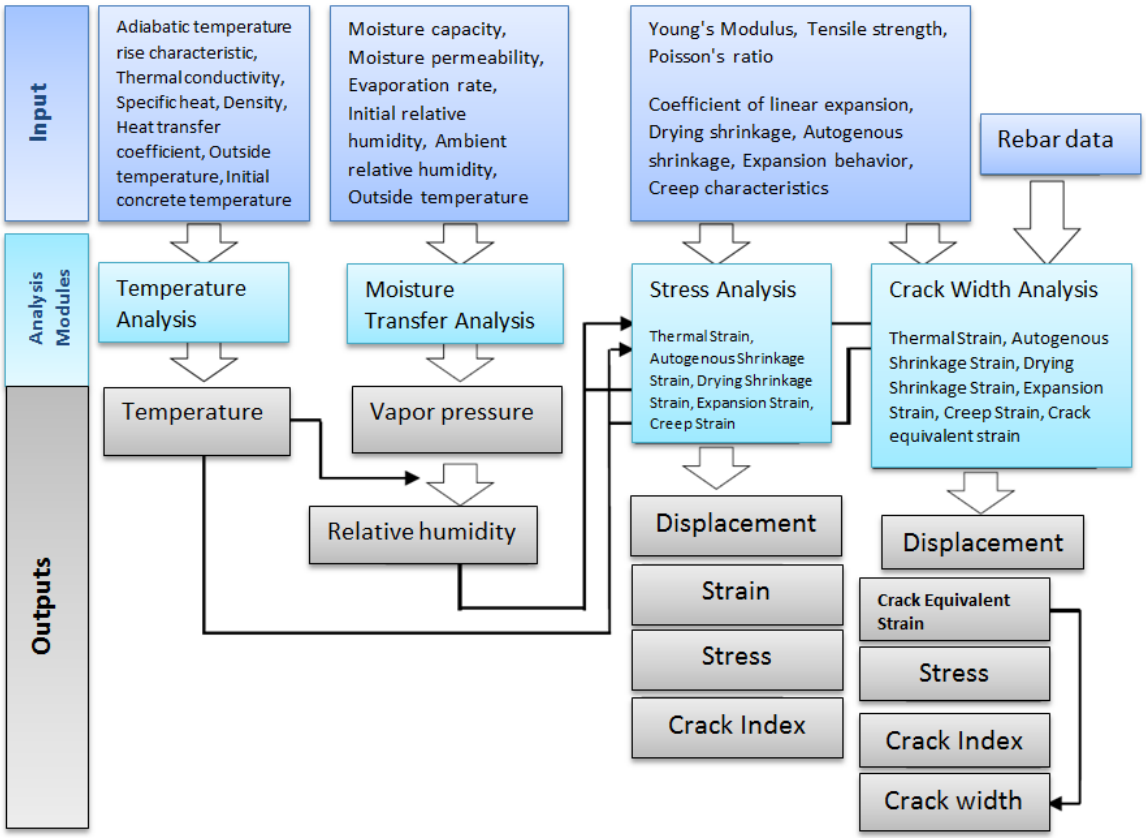

Fig.3.6 Temperature Analysis, Moisture Transfer Analysis, Stress Analysis and Crack Width Analysis Modules in JCMAC3 [1]

Figure 3.6 shows the flow of crack generation due to restrained volume changes due to temperature, autogenous shrinkage, drying shrinkage in reinforced concrete. Since, the volume change illustrated in Fig.3.5 occurs at the initial stage of concrete placement, JCMAC 3 analyse stress caused by initial strain (temperature changes /autogenous shrinkage / drying shrinkage/expansion strain) occurring in concrete from the time of construction to the time of use where strains are comprehensively analysed as shown in Fig.3.6.

3.2.2 Analysis Modules in JCMAC3[1]

JCMAC 3 is consists of four analysis modules such as temperature module, moisture transfer module, stress module (sequential linear elastic analysis) and a crack analysis module that considers stress release accompanying occurrence of cracks. As initial stresses, it is possible to analyse temperature, drying shrinkage, autogenous shrinkage, chemical expansion and contraction of expanding materials and so on singularly and complexly, respectively.

(1) Temperature Analysis Module

(a) Adiabatic Temperature Rise Model [1]

In temperature analysis module, JCMAC3 corresponds to the adiabatic temperature rise behaviour as below

$$Q(t) = Q_{\infty}\left(1 - e^{-rt}\right) \qquad \text{(Conventional Equation)} \qquad \text{Eq.3.1}$$

$$Q(t) = Q_{\infty}\left[1 - \exp\left\{-r\left(t - t_{0,Q}\right)^{s}\right\}\right] \quad \text{(Time dependent equation)} \qquad \text{Eq.3.2}$$

Where, s : Coefficient concerning adiabatic temperature rise rate when low heat generation type cement is used

If、 $t_{0,Q}$=0, s=1 , the above equation becomes a general adiabatic temperature rise formula.

$$Q(t) = Q_{\infty}\left[1 - \exp\left\{-r \cdot t\right\}\right]$$

In general, since it is calculated by time (hour) instead of day (day), if the above expression is expressed by (hour), the equations becomes as follows.

$$Q(t') = Q_{\infty}\left[1 - \exp\left\{-r\left(\frac{t'}{24} - \frac{t'_{0,Q}}{24}\right)^{s}\right\}\right] \qquad \text{Eq.3.3}$$

$$Q(t') = Q_{\infty}\left[1 - \exp\left\{-\frac{r}{24}t'\right\}\right] \qquad \text{Eq.3.4}$$

Therefore, the amount of temperature increase per unit time,

$$\frac{dQ(t')}{dt'} = \frac{Q_\infty rs}{24} \cdot \left(\frac{t'}{24} - \frac{t'_{0,Q}}{24} \right)^{s-1} \cdot \exp\left\{ -r \left(\frac{t'}{24} - \frac{t'_{0,Q}}{24} \right)^{s} \right\} \qquad \text{Eq.3.5}$$

$$\frac{dQ(t')}{dt'} = \frac{Q_\infty r}{24} \cdot \exp\left\{ -\frac{r}{24} t' \right\} \qquad \text{Eq.3.6}$$

By multiplying the above equation by the heat capacity (ρc), the amount of heat generated per unit time and unit volume is finally calculated.

(b) Effective Material Age [1]

In JCMAC3 effective material age is considered in the thermal and stress analysis considering the effect of temperature history of the material as below

$$t_e = \sum_{i=1}^{n} \left\{ \Delta t_i \cdot \exp\left[13.65 - \frac{4000}{273 + T(\Delta t_i)/T_0} \right] \right\} \qquad \text{Eq.3.7}$$

Where, t_e : Effective material age (day) considering the influence of temperature history

Δt_i : Period of constant temperature continuing in concrete (day)

$T(\Delta t_i)$: Concrete temperature for Δt_i ℃)

T_0 : It is a value that makes temperature non-dimensional (1℃)

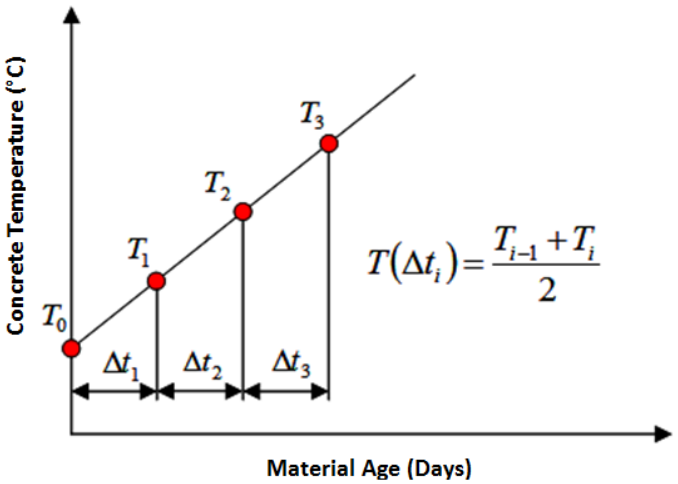

Fig.3.8 Temperature of an element in the step calculated by the average temperature between steps [1]

Calculation of Effective Material Age in JCMAC 3

Effective age should be determined for each element. Temperature is changing between the steps, hence temperature of an element in the step should be calculated by taking the average temperature between steps. Effective material ages are calculated based on the time between steps.

(2) Moisture Transfer Analysis Module [1]

JCMAC3 can calculate the humidity distribution of the concrete by moisture transfer analysis besides the temperature distribution of concrete by temperature analysis. Moisture migration analysis is not necessary when drying shrinkage is not taken into consideration, but moisture transfer analysis is required because humidity distribution inside the member is required when considering drying shrinkage. JCI-TC 911 and CEB formula can be used to calculate drying shrinkage strain from relative humidity.

(3) Stress Analysis Module[1]

In stress analysis modules JCMAC3 analyse initial stress due to temperature and humidity change. It is a linear elastic analysis (sequential elasticity analysis) that does not take cracks into consideration and is used for determining stress and crack index.

(a) Strength Development

In JCMAC3 time dependent strength development of concrete such as compressive strength, tensile strength and Young's modulus is based on effective material age considering temperature history of concrete.

(b) Autogenous Shrinkage Strain

Considerable autogenous shrinkage strain of concrete is a problem with relatively high-strength concrete with a smaller water binder ratio. In past studies it has been pointed out that autogenous shrinkage is affected by cement and admixture type, water binder ratio, unit coarse aggregate quantity. Again, autogenous shrinkage strain of concrete subjected to high temperature history has the tendency to increase has been recognized. In the guidelines and others, empirical formulas based on a number of experiments are used for determining autogenous shrinkage strain, and empirical formulas are proposed according to the type of cement used, the water cement ratio, temperature history, and the like. For stress analysis by JCMAC3, it is possible to consider autogenous shrinkage by entering these conditions.

(c) Expansion Strain

Expansive additives are utilized in concrete as a crack prevention countermeasure. Since the behaviour of the expanding material using the expansive additives is affected by the type and amount of the expansive additive to be used, the formulation and arrangement of the concrete, the shape and constraint of the member, the construction conditions such as curing, it is difficult to quantitatively evaluate the expansion behaviour accurately. In JCI Guidelines for Control of Cracking of Mass Concrete 2016 an approximate expression for calculating the expansion strain when a standard expanding material with a usage amount of 20 kg /m3 is used and JCMAC3 corresponds to this empirical formula. When using this empirical formula, it is necessary to superimpose it on the autogenous shrinkage strain. Although it is possible to calculate the effect of the expansion material approximately, the effect of the restraint by the reinforcing bars upon the expansion cannot be considered. Also, this approximation formula cannot be used when it is different from the standard usage.

In this context, JCMAC3 has adopted an analytical method that can take into consideration the restraints by reinforcing bars or others by the constant total energy law [7] that extended the idea of the law of constant work. The expansion strain energy is obtained from the Eq.3.8 as follows.

$$U(t_e) = U_\infty \,.\, (1\text{-}exp\ (-a\ (t_e\text{-}t_o)^b\ ) \qquad \text{Eq.3.8}$$

Where, $U(t_e)$=total energy at effective concrete age te, U_∞=ultimate value of the total energy, a and b= coefficient indicating the influence of the type of cement on the progressive characteristics of total energy, t_o=effective material age at the beginning of expansion.

(d) Calculation of creep strain by Rate Type Theory

If a continuous load is applied to the concrete, even if the stress is constant, the strain increases with the lapse of time. This is called creep strain. Creep strain has a great influence on the accuracy of stress analysis. The ratio of creep strain and elastic strain is called the creep coefficient, and the creep coefficient of sufficiently hardened concrete is about 1 to 2, but it may be 10 or more at less than 1 day of age. Effective elastic modulus method is used as a simple method to consider the influence of creep in Standard Specifications for Design of Concrete Structures, JSCE, 2007[4] where, the influence of creep is taken into consideration up to 3 days of age. Hence, the calculation of compressive stress in the temperature rising region becomes small, the influence of creep is excluded after 5 days of age, and the tensile stress in the temperature falling region is overestimated. For example, specifically, up to 3 days of age the Young's modulus is multiplied by 0.73 and after the 5th day of age the Young's modulus is multiplied by 1.0. Again from the 3rd to 5th day of age the reduction factor is calculated by linear interpolation. Reversely, in JCI Guidelines for Control of Cracking of Mass Concrete, Tokyo, 2016 [3], the effective Young's modulus is calculated by multiplying the Young's modulus by a coefficient of 0.42 at the temperature increasing and 0.65 at the temperature decreasing period, based on the consistency with the reinforcing bar stress acquired in experimental investigations. Although the effective elastic modulus is a simple calculation method, it does not take into consideration the stress history received by the concrete. Therefore, the creep model considering the stress history in JCMAC3 is as follows.

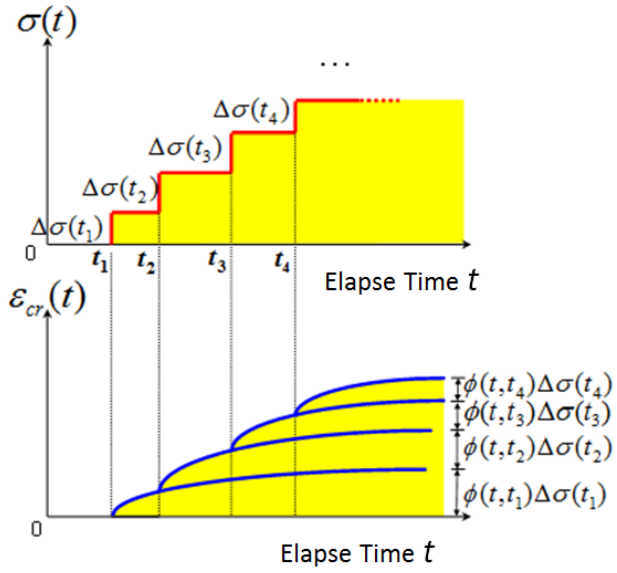

Fig.3.9 Creep strain when the working stress changes

In the case where the working stress varies under uniaxial stress, as shown in Fig. 3.9, it is considered that the stress history is constituted by a set of constant stress $\Delta\sigma(t_i)$ having different loading time t_i for each section. At this time, the creep strain is expressed as the sum of the creep strains generated under the constant stress $\Delta\sigma(t_i)$ as shown in the Eq.3.9.

$$\varepsilon_{cr}(t)=\sum\phi(t,t_i)\Delta\sigma(t_i) \qquad \text{Eq.3.9}$$

Here,: creep strain at age t, creep function, called creep function, is the creep strain at elapsed time t when = 1 acts. Generally, creep strain is expressed by equation (2) instead of equation (1).

Here, $\varepsilon_{cr}(t)$: creep strain at age *t*, $\phi(t,t_i)$: creep function、$\sigma(t_i)$=1 when creep strain at elapsed time t. Generally, creep strain is expressed by Eq.3.10 instead of Eq.3.9.

$$\varepsilon_{cr}(t)=\int_0^t\phi(t,\tau)d\sigma(\tau) \qquad \text{Eq.3.10}$$

It is difficult to solve the solution of Eq.3.10 analytically with respect to an arbitrary stress history. Therefore, Eq.3.10 will be solved approximately; the representative method is Step by Step method [8] and Rate type theory [9-10].

The Step by Step method can reflect arbitrary Creep functions directly in the calculation program, and creep strain in the multiaxial stress state. The disadvantage of step by step method is that it is necessary to memorize the history at all the time steps. In JCAMC3, it is different from the step by Step method, it is adopting the Rate type theory method that can calculate creep strain only from the history of the previous step, not all steps and calculates creep strain in incremental form.

(4) Crack Width Analysis Module

In crack width analysis module, nonlinear analysis is performed where cracks are expressed by releasing the stress of the concrete element exceeding the tensile strength based on the dispersed crack model applying crack equivalent strain corresponding to the fracture energy to the concrete element.

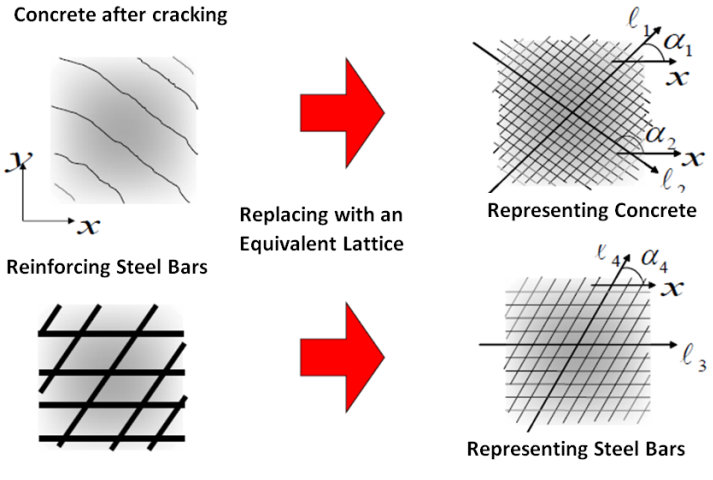

Fig.3.7 Concept of Orthotropic Model in JCMAC3 crack width analysis module [1]

In crack prevention measures of concrete structures, in consideration of required functions and durability, structural cracks are not allowed at all , There are countermeasures such as limiting the width of the crack to less than or equal to the limit value and allowing the occurrence of cracks. In JCMAC 3, it is possible to analyse the crack width by 3D FEM. In this analysis, concrete structure is treated as a continuum before crack occurred, but after cracking it is treated as an orthotropic model as shown in Figure 3 as a distributed crack model (Smeared Crack Model). Although the reinforcing steel bars are model by one dimensional truss element and entered one by one for each place, in the analysis, the element is considered as the RC element containing one dimensional truss element as rebar. And the effect of the rebar is taken into consideration in the form of the reinforcement ratio. This simplifies the description of the constitutional rule for easy convergence. The distribution cracked model, unlike the discrete crack model, can handle reinforced concrete as a continuous body even after cracking, and it is not necessary to set the crack generation position in advance, and the crack is expressed as "crack equivalent strain".

Moreover, in JCMAC-U, the load carrying capacity analysis module is incorporated. Therefore, in JCMAC 3-U, it is possible to evaluate the load carrying capacity of reinforced concrete members under the condition that the initial stress has been analysed and outputted by JCMAC 3.

References

[1] Japan Concrete Institute, JCMAC3 technical document on the computer program of thermal stress analysis for massive concrete structures, 2013.5.

[2] Japan Concrete Institute, JCI Guidelines for Control of Cracking of Mass Concrete, Tokyo, 2008.

[3] Japan Concrete Institute, JCI Guidelines for Control of Cracking of Mass Concrete, Tokyo, 2016.

[4] Japan Society of Civil Engineering, Standard Specifications for Design of Concrete Structures, JSCE, 2007.

[5] Japan Society of Civil Engineering, JSCE Standard Specifications for Concrete Structures, 2012.

[6] Architectural Institute of Japan: Recommendations for Practice of Crack Control in Reinforced Concrete Buildings (Design and Construction), pp.39-45, February 2006 (in Japanese).

[7] T. Tanabe and Y. Ishikawa, "Chemical Expansion Effect in Concrete and its Numerical Simulation Based on the Mechanical Energy Conservation Hypothesis," in JCI-RILEM International Workshop on Control of Mass Concrete and Related Issues Early Age Cracking of Structures (CONCRACK), Tokyo, 2017.

[8] Bazant, Z. P. and Wittman, F. H. : Creep and shrinkage in concrete structures, John Wiley & Sons Ltd., 1982

[9] 田辺忠顕：初期応力を考慮した RC 構造物の非線形解析法とプログラム，技報堂出版株式会社，pp.57～63, 2004.3

[10] Bazant, Z. P. & Panula, L., : Practical prediction of time-dependent deformations of concrete, Part II: basic creep, Material and Structures, Vol.11, pp.317-328, 1978

4

NUMERICAL MODELING AND SIMULATION OF THERMAL STRESSES IN RC BRIDGE DECK SLABS

4.1 INTRODUCTION

Application of multiple protection counter measures for highly durable concrete for deck slab was proved effective without any signs of early age thermal and shrinkage cracks in case of several short span bridges such as single span steel girder Mukai-sada-nai Bridge (length=45 m) and single span PC composite girder Hikohei Bridge. However, transverse early age cracks (crack width=0.2 mm) were occurred in different segments of the RC deck slab of the multiple span box girder Shinkesen Ohashi Bridge and Kosano viaduct. In general, it is assumed that the potentials for the early age transverse cracks in RC deck slab are increased in case of multiple span steel girder bridges due to its higher structural restraints against volumetric changes and tensile stresses in hardened slab due to stepping constructions. Therefore, it is important to define the influential factors for the occurrence of such early age cracks in RC deck slabs especially for multiple span deck girder bridges to prevent deterioration. In this context, the focuses of the current chapter is to evaluate the cracking risk of RC slabs of multiple span steel girder bridges by establishing accurate finite element models following systematic analytical scheme for simulating thermal stress in the restrained slab. First, laboratory investigations were conducted to measure free autogenous shrinkage, chemical expansion and compressive strength development for the regarding concrete. The obtained material property models were utilized in member level numerical models to simulate volume changes which were successfully verified by experimental results. Some important input parameters such as autogenous shrinkage, chemical expansion energy and creep coefficients were calibrated through this verification process. Second, a numerical model has been developed for 'Shinkesen Ohashi' RC slab with restraining steel girders confirming rational thermal and structural boundary conditions. The time dependent thermal behavior of the RC slab was satisfactorily verified with the monitored slab and girder temperature. Thermal analysis was followed by time dependent stress analysis where calibrated material properties were given as inputs. The analytically obtained concrete and steel strain for RC slab shows sufficiently good agreement with the measured data. The maximum tensile stress generated due to the volume changes in the RC slab obtained from the analysis indicates the possibility of the occurrence of early age cracks in some locations of the slab where the initially accumulated tensile stress due to the stepping construction of slab was comparatively large. The similar procedure is followed in simulating RC slabs on Kosano viaduct and consequently verified in terms of measured concrete temperature, strain and stress, thus verifying the established three levelled systematic FEM simulation procedure. It is to be noted that the highly durable concrete was also applied in RC deck slab construction of single span PC composite girder Hikohei post tensioned bridge where no cracks were generated. In this respect Chapter 4 also includes the numerical simulation of single span Hikohei bridge FEM model to confirm the thermal and volumetric changes in Hikohei bridge RC slab following the established systematic

FEM simulation scheme. The followed FEM numerical analysis approach has accurately simulated the early age volume changes of Hikohei bridge slab proving the low cracking risk of RC deck slab for single span PC composite girder bridges. The established three leveled systematic analysis scheme in the present research is intensively discussed in the following sections for Shinkesen Ohashi Bridge, Kosano viaduct and Hikohei Bridge FEM Models.

4.2 ESTABLISHING SYSTEMATIC FEM MODELING APPROACH FOR MULTIPLE SPAN STEEL GIRDER RC DECK BRIDGE (SHINKESEN OHASHI BRIDGE)

4.2.1 Construction of Shinkesen Ohashi Bridge

The new cross linking site of 438 m long Shinkesen Ohashi deck girder bridge along "Revival Road" in Tohoku is about 3 km from the estuary of the mountainous Kesengawa River in Iwate Prefecture. The height of the bridge is around 30 m from the ground surface [3] (Fig.4.1 to Fig.4.4). The bridge is highly susceptible to severe deterioration such as freezing and thawing, chloride attack and alkali silica reaction caused by deicing salt. Considering the severity of the conditions, a new initiative has been undertaken to secure highly durable bridge deck construction of Shinkesen Ohashi bridge ensuring multiple countermeasures against deterioration.

The application of blast furnace slag cement with low water-binder ratio was the key counter measure against frost damage, salt damage and ASR resistance. Expansive additive was applied to prevent cracks by compensating autogenous and drying shrinkage. Also limestone aggregate was used which could reduce drying shrinkage for its low shrinkage properties. Air content was set as 6% to achieve anti-frost performance. Seven days sealed curing was followed by 22 days wet curing applying three layers of special curing mats to control thermal changes and prevent evaporation. Moreover, epoxy coated reinforcing bars were applied for the protection against corrosion [1].

4.2.2 Scenario of Cracks in Shinkesen Ohashi Bridge

The concrete placement of Shinkesen Ohashi bridge slab was completed between 3rd June to 1st July in 2016 adopting special construction and curing methods such as appropriate concrete placement steps considering setting time of concrete and 7 days sealed curing followed by 22 days wet curing applying three layers of special curing mats to control thermal changes and prevent evaporation. Stepwise concrete placement was adopted in the construction of the RC slab segmented into thirteen placement lots to minimize the structural stresses.

However, minor transvers cracks were observed in Lot 1, Lot 2, Lot 3, Lot 8 and Lot 11 after removing the curing sheets (Fig.4.5 to Fig.4.7). The maximum crack width was 0.08mm in Lot 1 at the time of investigation in October 2016. Fig.4.8(b) and (c) shows the tensile strength of each lot at the day of Lot 13 concrete placement and reveals that the cumulative tensile stress in concrete is comparatively large in Lot 1, Lot 2 and Lot 3 due to the stepping construction. Initially, primary cracks were seemed to be generated in the concrete placed upon the permanent plywood forms and propagated towards the central axis of the slab (Fig.4.8(a),(b) and (c)). Effloresce observed in the bottom surface of the slab confirmed that some cracks were penetrating. Previous researches have revealed that autogenous shrinkage strain is relatively large while initial strength development rate is low for blast furnace slag cement[2]. Furthermore,

autogenous shrinkage can be even larger at high temperature caused by hydration heat of cement which can inhibit thermal and shrinkage cracks.

Fig.4.1(a) Shinkesen Ohashi bridge.

Fig.4.1(b) Continuous box girders and rubber shoe

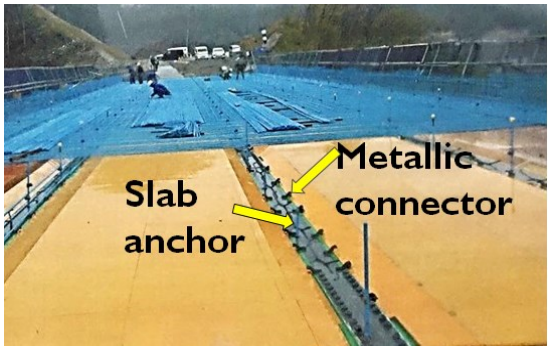

Fig.4.2(a) Temporary and permanent plywood forms and slab anchors

Fig.4.2(b) Slab anchors and mechanical connectors.

Fig.4.3(a) Epoxy coated reinforcement steel bars

Fig.4.3(b) Placement of durable concrete

Fig.4.4(a) Three layered special curing mats

Fig.4.4(b) Continued wet curing under curing mats

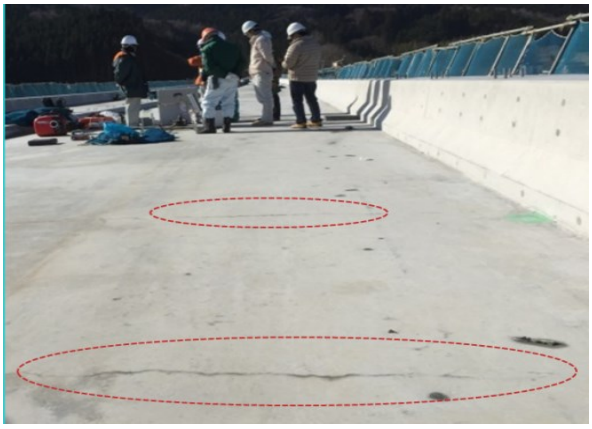

Fig.4.5(a) Minor transverse cracks observed after removal of curing sheet in Lot 1

Fig.4.5(b) Top surface crack width measured in Lot 1 (Crack 39)[4]

Fig.4.5(c) Bottom surface crack in Lot 1 (Crack 5) showing effloresence[4]

Fig.4.5(d) Bottom surface crack in Lot 1 (Crack 22) showing effloresence[4]

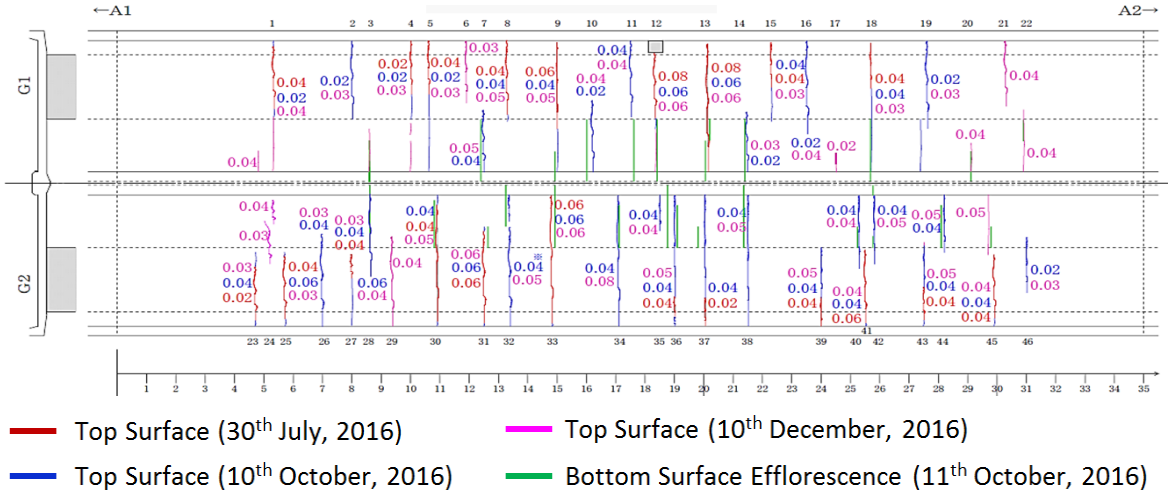

Fig.4.5 (e) Distribution of cracks in concrete placement Lot 1 according to the date of observation[4]

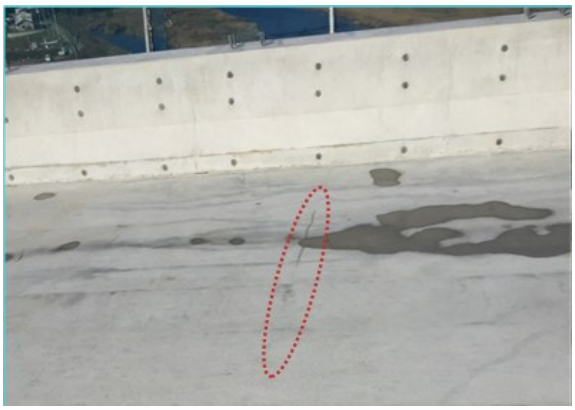

Fig.4.6(a) Minor transverse cracks observed after removal of curing sheet in Lot 2

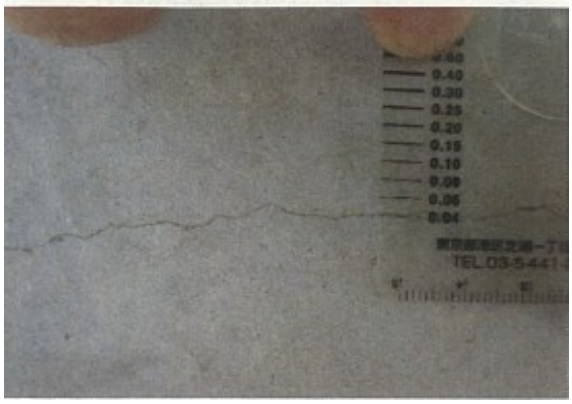

Fig.4.6(b) Top surface crack width measured in Lot 2 (Crack 4)[4]

Top Surface Crack 18

Fig.4.6(c) Top surface crack width measured in Lot 2 (Crack 18)[4]

Bottom Surface Efflorescence Crack 4

Fig.4.5(d) Bottom surface crack in Lot 2 (Crack 4) showing effloresence[4]

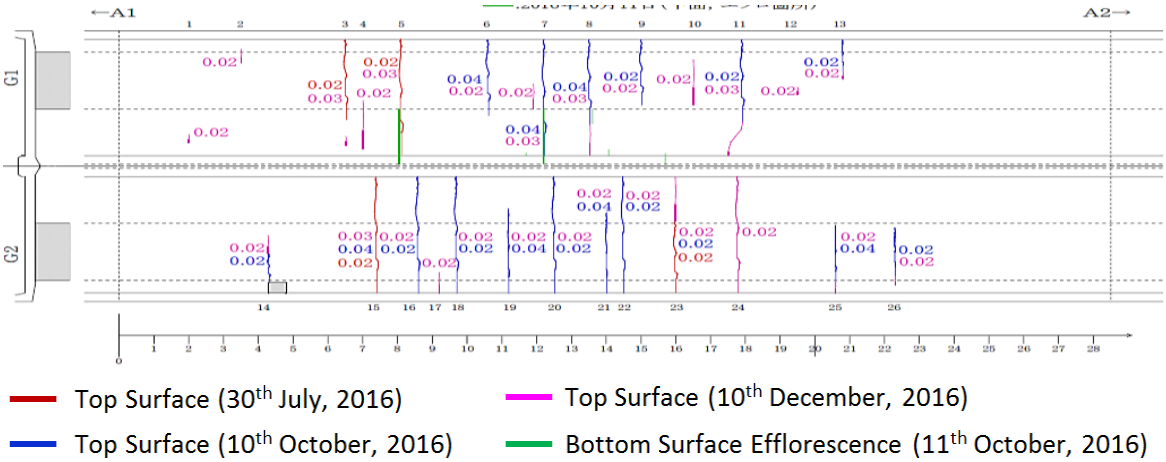

Fig.4.6 (e) Distribution of cracks in concrete placement Lot 2 according to the date of observation[4]

Fig.4.7(a) Minor transverse cracks observed after removal of curing sheet in Lot 3

Fig.4.7(b) Minor transverse cracks observed after removal of curing sheet in Lot 11

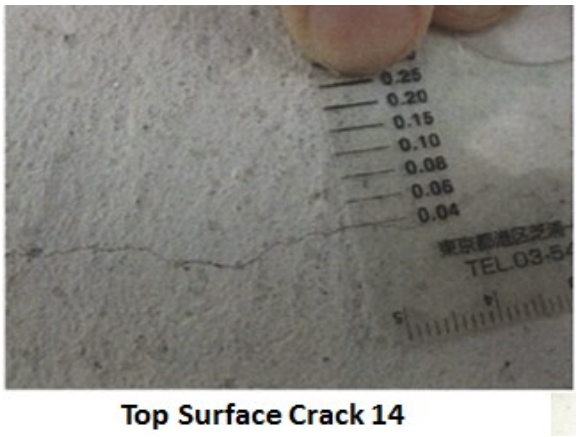

Fig.4.7(c) Top surface crack width measured in Lot 3 (Crack 14) [4]

Fig.4.7(d) Bottom surface crack in Lot 3 (Crack 14) showing effloresence[4]

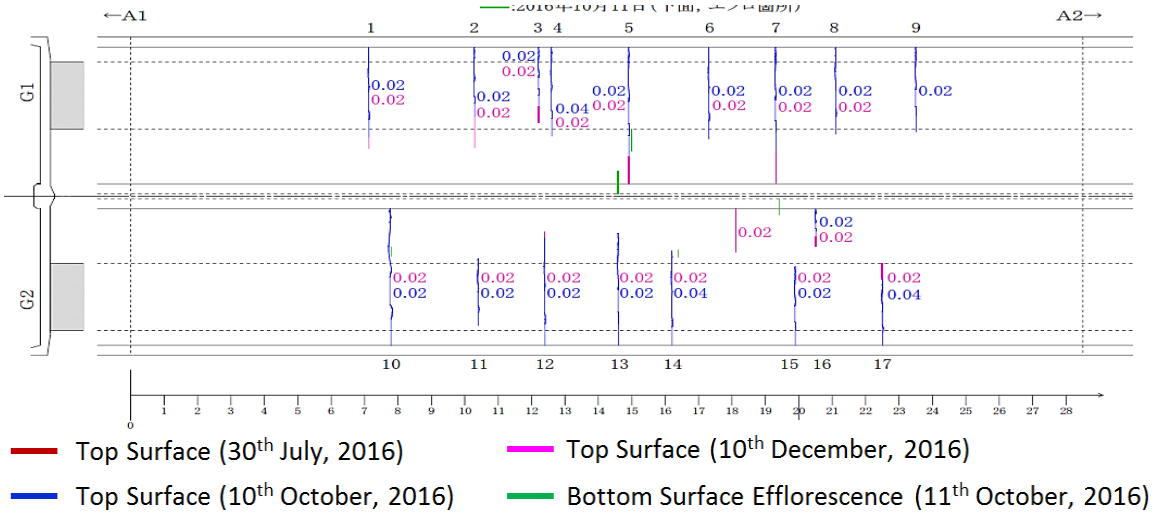

Fig.4.7 (e) Distribution of cracks in concrete placement Lot 3 according to the date of observation[4]

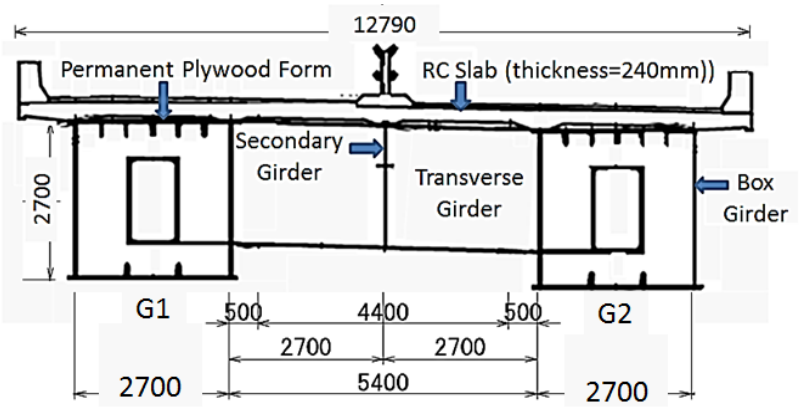

Fig.4.8 (a) Cross section of Shinkesen Ohashi deck girder bridge

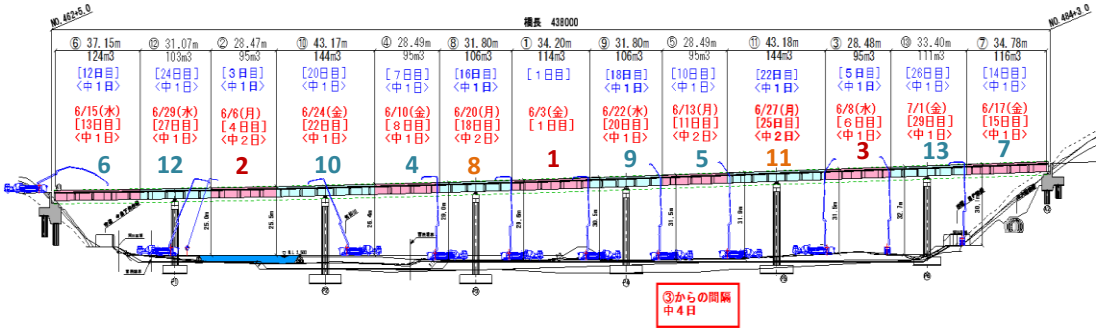

Fig. 4.8 (b) Sequence of stepping construction from Lo1 to Lot 13[4]

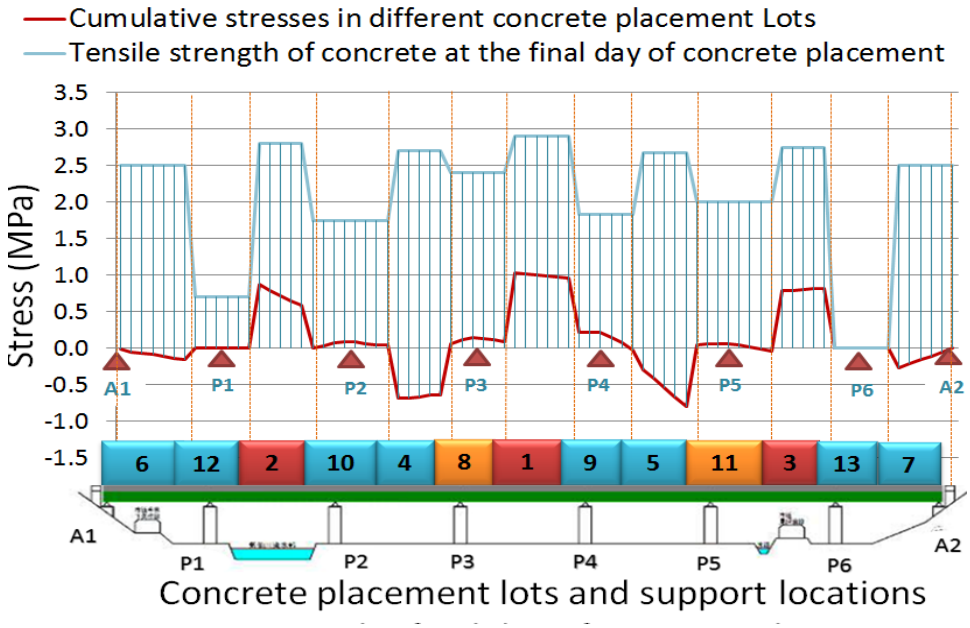

Fig.4.8 (c) Cumulative structural stress and tensile strength along different lots at the day of final concrete placement for Lot-13 (1st July, 2016) [4].

Recent investigations on crack propagation of Shinkesen RC slab have revealed that new cracks have been generated in several lots i.e. Lot 1, Lot 2, Lot 3, Lot 4, Lot 5, Lot 6 and Lot 13. Moreover, crack widths have been increased up to 0.20 mm exceeding the allowable limit (0.0035c where c is cover thickness) in highly corrosive area [6] like Tohoku region.

In this context, the present study aims at evaluating the significant influential factors for cracking of RC slab concrete by simulating volumetric changes and thermal stresses in Shinkesen Ohashi bridge deck slab FEM model utilizing material properties obtained from laboratory investigation. Laboratory investigations are conducted to determine the free autogenous shrinkage and restrained expansion along with setting time and time dependent compressive strength development for the same concrete mix applied in Shinkesen Ohashi bridge slab. The experimentally obtained properties are utilized as the input in the FEM systematic simulation procedure and the simulation results are verified in member levels for applications in real structural level simulating restrained volume changes in the Shinkesen Ohashi RC slabs to predict the risk of cracking. Sequentially, Shinkesen Ohashi RC slab FEM model is further validated with the data recorded in the RC slab of the Shinkesen Ohashi Bridge in real structural level. Eventually, the influential factors causing transverse cracking in RC slab on multiple span continuous steel girder bridges have been revealed through this established systematic FEM simulation procedure.

4.2.3 Level 1: Material Level Experimental Investigation and Modeling of Fundamental Properties of Shinkesen RC Slab Concrete

In level 1, laboratory investigations were performed to measure time dependent early age development of compressive strength, Young's modulus and free autogenous shrinkage without expansive additive. All the tests were performed separately under 20°C and 40°C constant room temperature to confirm the effect of temperature on the properties of the concrete.

Table 4.1 Concrete mix proportion

W/B %	s/a %	Air %	Unit Weight (kg/m^3)								
			W	C	Ex	S1	S2	G1	G2	Ad	AE
44.0	37.8	6	160	344	20	334	328	558	554	2.18	0.10

Table 4.2 Specimen descriptions

Specimen Designation	Number of Specimens				Initial Concrete Temp (°C)	Slump (cm)	Air (%)
	f'_c	E	Setting Time	Autogenous Shrinkage			
Lot-2015-20°C	3	-	1	2	19	12.5	5.9
Lot-2015-40°C	3	-	1	2	34	13.0	6.7
Lot-2016-20°C	3	-	1	2	19	12.0	5.7
Lot-2016- 40°C	3	-	1	2	34	10.5	5.8
Lot-2016-Expan*-20°C	3	3	1	-	20	12.0	5.2
Lot-2016-Expan-40°C	3	3	1	-	35	9.0	4.8

*Expan is used to indicate that expansive additive is applied in the corresponding specimens

(1) Concrete Materials and Mix Proportion

Concrete materials and mix proportion were same as Shinkesen Ohashi slab concrete where multiple protection durability design was applied. The type B blast furnace slag cement was utilized to mitigate ASR as well as to achieve anti-chloride performance securing water tightness. Water to binder ratio was set as 0.44 to achieve frost protection along with required strength development. Moreover, air entraining admixtures were used to keep the air content 6% to contribute in anti-frost performance. Expansive additive was added to compensate autogenous and drying shrinkage for suppressing cracks. Also limestone aggregates were used for total volume of coarse aggregate and for 50% of total volume of fine aggregate due to its low shrinkage properties. The detailed concrete mix design is summarized in Table 1 where, C= type B blast furnace slag cement, Ex= expansive additive, S1 = limestone crushed sand, S2 = land sand, G1 = coarse aggregate from crushed lime stone (Ryushin area), G2 = coarse aggregate from crushed lime stone (Waga area.), Ad = admixture for achieving workability and AE = air entraining Admixture. The grading of coarse aggregate satisfied the requirement of JIS A 5005, and the fine aggregates had an average fineness modulus of 2.73.

(2) Test Specimens

For the specimens, blast furnace slag cement was collected from two different production lots i.e., Lot-2015 and Lot-2016. Lot-2015 was previously used for JCI-SAS3-2 autogenous shrinkage test and small scale slab specimens[3] to confirm the restrained expansion and shrinkage for the designed concrete mix before the construction of the actual bridge. On the other hand, Lot-2016 was used in the construction of the actual bridge slab. Both Lot-2015 and Lot-2016 were used in the present laboratory investigations to evaluate their performances in 20°C and 40°C constant curing temperature. Test specimens are shown in Fig.4.9(a) and (b). Moreover, Table 4.2 demonstrates the test specimens with corresponding cement lot, curing temperature, use of expansive additive, initial concrete temperature, slump and percentage of air content. Details of the specimens are explained below.

Fig.4.9(a) Autogenous shrinkage specimens with embedded type strain gauge

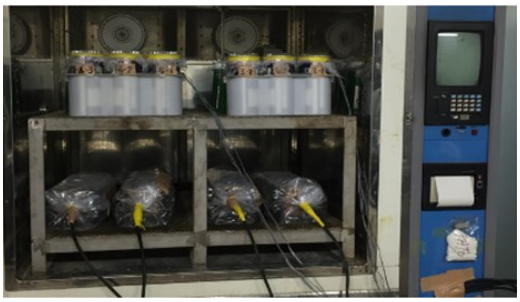

Fig.4.9(c) Specimens which are kept in 40°C curing temperature

(a) Compressive Strength and Young's Modulus

Cylindrical thin walled steel molds φ100×200mm were used for the time dependent compressive strength and Young's modulus development tests on 4th, 7th and 28th days from casting date (JIS A 1108). The specimens were water cured separately in 20°C and 40°C constant room temperature.

(b) Setting Time

Setting time tests were performed for all types of concrete mix i.e., with and without expansive additives both for 20°C and 40°C constant curing temperature according to JIS A 6204.

(c) Autogenous Shrinkage Strain

The free autogenous shrinkage specimens were cast in 100×100×400 mm steel molds. Autogenous shrinkage strain was measured by a low stiffness strain gauge embedded in the center of each specimen (Fig.4.9(a)). Sealed curing was applied for the specimens.

(3)Modeling of Fundamental Properties of Concrete according to the Experimental Results

(a) Compressive Strength, Tensile Strength and Young' modulus Development of Concrete

Test results of compressive strengths and Young's modulus are shown in Fig.4.10(a) and Fig.4.10(b) respectively. The compressive strength results represent the average value of three φ100×200mm concrete specimens of every kind. In addition, the compressive strength development result for 'Lot-2015-Expan-20°C' is taken from the reference[3] for comparison in Fig.5. On the other hand, Young's modulus development was measured only for Lot-2016-Expan-20°C and Lot-2016-Expan-40°C concrete. It is observed that the initial compressive strength and Young's modulus for the specimens cured under 40°C temperature were higher than those cured under 20°C. However, 20°C temperature cured specimens achieved the higher compressive strength and Young's modulus at the material age of 28 days. Moreover, compressive strength seems to be increased with the application of expansive additive.

The compressive strength development for the concrete mix Lot-2016-Expan-20°C shows good agreement with the JSCE2007[6] time dependent equations for development of compressive strength (Eq. 4.1(a)) whereas the corresponding Young's modulus development equation (Eq. 4.1(b)) underestimate the test results (Fig.4.10(a)(b)).

$$f_c'(t) = (t/(a+b.t)).d(i).f_{ck}' \qquad \text{Eq. 4.1(a)}$$

$$E_c(t) = 4700.(f_c'(t))^{0.5} \qquad \text{Eq. 4.1(b)}$$

Where, fc′(t) =time dependent compressive strength, f_{ck}'= concrete design standard strength, $E_c(t)$ = time dependent Young's modulus development, a=6.2, b=0.93 and d(i)=1.15 for i=28 days. The 28th days strength obtained from the laboratory investigations were given input for f_{ck}'.

However, JCI2016[7] compressive strength, tensile strength (Eq.3) and Young's modulus development equation can consider the temperature adjusted age of concrete, therefore, the parameters for JCI2016 compressive strength development equation were calibrated (Fig.4.10(b)) to utilize in the FEM simulation.

$$f_c'(t_e) = \frac{t_e - S_f}{a + b \cdot (t_e - S_f)} f_c'(t_n) \qquad \text{Eq. 4.1(c)}$$

Where,

t_e = Effective material age (day)

t_n : Strength control age of concrete cured under water at 20°C (day)

$f_c'(t_e)$: Compressive strength of concrete at t_e (N/mm^2)

a, b : Parameters that represent strength development, depending on type of cement and strength control age

a= 4.0 and b=0.9 calibrated for corresponding Lot-2016-Expan-20°C concrete

S_f : Temperature adjusted age corresponding to initiation of hardening, depending on type of cement (day)

$f'_c(t_n)$: Compressive strength of concrete at t_n (N/mm^2)

The splitting tensile strength of concrete can be determined by Eq. 4.1(d)

$$f_t(t_e) = C_1 \times f'_c(t_e)^{C_2} \qquad \text{Eq. 4.1(d)}$$

Where

$f_t(t_e)$: Splitting tensile strength of concrete at t_e (N/mm^2)

$f'_c(t_e)$: Compressive strength of concrete at t_e (N/mm^2)

C_1=0.13、C_2=0.85

(3) The modulus of elasticity (Young's modulus) of concrete can be determined by Eq. 4.1(e)

$$E_c(t_e) = C_3 \times f'_c(t_e)^{C_4} \qquad \text{Eq. 4.1(e)}$$

Where,

$E_c(t_e)$: Modulus of elasticity (Young's modulus) of concrete at t_e （N/mm2）

$f'_c(t_e)$: Compressive strength of concrete at t_e (N/mm^2)

C_3, C_4 : constants

C_3=6500, C_4=0.45 calibrated for Lot-2016-Expan-20°C concrete

The calibrated JCI2016 equation (Eq.4.1) (C3=6500, C4=0.45 calibrated for the Shinkesen RC slab) concrete is precisely calculate the Young's modulus development of the Lot-2016-Expan-20°C (Shinkesen RC slab concrete) as shown in Fig.4.10(b).

(b) Setting Time

Setting time results are summarized in Table 4.3 and illustrated in Fig.4.11 which reveals that the specimens cured under 40°C room temperature have hardened and gained strength faster than those specimens cured under 20°C room temperature. Setting time tests (JIS A 6204) for specimens cured at 20°C temperature confirmed initial and final setting time as 0.26 and 0.39 day respectively. Moreover, initial and final setting time for specimens cured at 40°C temperature was 0.12 and 0.16 day respectively. Therefore, the origin of strength and Young's modulus development, autogenous shrinkage and chemical expansion in the simulation was defined as the initial setting time experimentally obtained corresponding to 20°C and 40°C curing temperature. Measurement data and simulation results for strain were compared from the initial setting time corresponding to concrete temperature ignoring the unpredictable thermal expansion before hardening of concrete.

Table 4.3 Specimen descriptions

Setting time (hr-min)	Lot-2015 20°C	Lot-2016 20°C	Lot-2016-Expan 20°C	Lot-2015 40°C	Lot-2016 40°C	Lot-2016-Expan 40°C
Initial	7-00	6-05	6-10	3-10	2-45	2-55
Final	10-25	8-50	9-15	4-30	3-50	4-00

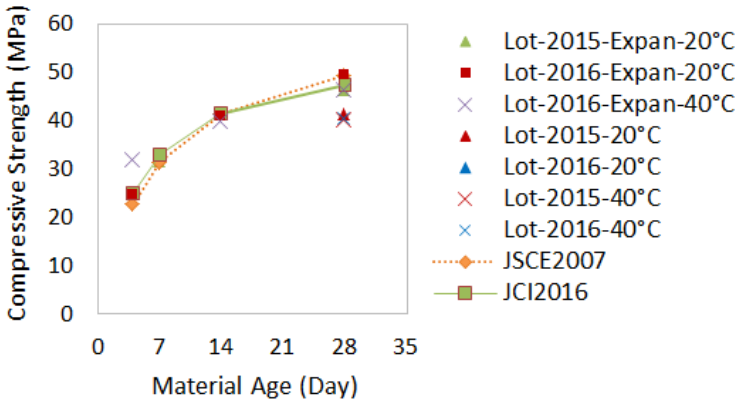

Fig.4.10(a) Compressive strength development

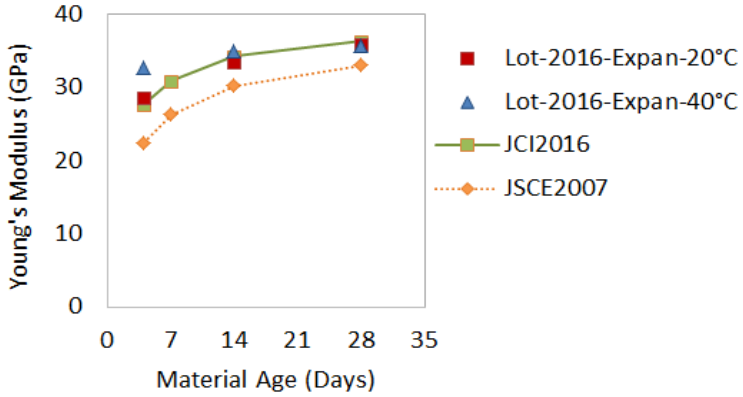

Fig.4.10(b) Young's modulus development

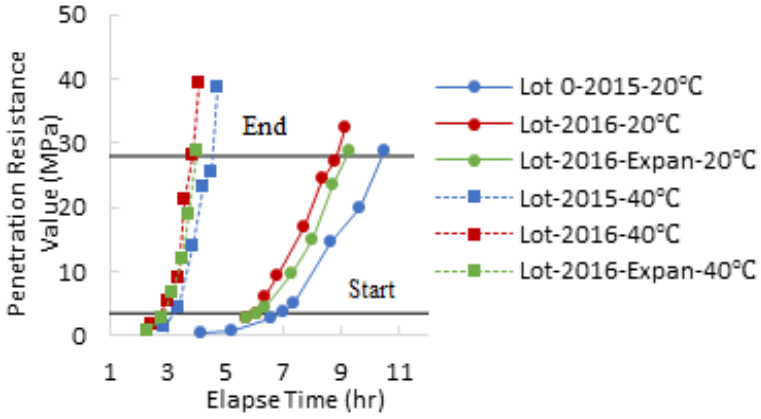

Fig.4.11 Setting time test result

(c) Autogenous Shrinkage Strain

Fig.4.12(a) and 4.12(b) illustrate the autogenous shrinkage strain obtained from the autogenous shrinkage specimens (measurement started at the time of concrete placement) without expansive additive for cement Lot-2015 and Lot-2016 respectively cured under 20°C and 40°C room temperature. Same kind of Lot-2015 specimens cured in 20°C (Lot-2015-20°C-Sp1 and Lot-2015-20°C-Sp2) and in 40°C (Lot-2015-40°C-Sp1 and Lot-2015-40°C-Sp2) exhibited variations in the maximum values of autogenous shrinkage. On the other hand, Lot-2016 specimens cured at 20°C (Lot-2016-20°C-Sp1 and Lot-2016-20°C-Sp2) and in 40°C (Lot-2016-40°C-Sp1 and Lot-2016-40°C-Sp2) room temperature did not show considerable differences in the maximum value of autogenous shrinkage. In reverse, Lot-2016 specimens cured under 40ºC constant temperature showed smaller autogenous shrinkage (max. autogenous shrinkage $=135\text{x}10^{-6}$) compared to that of specimens cured under 20°C temperature (max. autogenous shrinkage$=211\text{x}10^{-6}$). However, previous researches6) revealed that autogenous shrinkage for blast furnace slag cement in high adiabatic temperature history was larger than those cured under normal constant curing temperature i.e., 20°C.

Moreover, the autogenous shrinkage equation (Eq.4.2(a) for blast furnace slag cement) given in the 'JCI Guidelines for Control of Cracking of Mass Concrete 2016[7] as well as in 'JSCE Standard Specifications for Concrete Structures 2012[8] consider the effect of maximum temperature due to the hydration heat generation along with water-binder ratio on the occurrence of autogenous shrinkage (Fig.4.12(a) and 4.12(b)).

$$\varepsilon_{ag} = -\beta\varepsilon'_{as\alpha} \times (1-exp\,(-a \times (t'-t_s)^b))$$

$$\varepsilon'_{as\alpha} = 2350 \times exp\,(-5.8 \times (W/C)) + \varepsilon'_{asT} \qquad \text{Eq. 4.2(a)}$$

$$\varepsilon'_{asT} = 80 \times (1-exp\,(-1.210^{-6} \times (T_{max}-20)^4)$$

Where, β = coefficient indicates the influence of cement and admixture, t' = effective material age, t_s = initial setting time, $\varepsilon'_{as\alpha}$ = final value of autogenous shrinkage, a, b = coefficient expressing the progressive characteristics of autogenous shrinkage, W/C=water cement ratio, ε'_{asT} = autogenous shrinkage contributed by maximum temperature and T_{max} = maximum concrete temperature.

The test results obtained from the specimen cured in 40°C constant temperature indicate that the autogenous shrinkage obtained from the specimens cured in constant high temperature can be small due to early age rapid strength development. Because, in case of 40°C curing temperature, compressive strength and Young's modulus was observed relatively large (Fig.4.10(a) and (b)) in initial stage which may contribute in reducing contracting deformation producing smaller autogenous shrinkage.

Although, autogenous shrinkage rate at early age is observed higher in high temperature, it seems that temperature effect is not significant rather than water binder ratio on the maximum value of autogenous shrinkage for Shinkesen Ohashi slab concrete (Fig.4.12(c)). Hence, JSCE2012 autogenous shrinkage equation Eq.4.2(a)[8] considers the effect of water cement ratio, maximum concrete temperature and cement type has been calibrated with respect to the measured autogenous shrinkage in 20°C and 40°C curing temperature (Fig.4.12(c)) to utilize in the structural level simulation of Shinkesen Ohashi bridge slab instead of directly applying measured data from test specimens. The calibrated JSCE2012 autogenous shrinkage equation Eq.4.2(b) is as below.

$$\varepsilon_{ag} = -\beta\varepsilon'_{as\alpha} \times (1-exp\,(-a \times (t'-t_s)^b))$$
$$\varepsilon'_{as\alpha} = 2800 \times exp\,(-5.8 \times (W/C)) + \varepsilon'_{asT} \qquad \text{Eq. 4.2(b)}$$
$$\varepsilon'_{asT} = 10 \times (1-exp\,(-1.210^{-6} \times (T_{max}-20)^4)$$

Where, β =0.75 coefficient indicates the influence of cement and admixture, t′ = effective material age, t_s = initial setting time, $\varepsilon'_{as\alpha}$ = final value of autogenous shrinkage, a, b = coefficient expressing the progressive characteristics of autogenous shrinkage, W/C=water cement ratio, ε'_{asT} = autogenous shrinkage contributed by maximum temperature and T_{max} = maximum concrete temperature.

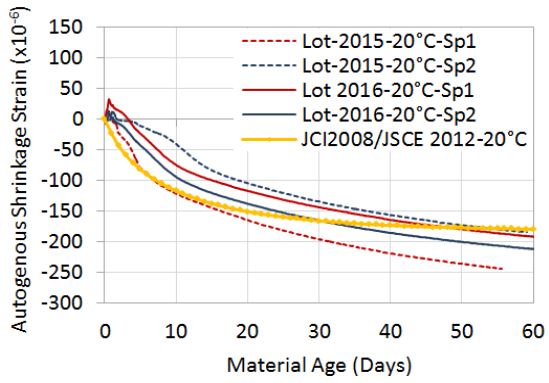

Fig.4.12(a) Autogenous shrinkage at 20°C curing temperature

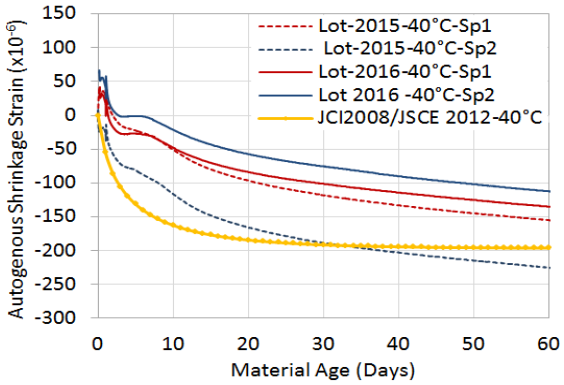

Fig.4.12(b) Autogenous shrinkage at 40°C curing temperature

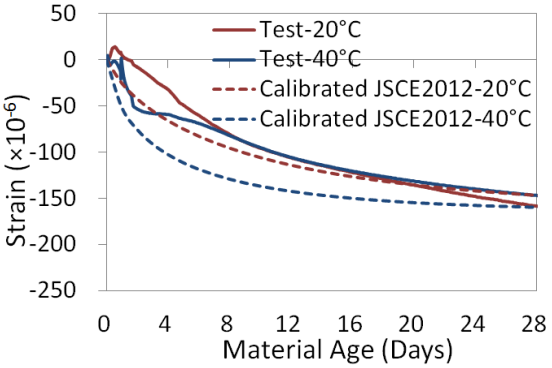

Fig.4.12(c) Calibration of JSCE2012/JCI2016 autogenous shrinkage equation with respect to test average autogenous shrinkage

Fig.4.12(d) Autogenous shrinkage specimens with embedded type strain gauge

4.2.4 Level 2: Numerical Simulation of FEM Member Level Specimen Models regarding Shinkesen Ohasi RC Slab Concrete

In level 2, JCMAC3 has been utilized for simulation of several restrained concrete specimens where fundamental concrete properties models for time dependent temperature adjusted compressive strength, tensile strength and Young's modulus development as well as autogenous shrinkage model calibrated from the test results were given as input. Furthermore,

some parametric assumptions such as expansion strain parameters for total expansion energy conservation model[9] and the reduction factors to calculate the effective Young's modulus of concrete taking into account the early age creep were determined in Level 2. The established simulation procedure has been verified in case of restrained expansion, autogenous shrinkage and creep for JCI-SAS3-2 autogenous shrinkage specimen and small scale RC slab specimen made previously with the same concrete mix applied in Shinkesen Ohashi bridge RC slab by Yokogawa Bridge Corporation[3].

(1) Experimental Investigations and Numerical Simulation of Thin Walled Tinplated Cylindrical Steel Mold Expansion Strain Specimen

(a) Experimental Investigation on Restrained Expansion Strain Specimen

Restrained expansion strain specimens were prepared according to JCI-S-009-2012 in the cylindrical thin walled tinplated steel molds φ100×200mm (Fig.4.13 (a)). The outline of the mold is illustrated in Fig.4.13(b). A commercially available lime type expansive additive was used which was applied in Shinkesen Ohashi bridge deck slab construction. A strain gauge is attached with glue at the center of the outer surface of the tinplated steel mold as shown in Fig.4.13(b). Circumferential strain was measured as the restrained expansion strain. The specimens were kept in sealed condition. Past researches have confirmed that the measured circumferential strain at the middle height of this specimen under sealed condition according to JCI-S-009-2012 is equivalent to the restrained expansion obtained from the JIS A6202 standard test[5].

The expansion strain results obtained from the thin walled steel mold cylindrical specimens cured in 20°C and 40°C constant temperature are shown in Fig.4.13(c) and (d) along with their average values. The observed averaged maximum restrained expansion strain for the specimens cured in 20°C temperature was 263×10^{-6} which followed by the occurrence of autogenous shrinkage. In case of 40°C curing temperature the maximum observed restrained expansion strain was 250×10^{-6} (Fig.4.13(e)). However, autogenous shrinkage rate at early age was observed higher for the specimens cured in high temperature.

Fig.4.13(a) Expansion strain specimens in thin walled tinplated cylindrical steel molds

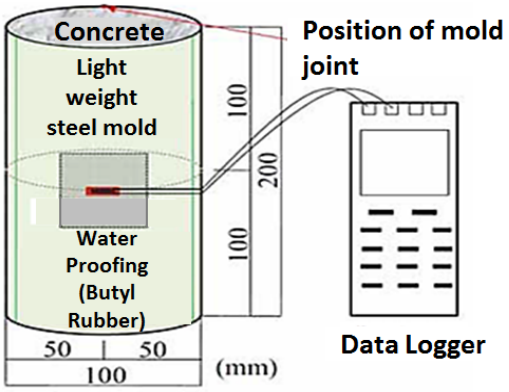

Fig.4.13(b) Outline of the cylindrical expansion strain specimen[5]

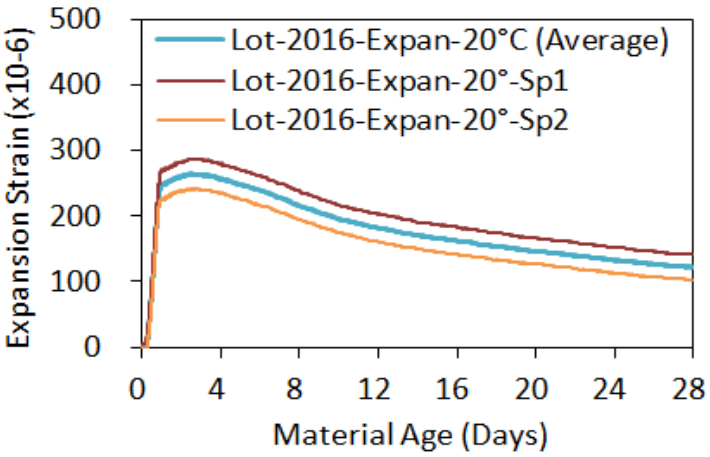

Fig.4.13(c) Expansion strain in 20°C curing temperature

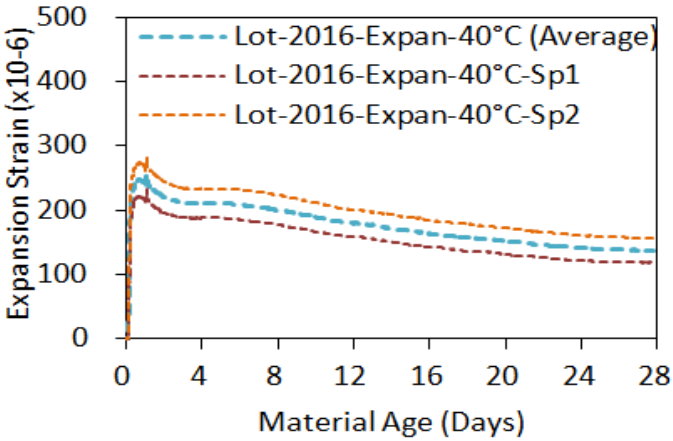

F ig.4.13(d) Expansion strain in 40°C curing temperature

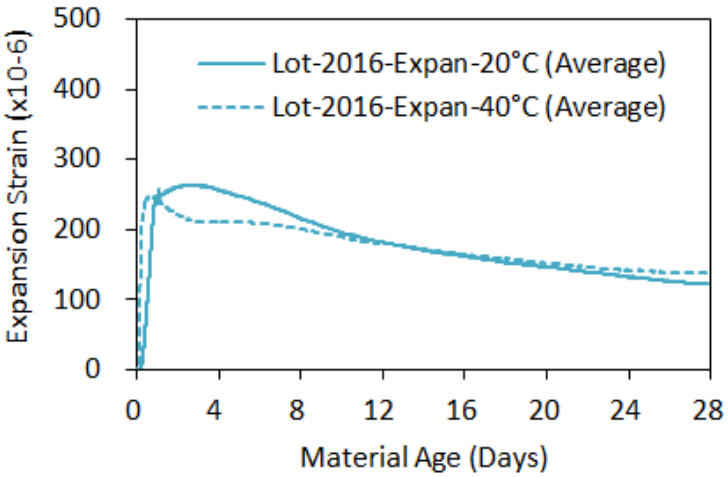

Fig.4.13(e) Comparison of average expansion strains in 20°C and 40°C curing temperature

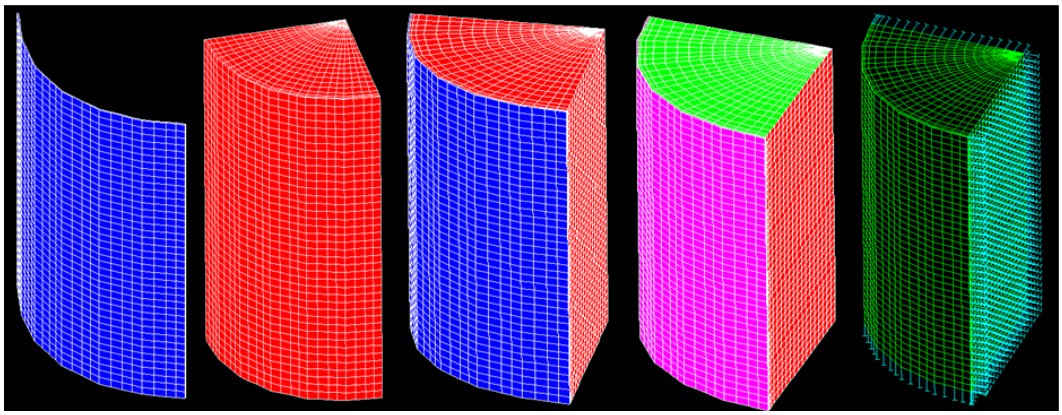

(a) (b) (c) (d) (e)

Steel Mold Solid Element Model
Concrete Solid Element Model
2D Heat Element as Heat Transfer Boundary Surface for Steel Mold
2D Heat Element as Heat Transfer Boundary Surface for Concrete
Structural Boundary

Fig.4.14 1/8th model for thin walled cylindrical tinplated steel mold expansion strain specimen in FEM (a) 3D solid element model for thin walled tinplated steel mold, (b) 3D solid element model for concrete specimen, (c) Perfect bond between steel mold and concrete specimen, (d) 2D heat transfer boundary surface on the outer surface of steel mold and the top surface of the concrete specimen and (e) Structural boundary conditions for 1/8th cylindrical model.

(b) Finite Element Model and Boundary Conditions

The 1/8th scaled specimen model was configured with 3D linear hexahedral isoparametric solid element (Fig.4.14(a) and 4.14(b)). Since the concrete inside the steel mold produces radial compressive stress and circumferential tensile stress against the mold due to the expansion of concrete, perfect bond was considered between the concrete and the mold (Fig.4.14(c)). 2D heat element was pasted upon the outer surface of the steel mold and the top surface of the concrete to set heat transfer boundaries on the exposed surfaces (Fig.4.14(d)). Structural boundaries were set to confirm the stability and the symmetry of the 1/8th cylindrical model (Fig.4.14(e)). Moreover, mesh sensitivity analysis was performed to confirm the appropriate mesh sizes of the cylindrical model for obtaining acceptable analytical results.

(c) Thermal Analysis Input

Adiabatic temperature rise model

Since the thermal analysis is followed by the structural stress analysis, Adiabatic temperature rise model [6] [7] was considered to conduct thermal analysis of the model both for 20°C and 40°C curing conditions as follows in Eq.4.3:

$$Q(t) = Q_{\infty}\left[1 - \exp\left\{-r\left(t - t_{0,Q}\right)^{s}\right\}\right] \quad \text{(Time dependent equation)} \qquad \text{Eq.4.3}$$

Where, $Q(t)$=adiabatic temperature rise at age of t days (°C)

$Q\alpha(t)$=ultimate adiabatic temperature rise (°C)

r and s =parameters representing the rate of adiabatic temperature rise

$t_{o,Q}$ = age of starting of adiabatic temperature rise

Heat Transfer Coefficient

The specimens were kept in curing room with constant temperature; hence there was no influence of the natural wind flow. Therefore, heat transfer coefficient was set as 6.0 W/m^{2o}C for the steel mold and 8.0 W/m^{2o}C for top surface of the concrete sealed by a cellophane plastic sheet. As the thermal strain was not taken in account for the present structural stress analysis, coefficient of thermal expansion was not considered in the model. Material properties for thermal analysis are summarized in Table 4.4.

Table 4.4 Input properties for thermal analysis

Thermal Properties	Concrete Specimen	Steel Mold
Heat Conductivity (W/m°C)	3.3	43
Specific Heat (kJ/kg°C)	1.15	0.47
Density (kg/m3)	2300	7890
Heat Transfer Coefficient (W/m2ºC)	8	6
Initial Temperature (°C)	20 and 35	20 and 40
Curing Temperature (°C)	20 and 40	20 and 40

(c) Structural Stress Analysis Input

Compressive Strength, Tensile Strength, Young's Modulus and Creep

Structural stress analysis followed consecutively after thermal analysis. JCI2016[7] equations with calibrated parameters defining time dependent development of compressive strength (Eq.4.1(c)), tensile strength (Eq.4.1(d)) and Young's modulus development (Eq.4.1(e)) were adopted in the stress analysis.

Effective Young's Modulus to Consider Creep Effect

The effect of early age creep of concrete was considered by applying the Effective Young's Modulus by a method of reducing the Young's modulus of concrete at the age of temperature increasing and decreasing period as recommended in JCI2016[7] shown in the Eq.4.4.

$$E_e(t_e) = \varphi(t_e) \times E_c(t_e) \qquad \text{Eq.4.4}$$

Where,

$E_c(t_e)$: Modulus of elasticity (Young's modulus) of concrete at t_e （N/mm2）

$\varphi(t_e)$： Reduction factor for modulus of elasticity because creep is large in hardening process.

Until the temperature adjusted effective material age when temperature rise becomes the maximum:

$$\varphi(t_e)=0.42$$

Again, after one day in temperature adjusted effective material age as from the age at the maximum temperature:

$$\varphi(t_e)=0.65$$

$\varphi(t_e)$ is linearly interpolated between the above both temperature adjusted effective material age.

Expansion strain model

Expansion strain model based on the total energy conservation hypothesis[9] is adopted in the present study to simulate the expansion strain due to the application of expansive additive. The expansion strain energy is obtained from the Eq.4.5 as follows.

$$U(t_e) = U_\infty . (1\text{-}exp\ (\text{-}a\ (t_e\text{-}t_o)^b) \qquad \text{Eq. 4.5}$$

Where, $U(t_e)$=total energy at effective concrete age t_e, U_∞=ultimate value of the total energy, a and b= coefficient indicating the influence of the type of cement on the progressive characteristics of total energy, t_o=effective material age at the beginning of expansion. These parameters have been determined as U_∞= $100\text{x}10^{-6}$, t_o= 0.3, a= 1.5 and b= 1 for Shinkesen Ohashi bridge slab concrete mix on the basis of extensive parametric studies by changing values of U_∞, a and b systematically to obtain good agreement with the average expansion strain results acquired from the thin walled cylindrical tinplated steel mold specimens cured under 20°C and 40°C curing temperature shown in Fig.4.13(c).

Input Autogenous Shrinkage Strain

The free autogenous shrinkage strain obtained from the specimens without expansive additive cured under 20°C and 40°C room temperature (Fig.4.12(a) and (b)) have been directly applied as input for the simulation. Since autogenous shrinkage equation (Eq.4.1) given by JSCE2012[8] and JCI2016[7] consider maximum temperature effect due to hydration heat generation, autogenous shrinkage values obtained from that equation were also given as inputs for 20°C and 40°C curing temperature to compare the effect of autogenous shrinkage considering maximum concrete temperature on the simulation of expansion strain model.

(d) Simulation Results

Fig.4.15(a) illustrates the x-directional strain distribution on the 1/8th model at 28th day of concrete material age. The strain along x-axis on the measurement point at the center height of the mold acts as circumferential strain Fig.4.15(b). The strain distribution demonstrates that the average circumferential strain is about $150\text{x}10^{-6}$ at the center height of the mold at material age of 28 days, while the maximum expansion occurs at the top surface of the concrete specimen. Fig.4.15(c) illustrates the simulation results for 20°C temperature curing condition.

The maximum expansion strain obtained from utilizing measured autogenous shrinkage is slightly larger than the measured expansion strain data while the decreasing trend is same as the measured results. On the other hand, the analysis results acquired from utilizing autogenous shrinkage equation (Eq.4.1) shows less expansion due to higher autogenous shrinkage at

temperature increasing age of concrete. However, both of the analysis results show nearly the same expansion strain at 28th day material age of the concrete. Fig. 4.15 (d) depicts the analytical results for 40°C temperature curing condition. The maximum expansion strain obtained from utilizing measured autogenous shrinkage is also slightly larger than the measured expansion strain result due to relatively smaller autogenous shrinkage. In reverse, the analysis results applying the autogenous shrinkage Eq.4.2(a) shows reduced expansion because of considering higher autogenous shrinkage at temperature increasing age of concrete. Therefore, test results for autogenous shrinkage in constant high temperature curing condition seems to be less conservative compared to the autogenous shrinkage equation recommended by JSCE2012[7]/JCI2016[8] in simulating the shrinkage compensating phenomenon of expansion strain in restrained concrete.

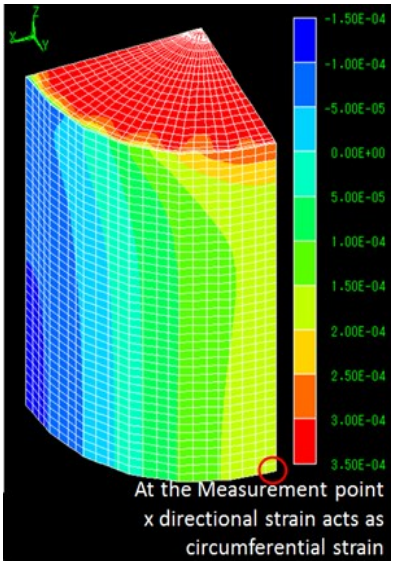

Fig.4.15 (a) Strain contour in x-axis at the material age of 28 days for 20°C curing temperature

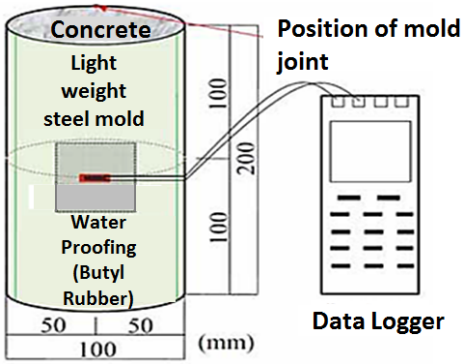

Fig.4.15(b) Strain measurement location

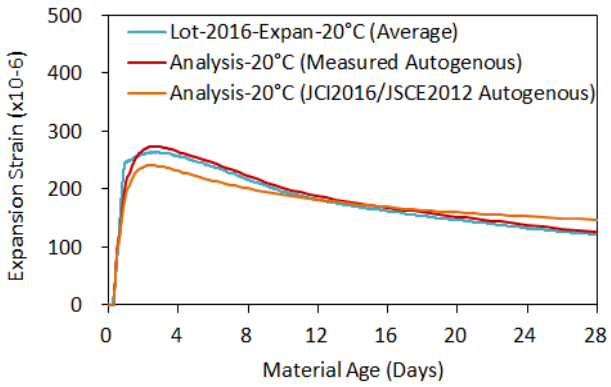

Fig.4.15 (c) Simulation of expansion strain in 20°C curing temperature

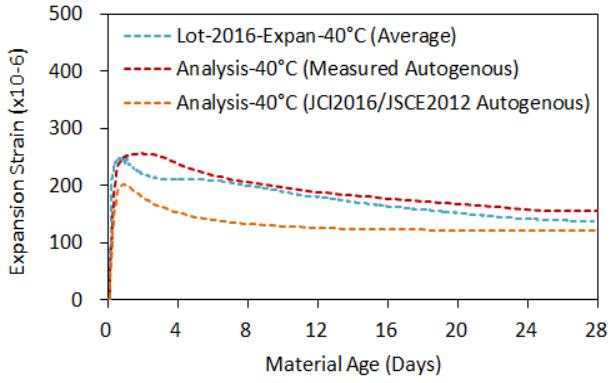

Fig.4.15 (d) Simulation of expansion strain in 40°C curing temperature

(2) Verification of the Input Autogenous Shrinkage, Expansion Strain Parameters and Creep for Restraint Concrete Specimens

(a) JCI-SAS3-2 Autogenous Shrinkage Strain Specimen

JCI-SAS3-2 specimen for measuring restrained autogenous shrinkage was previously investigated by Yokogawa Bridge Corporation to confirm the shrinkage compensating performance of Shinkesen Ohashi bridge slab concrete due to the expansion even under restrained condition3). The measured rebar strain data obtained from JCI-SAS3-2 specimen (Fig.11(a))[3] was utilized to verify the FEM simulation procedure in member level developed in the current study. 100x100x1500 mm JCI-SAS3-2 concrete specimen is restraint with φ32mm steel bar. 3D solid hexahedral isoparametric solid elements were considered for concrete material and 1D truss elements were applied as steel bar where perfect bond is modeled between concrete and steel reinforcement in the 1/8th FEM symmetric model (Fig.4.16(a)-(c)).

Fig.4.16(a)JCI-SACS3-2 specimens[3]

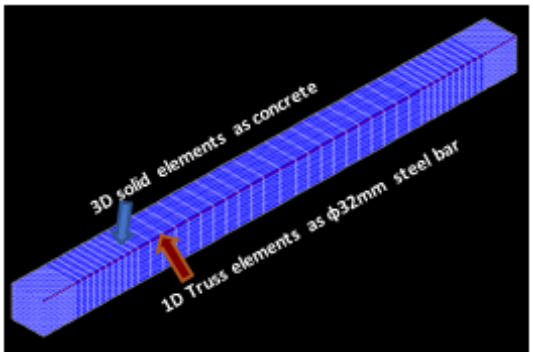

Fig.4.16(b) JCI-SACS3-2 1/8th model in FEM

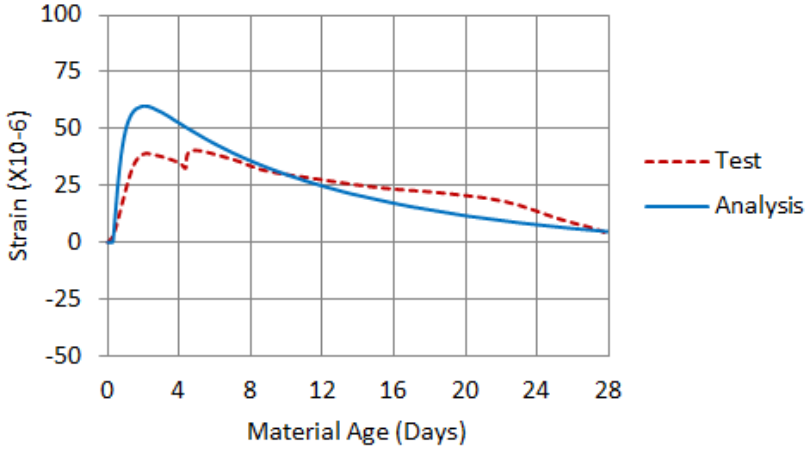

Fig.4.16(c) Simulation of JCI-SACS3-2 specimen model

The input properties for thermal analysis i.e. heat conductivity, specific heat, density were same as described in Table 4.4. Heat transfer coefficient was set as 6.0 W/m^{2o}C. Initial concrete temperature was 22.5°C while the constant curing temperature was 20°C. Furthermore,

structural stress analysis input procedure was same as cylindrical expansion strain model. Since the JCI-SAS3-2 specimen was made using cement lot-2015, the corresponding 28th day compressive strength (Fig.5(a)) was given as the input for compressive strength (Eq.4.2) followed by tensile strength (Eq.4.3) and Young's modulus development (Eq.4.4). The test average autogenous shrinkage strain for Lot-2015-20C° under 20C° curing temperature was given as input while initial thermal expansion due to the large coefficient of thermal expansion prior to setting was deducted.

The reduction constant for creep, and parameters for expansion strain model were same as for thin walled steel mold cylindrical expansion strain model. The origin of the measurement and simulation was defined as the initial setting time of concrete (around 7 hours of concrete placing for cement Lot-2015 under 20C° curing temperature). Eventually, Fig.4.16(c) proves the good agreement of the simulation results with the measured restrained expansion and autogenous shrinkage until 28 days of material age.

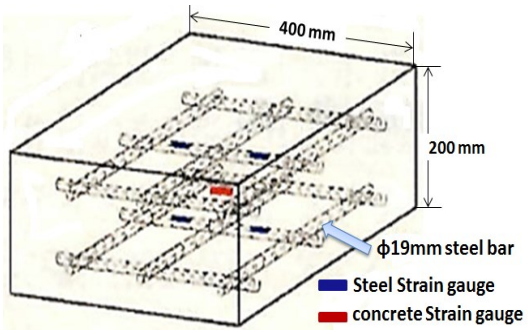

Fig.4.17(a) RC slab specimen[3]

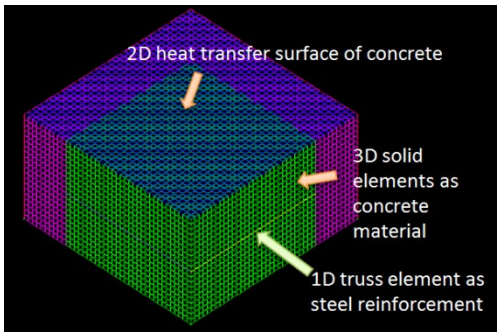

Fig.4.17(b) 1/8th RC slab specimen model in FEM

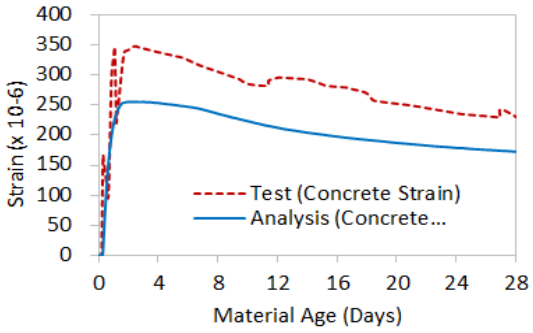

Fig.4.17(c) Simulation of concrete strain in RC slab

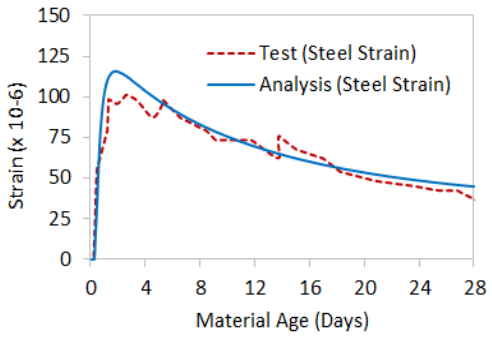

Fig.4.17(d) Simulation of rebar strain in RC slab

(b) RC Slab Specimen

The small scale 400x400x200 mm RC slab specimen was experimentally investigated by Yokogawa Bridge Corporation to understand the expansion and the shrinkage behavior of RC slab with Shinkesen bridge slab concrete mix under the internal restraint due to the reinforcing bars (Fig.4.17(a))[3]. The specimen was kept at 20C° room temperature until 28 days under sealed condition around five surfaces of the specimen except the top surface with continuous wet curing. Hence, smaller autogenous shrinkage was expected in this specimen compared to that of the test prism specimens under fully sealed curing (Fig.4.12(a) and (b)). The measured concrete

and rebar strain obtained from the RC slab specimen (Fig.4.17(c) and Fig.4.17(d)) were utilized in another member level verification for the FEM simulation procedure followed in the present study. The numerical model was configured with 3D solid hexahedral isoparametric solid elements for concrete and 1D truss elements for reinforcing bars for the 1/8th scale FEM model (Fig.4.17(b)). Thermal and stress analyses inputs were same as JCI-SAS3-2 specimen. Fig.4.17(c) shows that maximum restrained expansion strain in concrete is about 260x10^{-6} in simulation whereas the measured maximum restrained concrete strain is nearly 350x10$^{-6.}$ The discrepancy between simulation and measurement is due the fact that the maximum expansion energy parameter (U_{α} =100) was determined with the basis of average expansion strains (250x10^{-6}) obtained from the measurement of thin walled steel mold cylindrical specimens. Fig.4.17(d) presents good agreements between simulation and measurement in case of rebar strain.

(3) Brief Summary of the Simulation Results in Member Level

The FEM simulation procedure has been successfully verified in member levels in simulating the volume changes in the early age of concrete with slag cement and expansive additive utilizing several material level experimental results. It has been confirmed that the calibrated material parameters for total expansion strain energy model, experimentally obtained input autogenous shrinkage, appropriate utilization of creep reduction factors and confirmed time dependent compressive strength development of the concrete are the key factors for obtaining good agreements in FEM simulations for several member level specimens. It can be conferred that the present simulation method followed by several material and member level verifications can be effectively applicable in real structural level simulation of Shinkesen Ohashi bridge FEM model evaluating early age thermal and volumetric changes along with cracking risk of the similar RC deck slabs.

4.2.5 Level 3: Structural Level Verification of Shinkesen Ohashi Bridge RC Slab FEM Model

(1) Locations of Temperature and Strain Data Monitoring in the Deck Slab

Embedded strain gauges with thermocouples were installed to measure concrete strain and temperature in longitudinal (X), transverse (Y) and vertical (Z) axes in the Shinkesen Ohashi deck RC slab in the concrete placement Lot-8 upon Pier-3 (Fig.4.18(a) and (c)) at locations A (position of RC slab directly connected to the steel girder) and B (center of the flexural part of the RC slab) (Fig.4.18(c)) whereas; C and D were additionally accounted for temperature and stress simulation in Lot 8 upon pier 3. Moreover, longitudinal and transverse concrete strains were monitored at the end of Lot 8 shown in Fig.4.18(c). The positions of embeded strain gauges are designated as A_End and B_End. Moreover, girder temperature and ambient temperature was measured at locations G and T respectively (Fig.4.18(c)).

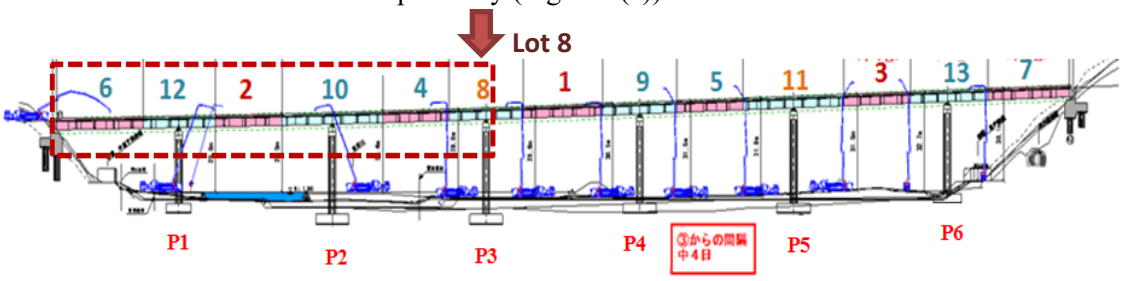

Fig.4.18 (a) Locations of data monitoring in concrete placement Lot 8 upon Pier 3 and the modeled section of Shinkesen Ohashi bridge

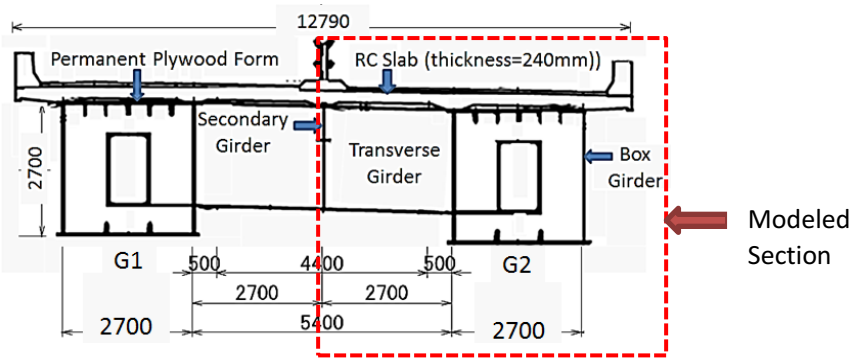

Fig.4.8(b) Cross section of Shinkesen Ohashi deck girder bridge showing modeled section

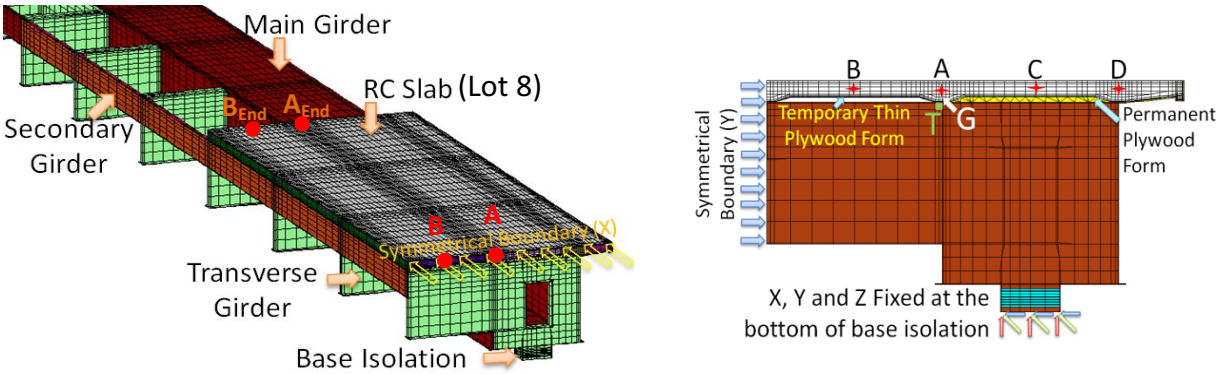

Fig.4.18(c) Shinkesen Ohashi Bridge FEM 1/4th model considering concrete placement Lot 8 upon Pier 3

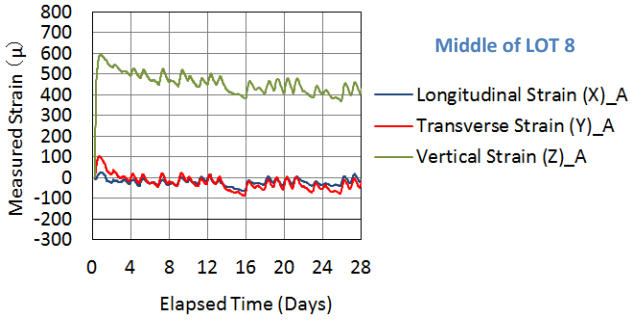

Fig.4.18(d) Monitored concrete strains at the measurement location A at the middle of Lot 8 upon Pier 3

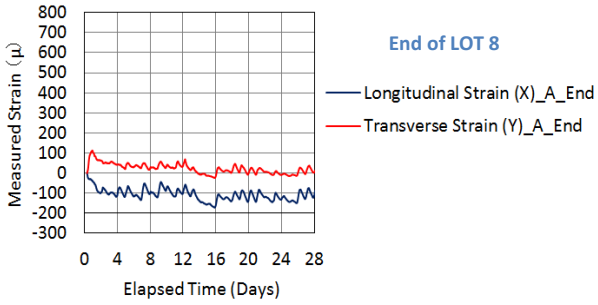

Fig.4.18(e) Monitored concrete strain at the measurement location A_End at the end of Lot 8 adjacent to hardened Lot 1

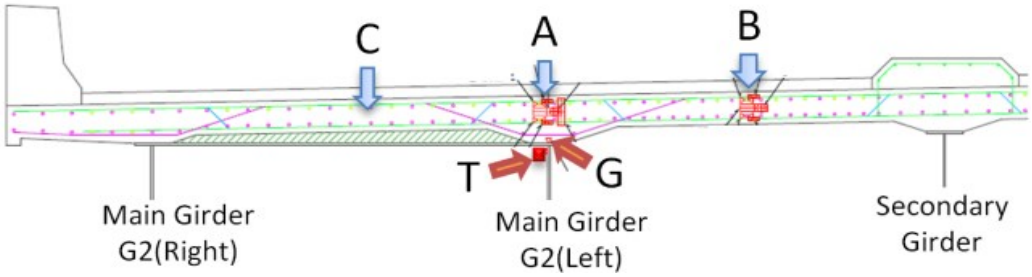

Fig.4.18(f) Locations of measurement (A: directly connected with main girder and B: in flexural part of RC slab) in the Shinkesen Ohashi Bridge deck RC slab

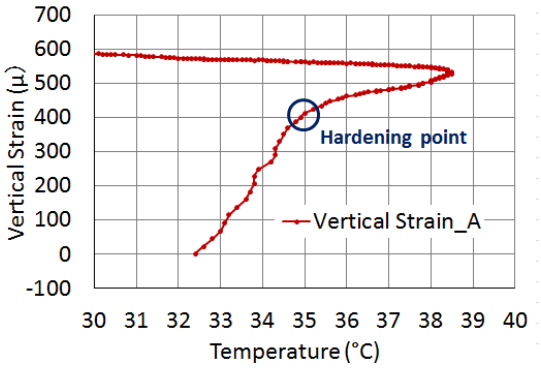

Fig.4.18(g) Vertical strain history defining hardening point with respect to concrete temperature rise due to hydration heat

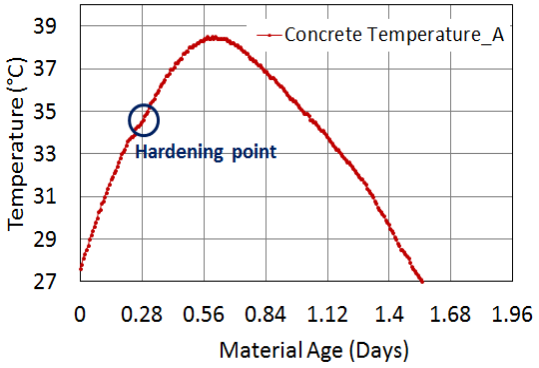

Fig.4.18(h) Temperature rise history and hardening time with respect to material age

Measured strains and temperature were utilized to validate the Shinkesen Ohashi bridge FEM model. On 22nd June, 2015, after placing of concrete temperature measurement started in the morning at 8:40 am at location A upon pier 3. Concrete placement was finished at 11:30 am upon pier 3, and measurement of strain was started at 15:30. Therefore, it is to be noted that, strain measurement was started after 6 hours 50 minutes (0.28 day) after initiation of concrete temperature measurement.

(2) Significance of Measuring Three Directional Strains for Structural Level Verification of FEM Model

In real structural level verification of RC deck bridge models, three directional concrete strains which are considered to be under different restraint conditions were taken into account.

Longitudinal Strain

Mmeasured longitudinal strain in RC slab was observed under the highest external restraints due to the continuous composite connections of the main girders and RC slab at location A and flexural part of RC slab at location B. It should be noted that the development of tensile stress due to the external restraint against volumetric changes of concrete along the longitudinal direction is the key factor for generation of transverse cracks in RC deck slab. This is why; recorded longitudinal strains were efficiently utilized to validate the model corresponding to the restrained longitudinal strain along bridge axis at locations A and B (Fig. 4.18 (c),(d), (e) and (f)).

Transverse Strain

Transverse strain in RC slab is governed by the transverse reinforcement, non-uniform shape of the RC slab, the stay-in-place (SIP) plywood forms and the supporting girders. Therefore, some modeling assumptions such as modeling of permanent plywood forms were conveniently verified utilizing monitored transverse strain data (Fig. 4.18 (c),(d), (e) and (f)).

Vertical Strain

Since there was no steel reinforcement in vertical direction, structural restraints in vertical direction was negligible which can be the key measure for verification of chemical expansion and autogenous shrinkage under very low restraints. Moreover, hardening point of

concrete can also be determined from the vertical strain history with respect to temperature rise due to the hydration heat generation of concrete in absence of severe structural restraints (Fig. 4.18 (f),(g), and (h)).

(3) Structural Model, Structural Boundary Conditions, Element Types and Element Discretization

Full scale Shinkesen Ohashi continuous span deck girder bridge FEM model consists of RC deck slab, main box girder, secondary girder, transverse girders, permanent and temporary plywood forms and rubber bearings (Fig.4.19(a),(b) and (c)). Approximately 1/4th segment of the bridge was modeled with symmetric structural boundary conditions considering multiple spans along with unique modeling approach regarding rubber bearing for accurate simulation of thermal and volumetric expansion-contraction behavior of the full-scale bridge model.

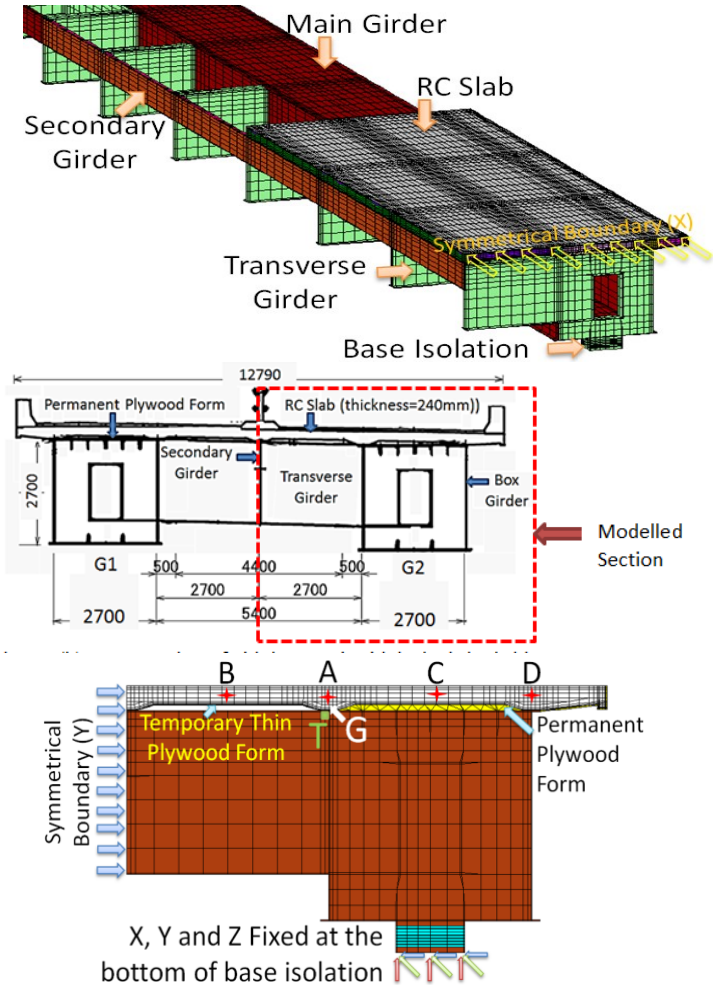

Fig.4.19(a) FEM Modeling of Shinkesen Ohashi bridge with symmetric structural boundary conditions

RC Slab

The RC slab on the Shinkesen Ohashi bridge was modeled with 3D hexahedral isoparametric heat generating solid elements as concrete (Fig.4.19(b). The thermal and some of mechanical properties of the heat generating concrete elements are depicted in Table 4.5.

Steel Reinforcement

The embedded steel reinforcements in RC slab have been modeled with one dimensional truss elements (Fig.4.19(c)). The thermal and some of mechanical properties of the steel are depicted in Table 4.5.

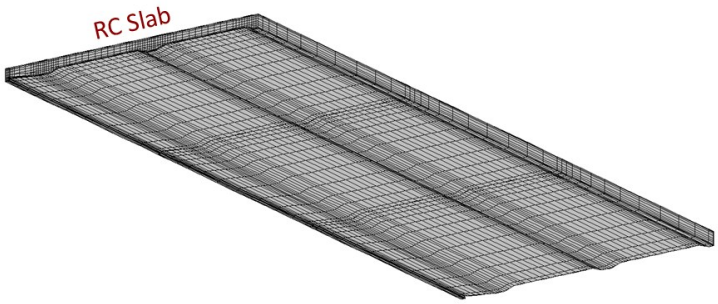

Fig.4.19(b) 3D hexahedral isoparametric heat generating solid elements used for RC slab FEM model

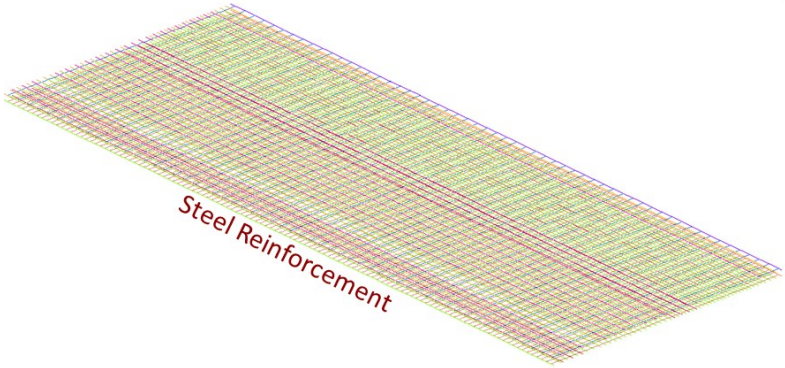

Fig.4.19(c) 1D truss element reinforcing steel model embedded in concrete deck slab

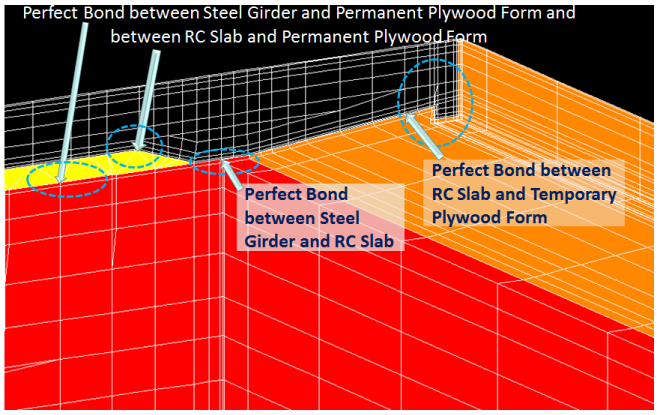

Fig.4.19(d) Perfect bond considered in case of connections between heat generating element RC slab, non-heat generating plywood-styrofoam composite permanent form and steel girders.

Table 4.5 Thermal and stress analysis inputs for member and structural level FEM models

Thermal Properties	Concrete	Steel bar	Steel Girder	Plywood Form	Rubber Bearing
Heat Conductivity (W/m°C)	2.7	43	43	0.13	0.19
Specific Heat (kJ/kg°C)	1.15	0.47	0.47	1.22	2.00
Density (kg/m3)	2300	7890	7890	545	1.23
Young's Modulus (MPa)	JCI2016	$2x10^5$	$2x10^5$	17000	Lower bound=1.5 Upper bound=5200
Poisson's Ratio	0.2	0.3	0.3	0.3	0.45
CTE ($x10^{-6}$/°C)	8.4	10	9	4.5	4.5

Steel Girders

Main box girders, transverse girders and secondary girders in Fig.4.19(a) were modeled with 3D hexahedral isoparametric non-heat generating solid elements. The connections between steel girders and the RC slab were modeled as perfect bond for true representation of the existing shear connectors and metallic slab anchors as shown in Fig.4.19(d). The thermal and mechanical properties are shown in Table 4.5.

Permanent and Temporary Plywood Forms

Permanent plywood forms between RC slab and main girders and temporary plywood forms at the bottom surfaces of other portions of the RC slab were modeled with non heat generating 3D sloid elements considering perfect bond with appropriate thermal and mechanical properties (Table 4.5) for accurate simulation of thermal and volumetric expansion-contraction behavior of the early age concrete ensuring real structural conditions. Since the Young's modulus of plywood (17000 MPa) is significantly smaller than the Young's modulus of hardened concrete, it is believed that the modeling of plywood considering perfect bond will not cause any unexpected stress generation in RC slab.

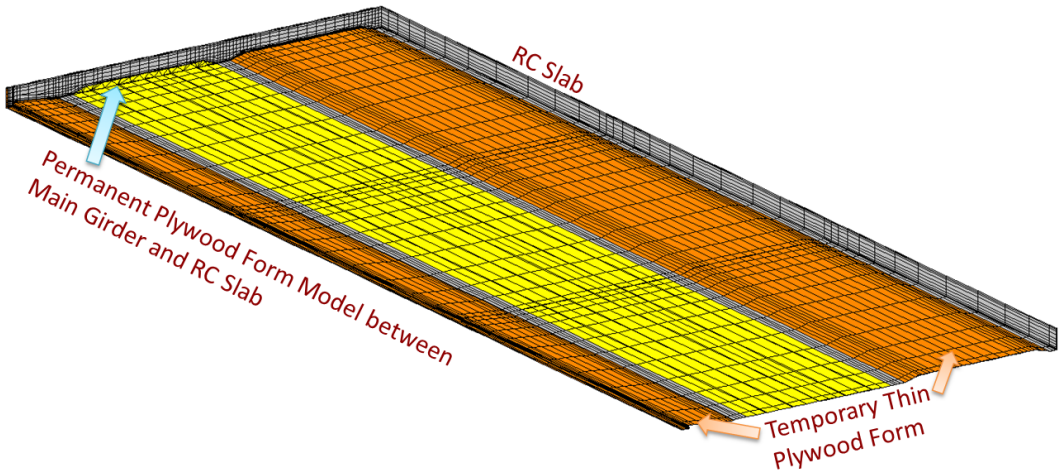

Fig.4.19(e) Three dimensional hexahedral isoparametric non-heat generating solid elements used for permanent and temporary plywood form model

Rubber Bearing

Cure adhesion multilayer rubber bearings with alternately piled up rubber and steel plate installed in case of Shinkesen Ohashi bridge were modeled with equivalent stiffness (lower bound of Young's modulus=1.5 MPa and upper bound of Young's modulus=5200 MPa) calculated according to the rule of mixture for composite materials considering multilayered rubber sheets and steel plates to ensure accurate simulation regarding appropriate movement of the girders due to the thermal changes. However, thermal deformation of base isolation itself was not considered for simplification of the analysis (Table 4.5).

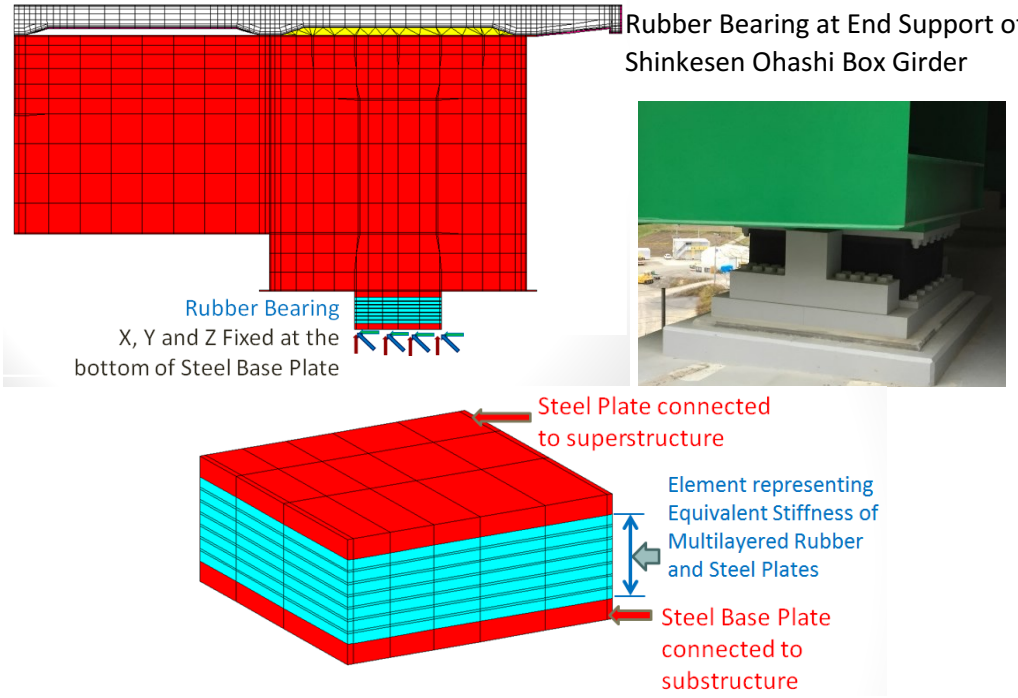

Fig.4.19(f) Three dimensional hexahedral isoparametric heat generating solid elements used for RC slab FEM model

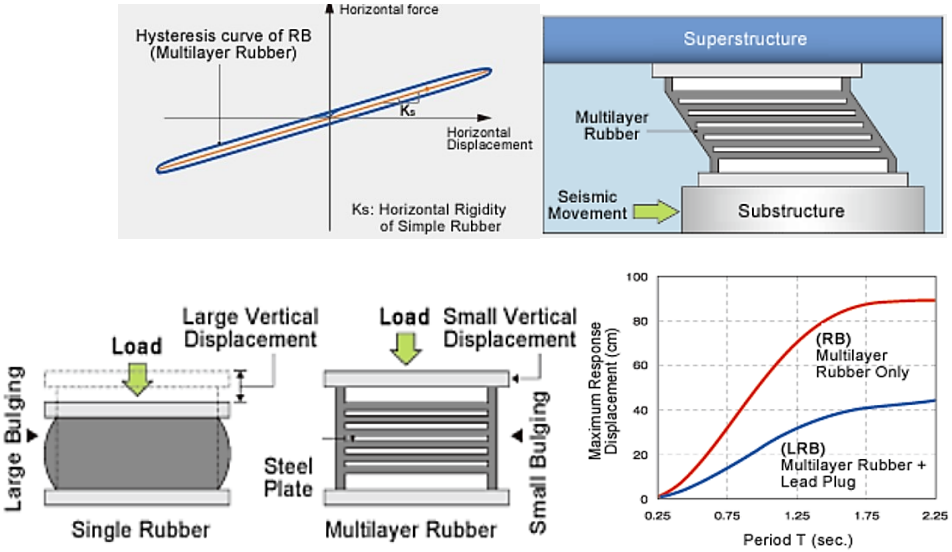

Fig.4.19(g) Basic characteristics of multilayer rubber bearing with lead plug [10]

Horizontal displacement of rubber bearing generaly depends on the horizontal rigidity of the simple rubber (say, Young's modulus=1.47 MPa). However, existence of lead plug can increase damping reducing maximum response displacement of the rubber bearing (Fig.4.19(g)) [10]. In this context, according to the rule of mixture[11], the lower bound and upper bound of the equivalent Young's modulus representing stiffness of rubber bearing can be obtained for composite action of alternately piled up rubber, steel plate and lead plug following Eq. 4.6(a) and Eq.4.6(b) respectively

Lower bound of Young's modulus, $$E_c = \left(\frac{f}{E_f} + \frac{1-f}{E_m} \right)^{-1}$$ Eq. 4.6(a)

Upper bound of Young's modulus, $$E_c = fE_f + (1-f)E_m$$ Eq. 4.6(b)

Where, E_f = Young's modulus of fiber (steel plates and lead plug)
E_m = Young's modulus of matrix (rubber) and
f = Volume fraction of fiber (steel plates and lead plug)

The calculated lower bound of Young's modulus (1.5 MPa) is nearly similar value as that of rubber (1.47 MPa). The upper bound of the equivalent Young's modulus was obtained 5200 MPa which has been successfully utilized in verification of Shinkesen Ohashi bridge model regarding three directional concrete strains and simulation of stresses. However, the effect of the lower and upper bound of Young's modulus of the rubber bearing has also been compared.

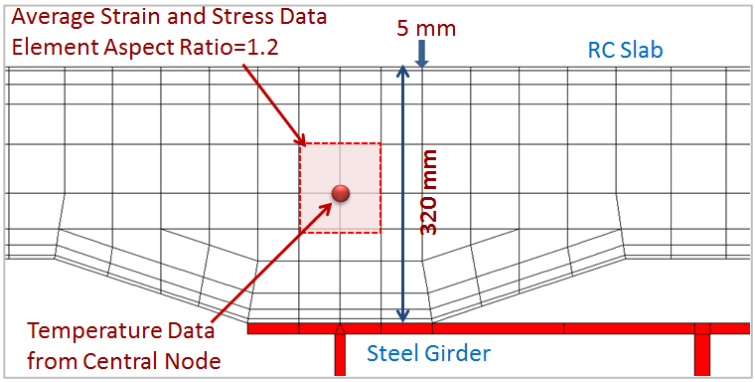

Fig.4.19(h) Mesh discretization and measurement nodes and elements in RC slab at the location connected to steel girders (location A)

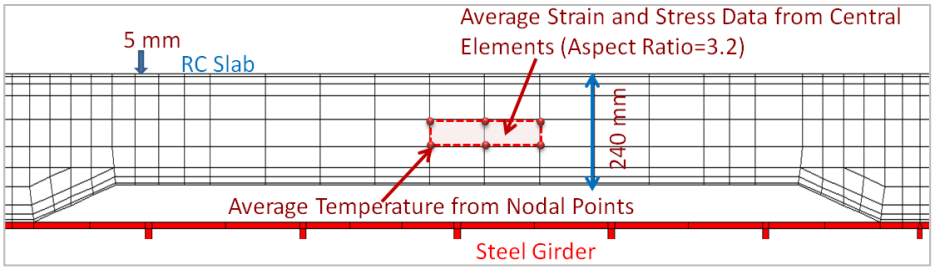

Fig.4.19(i) Mesh discretization and measurement nodes and elements in RC slab (location B and C)

Element Discretization

The slab thickness at the location of the connections with steel girders was 320 mm whereas the thickness of the slab in free portions was 240 mm. The thickness of elements were increased from the heat transfer top surface to the center of the slab and again decreases from the center to the bottom heat conduction surface of the RC slab. The thickness of the elements at heat transfer surface and heat conduction surface was kept small (5mm) for accurate temperature analysis considering heat transfer and heat conduction to different material.

Simulation results for temperature can only be obtained from nodal points. In present simulation, the temperature results were obtained from nodal points at the center of the RC slab along thickness direction. On the other hand, simulation results for stress and strain are acquired from the elements. Therefore, the aspect ratio of the elements at the central position along thickness direction in the RC slab was kept 1.2 at location A (upon girder). The maximum aspect ratio was kept 3.2 at other measurement locations such as B and C to obtain satisfactory results with respect to stress analysis (Fig.4.19(h) and (i)).

(5) Thermal Boundary Conditions

Heat transfer coefficients for different heat transfer surfaces of the bridge were determined from parametric studies in thermal analysis considering the depending on formwork type, curing method, curing duration, ambient temperature, wind velocity and ambient moisture conditions for accurate thermal stress analyses.

As shown in Fig.4.19(j), the heat transfer coefficient of the top three layered special curing surface of the RC slab has been kept 6.0 W/m^2/°C. Exterior surface of the girders were consider free to exposure to wind flow, therefore the heat transfer coefficient was decided as 14.0 W/m^2/°C. Since flow of wind is obstructed inside the box girder, the heat transfer coefficient of the interior surface of the box girder is anticipated as 12.0 W/m^2/°C. Furthermore, although the JCI crack control guidelines for mass concrete (2016) recommends 8.0 W/m^2/°C as heat transfer coefficient, since the temporary plywood for was accurately modeled considering appropriate thermal properties, the heat transfer coefficient of the temporary plywood form was defined as 12.0 W/m^2/°C considering the free wind flow condition in Shinkesen Ohashi bridge site.

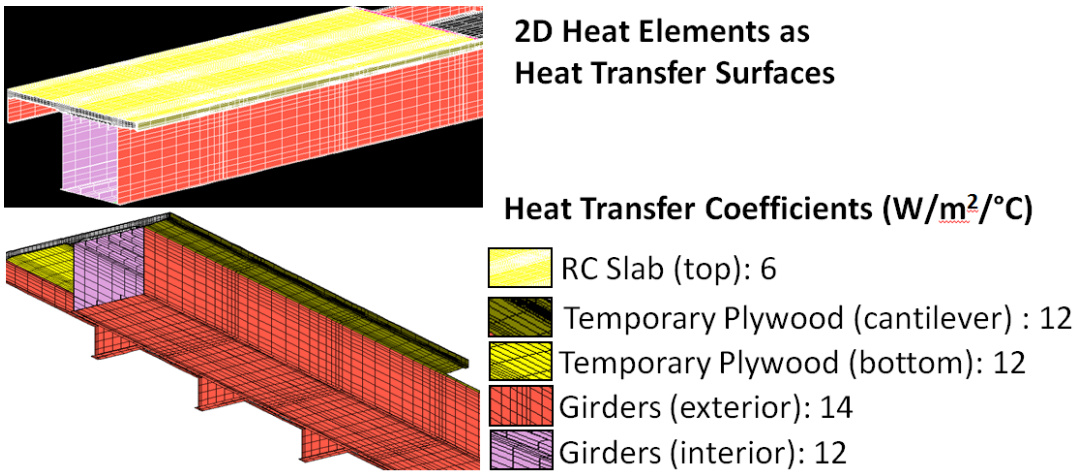

Fig.4.19(j) Heat transfer surfaces applied upon Shinkesen Ohashi FEM model

(4) Thermal Analysis Input

(a) Ambient temperature

The ambient temperature (Fig.4.19(k)) was recorded inside the main girder (Fig.4.18(c), location T). Radiation due to direct sunlight was observed in slab concrete temperature compared to the girder temperature (average temperature differences=7°C in day time); accordingly, calibrated ambient temperature was considered for top surface of the RC slab. Conversely, measured ambient temperature was applied on other heat transfer surfaces of the bridge.

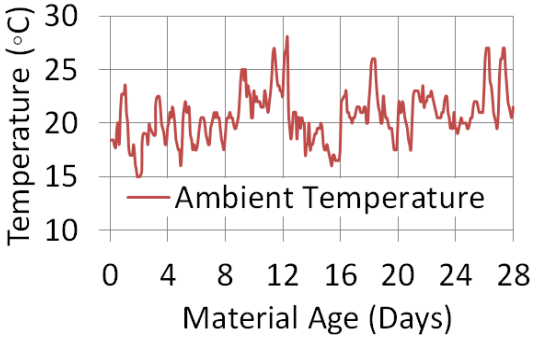

Fig.4.19(k) Measured and applied ambient temperature at the girder location T (in Fig.4.18(c))

(b) Adiabatic temperature rise model

The thermal behavior corresponding to concrete temperature in the RC deck slab concrete was calibrated following adiabatic temperature rise model (Eq.4.3) [6][7][8] and the monitored temperature data in the real bridge slab in the site comparing with the measured adiabatic temperature rise data for Shinkesen Ohashi deck concrete (Fig.4.19(l)). The ultimate adiabatic temperature rise and parameters were calculated based on the unit cement content=364 kg/m^3 and initial temperature of concrete=24°C.

$$Q(t) = Q_{\infty}\left[1 - \exp\left\{-r\left(t - t_{0,Q}\right)^{s}\right\}\right] \quad \text{(Time dependent equation)} \qquad \text{Eq.4.3}$$

Where, $Q(t)$=adiabatic temperature rise at age of t days (°C)

$Q\alpha(t)$=ultimate adiabatic temperature rise (°C) =58.82°C

r=0.975 and s=1, parameters representing the rate of adiabatic temperature rise

$t_{o,Q}$ = 0, age of starting of adiabatic temperature rise

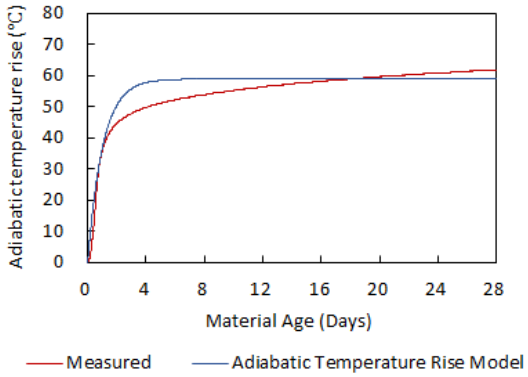

Fig.4.19(l) Comparison of the measured adiabatic temperature rise data with adiabatic temperature rise model[6][7][8] for Shinkesen Ohashi Bridge deck slab concrete

(5) Stress Analysis Input

Structural stress simulation inputs for concrete are same as the inputs for the member level verified models described previously. However, calibrated JSCE2012 equation (Eq.4.1(b)) was adopted to calculate the temperature dependent autogenous shrinkage. Thermal and some of mechanical properties for deck slab concrete, steel (reinforcing bars and girders), and plywood forms are summarized in Table 4.5.

(6) Starting Point of Thermal and Structural Stress Analysis

Concrete exhibits as a plastic material with a very large coefficient of thermal expansion and a large deformation capability during its initial period before hardening. The strain measurement results before the hardening of concrete incorporate very large strains and comparatively smaller stresses due to such plastic nature. These early stage measurements can also include undesirable strains for example due to the movement of formwork. Considering these facts, the starting point of the strain measurement was determined as the starting point of hardening that can be equivalent to the initial setting time of concrete.

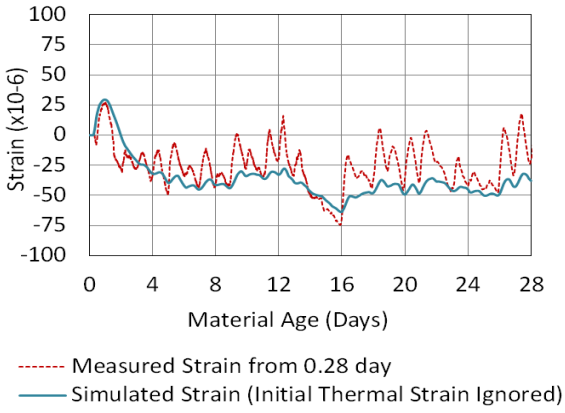

Fig.4.20(a) Comparison of simulation and measurement results in verification process ignoring initial thermal strain in the simulation until 0.28 day.

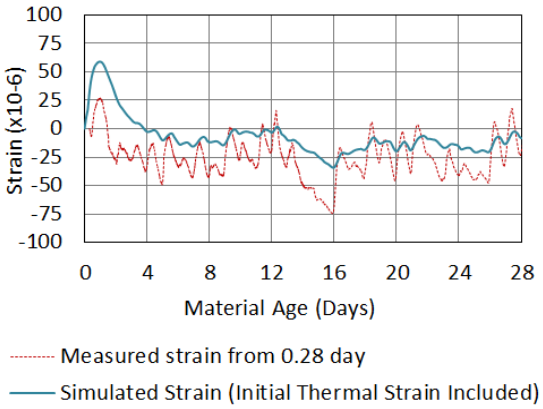

Fig.4.20(b) Significant differences between the measurement and the simulation as the initial thermal strain in very early age of concrete is taken into account in the simulation results.

In the real structural monitoring of Shinkesen RC slab, temperature measurement of concrete was started just after the concrete was placed at the location of thermocouples in the Lot 8 upon Pier 3. However, concrete strain measurement was started four hours after the finishing of the newly placed concrete at the same measurement location. It is confirmed that the starting time of strain measurement was 6 hours 50 minutes (0.28 day) later than the starting time of temperature measurement. The time lapse between temperature measurement and strain measurement is 0.28 day which also approximately corresponded to the initial setting time of Shinkesen Ohashi concrete (Lot-2016-Expan 20°C, initial setting time 6 hour 10 minutes (0.26 day)) acquired from the laboratory investigation depicted in Table 4.3. Furthermore, the Fig.4.18(g) and (h) explains the vertical strain measurement history at Lot 8 defining hardening point with respect to concrete temperature rise caused by the heat of hydration.

Since the temperature measurement was started just after concrete placing, thermal and structural stress analyses were started considering the same starting time of temperature measurement. However, starting time of strength development, autogenous shrinkage and expansion strain was considered from the 0.28 day material age of concrete in the structural stress simulation corresponding to the strain measurement starting time. It should be noted that the

simulated thermal strain from the starting time of analysis until the material age of 0.28 day was ignored in the verification process. Even though the simulations were started at the time of concrete placing, measurement results were compared from 0.28 day of concrete age as shown in Fig.4.20(a). Conversely Fig.4.20(b) represent the significant differences between the measured and the simulated strain when the initial thermal strain in the very early age of concrete is taken into account in representing the simulation results.

(7) Thermal and Structural Stress Analysis Results

(a) Simulation of Temperature and Strain for Structural Level Verification

Fig.4.21 (a), (b) and (c) depict satisfactorily good agreement (except radiation effect) between the simulated and the measured temperature history at G (steel girder), A (concrete upon girder) and B (concrete upon temporary plywood form) respectively. Moreover, simulation of longitudinal, transverse and vertical strains in concrete at A (upon girder) exhibit satisfactory agreement with corresponding measured strains (Fig.4.22 (a), (b), and (c)).

However, simulated vertical strain under in Fig. 4.22(c) represent that the input temperature dependent autogenous shrinkage acquired from calibrated JSCE2012 equation (Eq.4.1(b)) is larger than that occurred in Shinkesen Ohashi real slab under prolonged wet curing. Moreover, simulated concrete strains at C (upon permanent plywood forms) also confirm the similar expansion and contraction behaviour as measurements. Eventually the Shinkesen Ohashi bridge FEM model is validated for thermal stress analysis as well as for parametric studies forward.

(b) Simulation of Stress

The occurrence of maximum longitudinal stress (approximately 2.0 MPa) and transverse stress (1.0 MPa) is followed by the occurrence of maximum temperature in concrete at C upon permanent plywood forms (Fig.4.23(a), (b), and (c)). This reveals that thermal cracks might be initiated in concrete upon permanent plywood forms in few segments of the RC slab where cumulative structural tensile stress is large because of stepping construction of the bridge deck (Fig.4.8(c)). Furthermore, the effect of the stiffness of the rubber bearing was evaluated by comparing the simulated stress regarding upper bound (5200 MPa) and lower bound (1.5 MPa) of Young's modulus of the rubber bearing which revealed that higher stiffness of rubber bearing can increase the thermal stress in concrete when a large gradient of ambient temperature may occur (Fig.4.23(c).

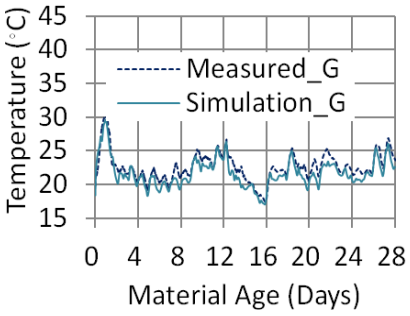

Fig.4.21(a) Simulation of girder temperature (G)

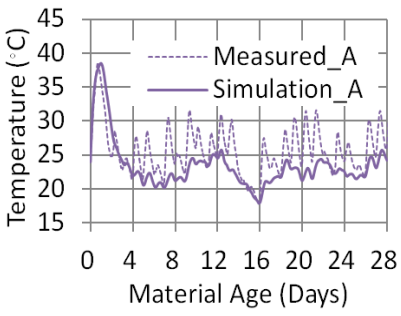

Fig.4.21(b) Simulation of concrete temperature (A)

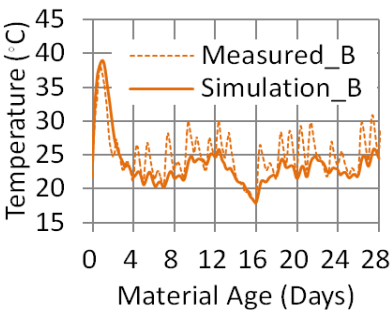

Fig.4.21(c) Simulation of concrete temperature (B)

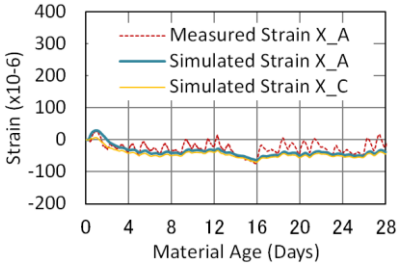

Fig.4.22(a) Simulation of longitudinal strain (X)

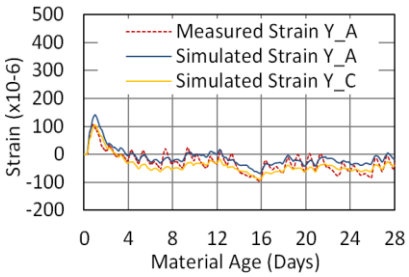

Fig.4.22(b) Simulation of transverse strain (Y)

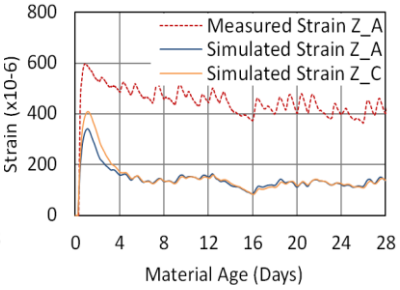

Fig.4.22(c) Simulation of vertical strain (Z)

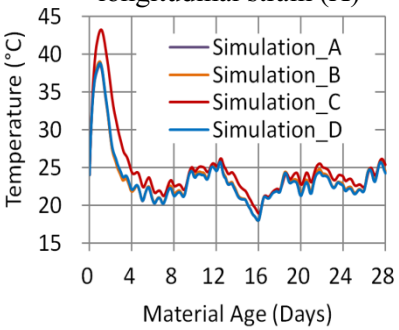

Fig.4.23(a) Simulation of temperature

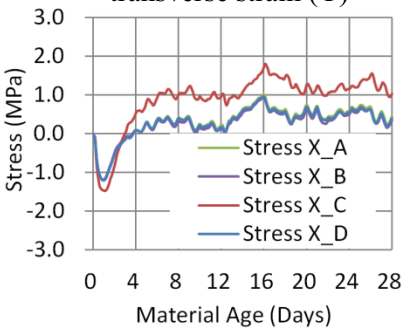

Fig.4.23(b) Simulation of longitudinal stresses

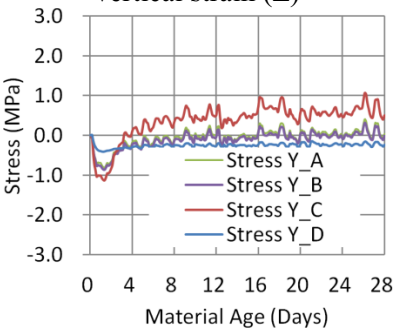

Fig.4.23(c) Simulation of transverse stresses

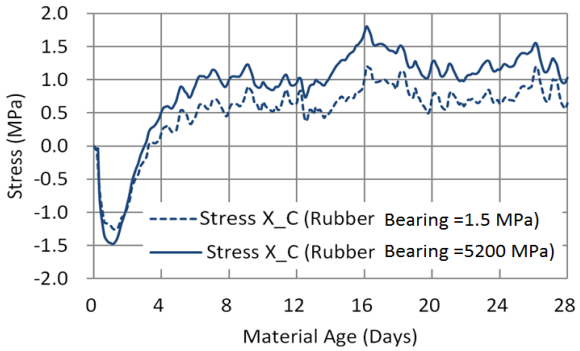

Fig.4.23(d) Effect of rubber bearing on simulated stresses

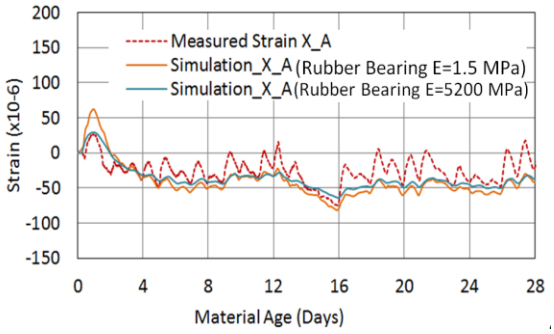

Fig.4.23(e) Effect of rubber bearing on simulated longitudinal strain

(c) Comparison of Simulation Results between JSCE2007[6] and JCI 2016[7] regarding Strength Development and Reduction Factors for Calculating Creep

In JSCE2007[6] and JCI2016[7], the compressive strength development is same, while JSCE2007 underestimates the Young's modulus development of concrete compared to the test results (Fig.4.10(a) and (b)). On the other hand, the reduction factors for the Young's modulus to consider the creep effect are different for JSCE2007 and JCI2016. For example, JSCE2017 consider φ(t) = 0.73 for temperature rising period (until 3 days of concrete material age) and φ(t) =1.00 for temperature decreasing period (from 5 days of concrete material age). Moreover, JCI2016 has specified $\varphi(t_e)$=0.42 until the temperature adjusted effective material age when temperature rise becomes the maximum and $\varphi(t_e)$=0.65 after one day in temperature adjusted effective material age as from the age at the maximum temperature.

Therefore, it is necessary to confirm the creep effect analysed for both JSCE2007 and JCI2016. From the comparison of strains and stresses in Fig 4.23(f) and Fig.4.23(g), it has been revealed that there are no significant differences of strains and stresses between the analysis results following JSCE2007 and JCI2016 guidelines. Therefore, it is confirmed that utilizing the reduction factors for the Young's modulus in JSCE2007 and JCI2016 corresponding to the strength and Young's modulus Equations respectively to consider the creep effect on the simulated stress will produce approximately same simulation output.

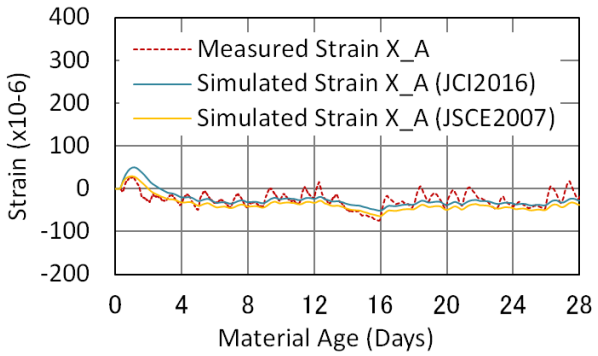

Fig.4.23(f) Comparison of longitudinal concrete strains obtained from analyses considering JSCE2007 and JCI2016 along with measured strain in Shinkesen Ohashi Bridge RC slab.

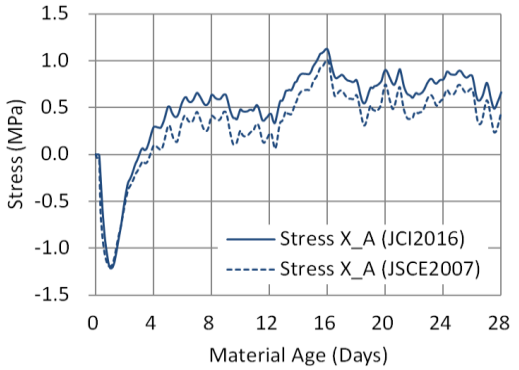

Fig.4.23(g) Comparison of longitudinal stresses at location A where RC slab directly connected to the box girder

(8) Brief Summary of the Structural Level Simulation of Shinkesen Ohashi RC Deck Slab

The three level systematic FEM simulation procedure followed in the present study was successfully verified in material and member level specimens and real structural level Shinkesen Ohashi bridge model in terms of concrete temperature and early age thermal and volumetric strains in RC slab concrete. The unique modeling approaches for permanent and temporary plywood forms, composite behavior of rubber bearing and appropriate 2D heat transfer surfaces are the significant factors for accurate thermal stress simulation. The calibrated expansion strain energy, calibrated autogenous shrinkage, reduction factors for Young's modulus considering creep effect and appropriate coefficients of thermal expansion of concrete were the key factors for obtaining satisfactory agreements in the simulation of thermal and structural stress. Simulation of stress in RC slab reveals the initiation of preliminary thermal cracks in concrete placed upon permanent plywood forms (location of maximum concrete temperature) different segments of the RC slab where the cumulative structural tensile stress was large because of stepping construction of the bridge deck.

4.3 VERIFICATION OF THE SYSTEMATIC FEM SIMULATION PROCEDURE UTILIZING THE FIELD MONITORING OF RC SLAB ON KOSANO VIADUCT

4.3.1 Construction and Cracking Scenerio of Kosano RC Slab

The construction of 260m long RC deck slab on the four continuous span non-composite steel girder Kosano Viaduct along general highway no.45 in Kamaishi was performed from 27th March 2018 to 20th April 2018 adopting multiple protection counter measures to secure highly

durable RC slab with special construction and curing methods such as appropriate concrete placement steps considering setting time of concrete and 28 days wet curing applying special curing mats to control thermal changes and prevent evaporation (Fig.4.25(a)). Stepping concrete placement was applied with sequential seven placement lots to minimize the structural stresses (Fig.4.26(a) and (b)). Instrumented monitoring of the RC slab has been continued to measure expansion and contraction behavior of concrete along longitudinal, transverse and vertical direction of the bridge deck (Fig.4.25(b)) regarding temperature, volumetric strains and effective stresses in concrete.

However, minor transvers cracks were appeared in Lot 1, Lot 2, Lot 5, Lot 6 and Lot 7 after completion of 28 days wet curing. The maximum crack width is 0.10 mm in Lot 5 where the tensile stress generation is large (1.3 MPa) due to stepping construction (Fig.4.25(a) and (b)). Similar to the Shinkesen Ohashi RC slab, primary cracks were generated initially in the concrete placed upon the permanent plywood forms.

Fig.4.24(a) Bird's eye plan view of Kosano site

Fig.4.24(b) Kosano Viaduct at Kamaishi, Iwate Prefecture

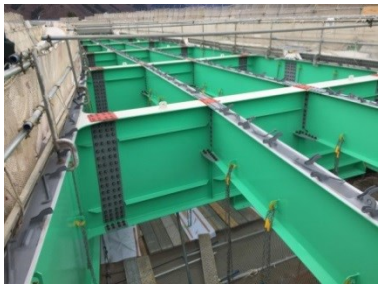

Fig.4.24(c) Four span continuous steel girders

Fig.4.24(d) Permanent and temporary plywood forms for RC slab

Fig.4.24(e) Steel reinforcement

Fig.4.24(f) Monitoring of concrete temperature, strain and stress

Fig.4.24(g) Durable concrete placing and compaction

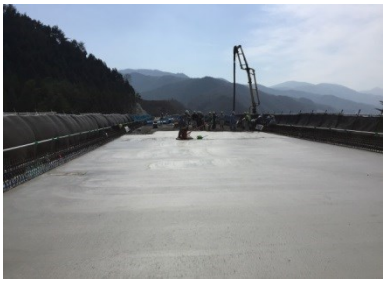

Fig.4.24(h) Finished surface of Kosano RC slab

Fig.4.24(i) 28 days wet curing of Kosano RC slab

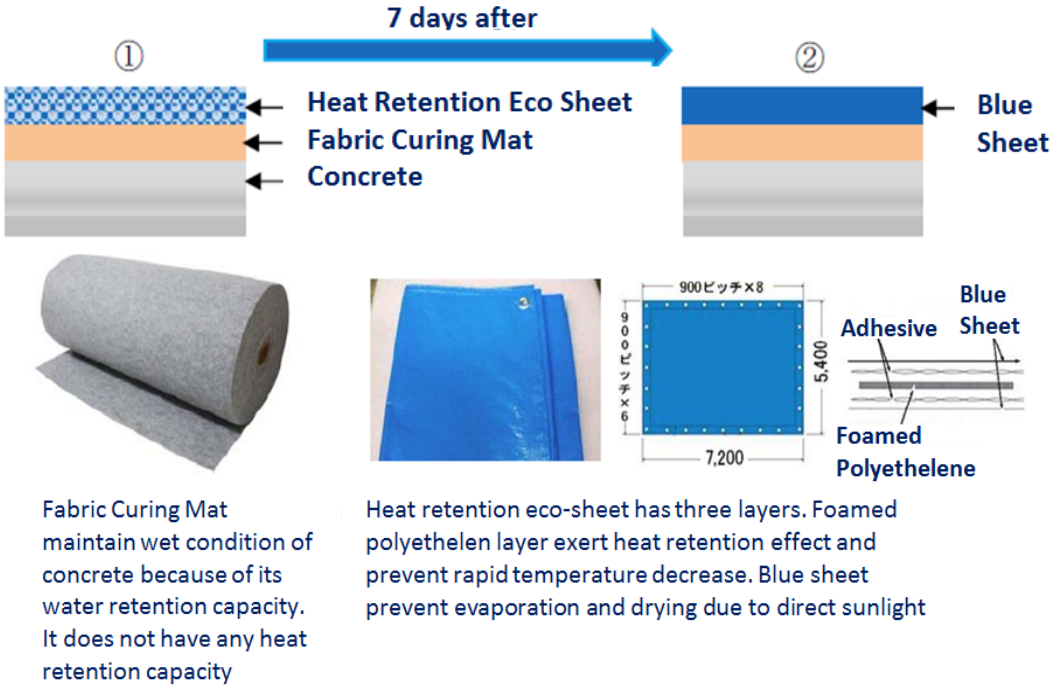

Fig.4.25(a) Special curing method applied in Kosano RC slab

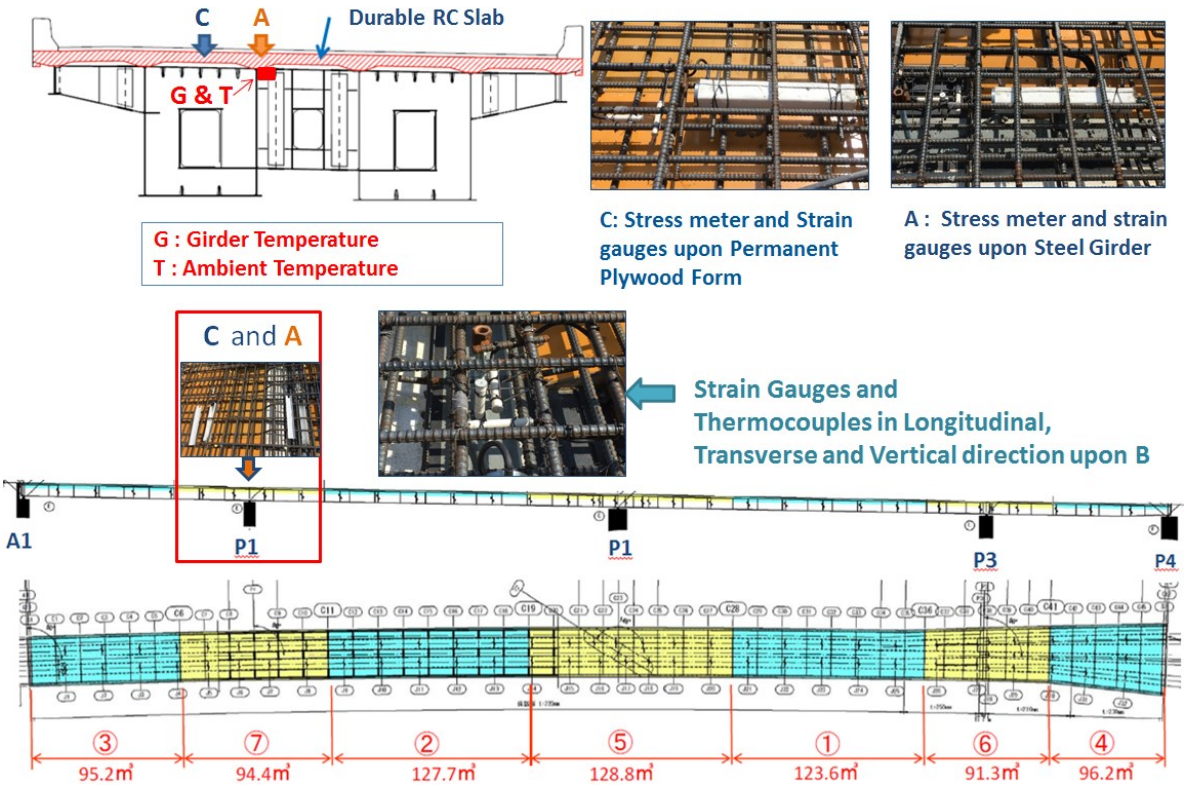

Fig.4.25(b) Instrumented monitoring regarding ambient, girder and concrete temperature, three directional concrete strain and effective stresses in concrete along the bridge axis

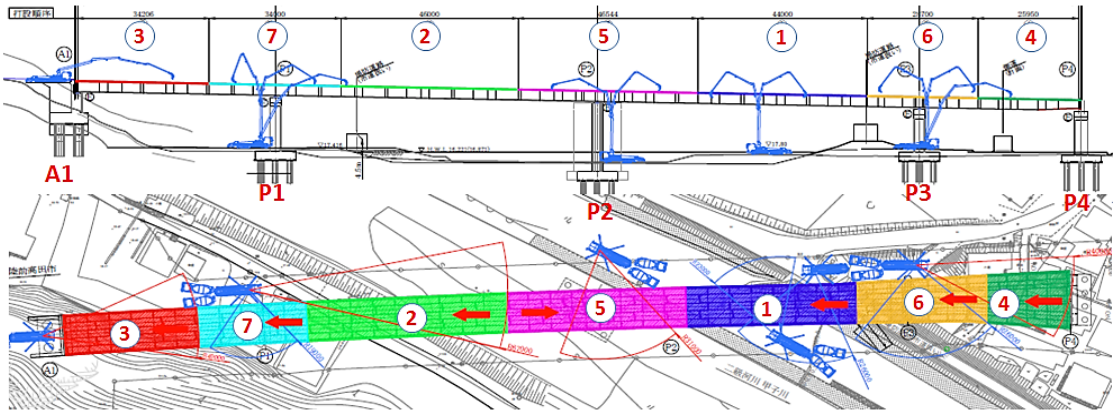

Fig.4.26(a) Stepping construction in seven concrete lots in Kosano RC slab

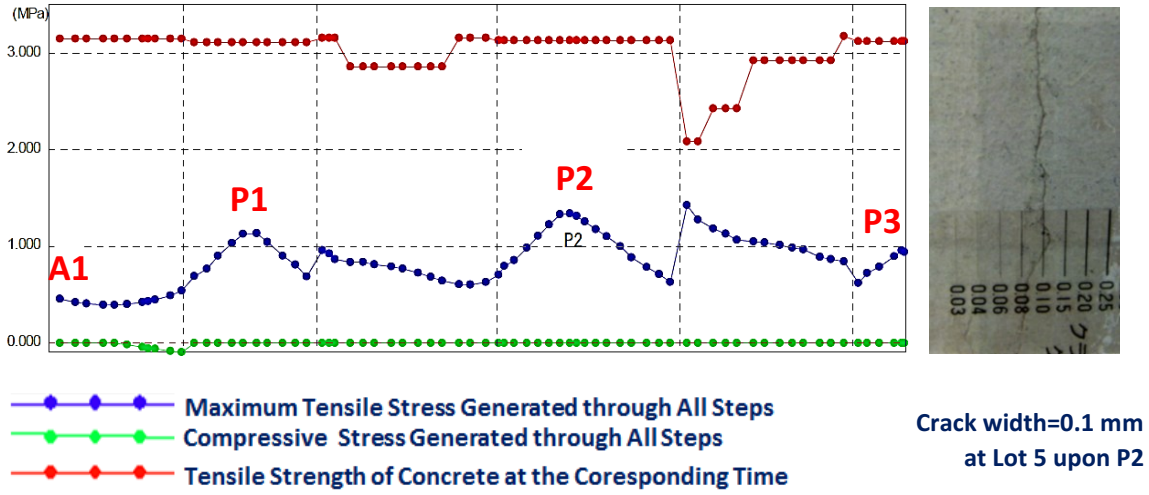

Fig.4.26(b) Generation of tensile stresses due to stepping construction

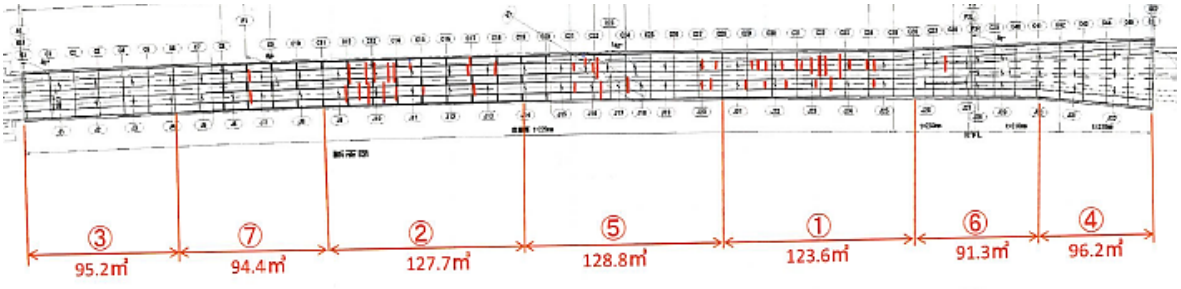

Fig.4.26(c) Crack map of Kosano RC slab

4.3.2 Comparison of Thermal Characteristics of Kosano RC Slab Concrete and Shinkesen RC Slab Concrete

The measured temperature and stresses in Kosano viaduct RC slab concrete upon steel girder (Location A) and upon permanent plywood form (Location C) were compared with the corresponding simulated temperature and stresses in Shinkesen RC slab concrete. The measured concrete temperature and stresses in Kosano RC slab concrete exhibited the same trends simulated in case of Shinkesen Ohashi RC slab (Fig.4.27(a), (b), (c) and (d)). Thus, the occurrence of highest temperature and thermal stress of concrete due to the hydration heat generation and low conductivity of the permanent plywood form was verified by the instrumented monitoring of Kosano RC slab which proved the applicability and efficiency of the three levelled systematic FEM simulation procedure for the full-scale structural simulation of the multiple span continuous steel girder bridges.

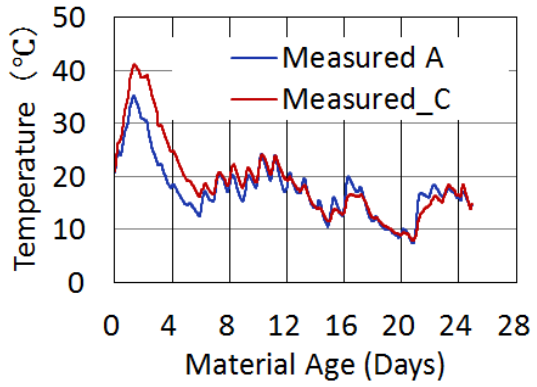

Fig.4.27(a) Measured temperature at location A and C in Kosano Viaduct RC Slab

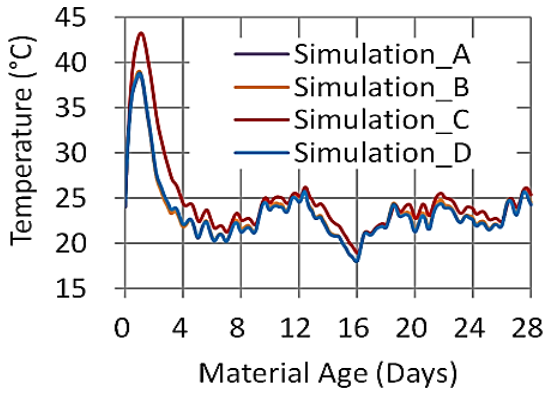

Fig.4.27(b) Simulation of temperature at location A, B, C, D in Shinkesen RC Slab

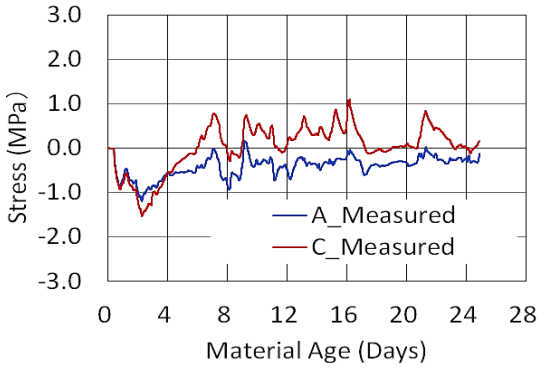

Fig.4.27(c) Measured lomgitudinal stresses at location A and C in Kosano Viaduct RC Slab

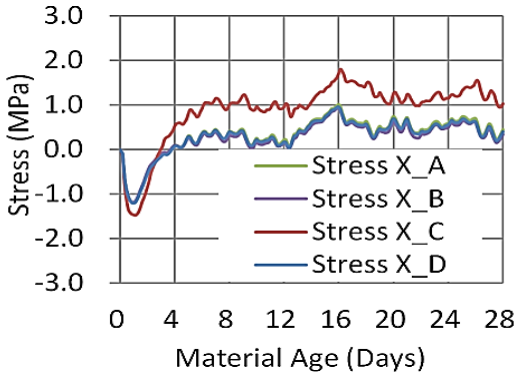

Fig.4.27(d) Simulation of longitudinal stresses at location A, B, C and D in Shinkesen RC slab

However, the three leveled systematic simulation procedure has been further applied in simulating the monitored temperature, strain and stress in Kosano RC slab concrete to confirm its applicability and generalization of the FEM models.

4.3.3 Level 1: Material Level Experimental Investigation and Modeling of Fundamental Properties of Kosano Viaduct RC Slab Concrete

Laboratory investigations were performed to determine some fundamental properties of Kosano concrete (Table 4.6) such as time dependent compressive strength development, Young's modulus development, Setting time, thermal expansion coefficient, adiabatic temperature rise and free autogenous shrinkage. The obtained properties were utilized for establishing concrete property models applicable for Kosano RC slab concrete as inputs in member level and real structural level FEM models.

Table 4.6 Concrete mix proportion for Kosano RC slab

Mix.	Design Slump (cm)	Design Air Content (%)	W/B (%)	W/C (%)	s/a (%)	Unit Weight (kg/m^3)							
						W	Slag Cement B	S1	S2	G1	G2	Ex	Admixture 15L
1	12 ±2.5	5～6	45.3	48.0	46.3	163	340	414	415	294	686	20	2.12
2	12 ±2.5	5～6	—	45.3	46.3	163	360	414	415	294	686	—	2.34

(1) Compressive Strength, Tensile Strength and Young's Modulus Development Model

Time dependent compressive strength development model for Kosano RC slab concrete was established according to JCI2016[7] (Eq.4.1(c)) with calibrated parameters such as a=4.5 and b=0.83 (Fig.4.27(a)). Accordingly, time dependent tensile strength and Young's modulus development models were fixed same as JCI2016[7] (Eq.4.1(d) and (e)) (Fig.4.27 (c)). Moreover, JSCE2007 models were also compared with the obtained test data (Fig.4.27(b) and (d)).

(2) Setting Time

According to the laboratory investigation initial and final setting time for Kosano RC slab concrete were 0.23 and 0.34 day respectively.

(3) Coefficient of Thermal Expansion

The coefficient of thermal expansion was determined as 7.5×10^{-6} according to the laboratory investigations.

(4) Adiabatic Temperature Rise

The maximum temperature rise of Kosano RC slab concrete was determined as 53.5°C in semi-adiabatic condition.

(5) Free Autogenous Shrinkage

The free autogenous shrinkage was measured in 20°C curing temperature and 60% relative humidity condition as well as in semi-adiabatic condition. Since the calibrated JSCE2012/JCI2016 equation (Eq. 4.2(b)) applied in Shinkesen Ohashi concrete showed good agreement with the test data for the Kosano RC slab concrete, Eq.4.2(b) is further adopted as Kosano concrete free autogenous shrinkage model.

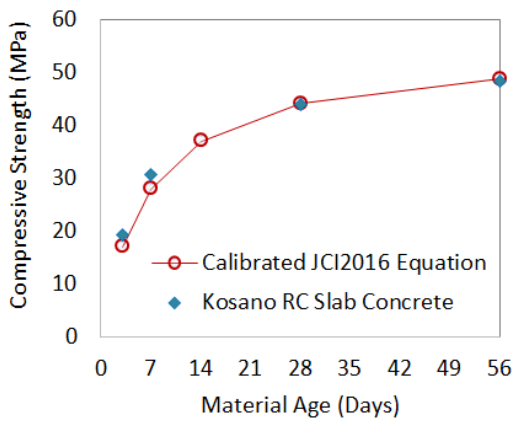

Fig.4.27(a) Calibrated JCI2016 compressive strength development model

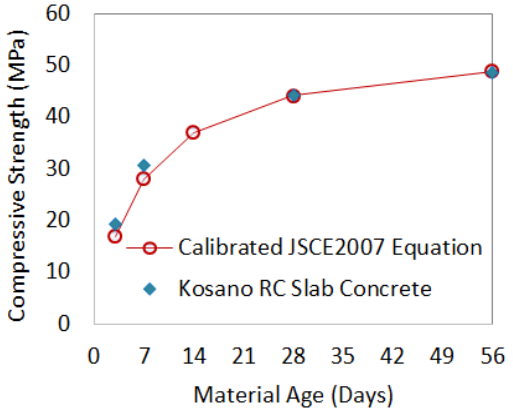

Fig.4.27(b) JSCE2007 compressive strength development model

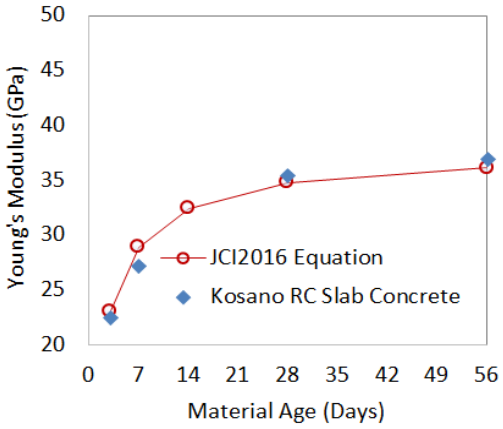

Fig.4.27(c) JCI2016 Young's modulus development model

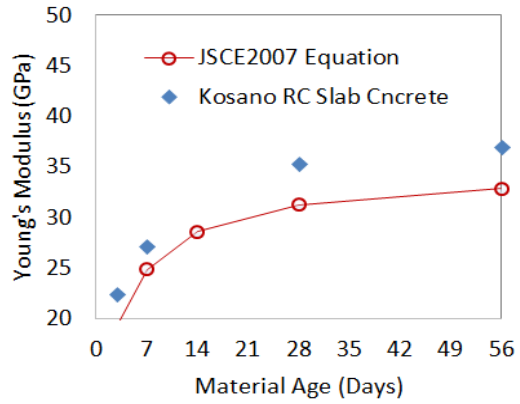

Fig.4.27(d) JSCE2007 Young's modulus development model

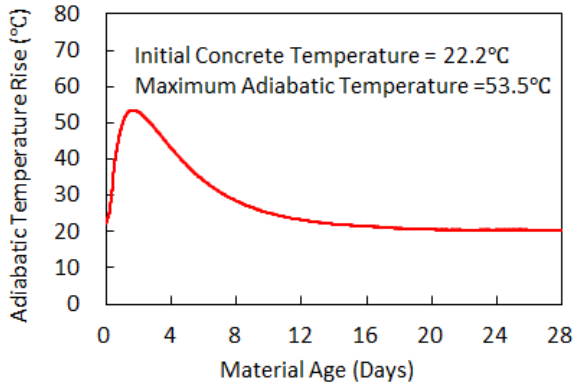

Fig.4.27(e) Temperature rise of Kosano concrete in Semi-adiabatic condition

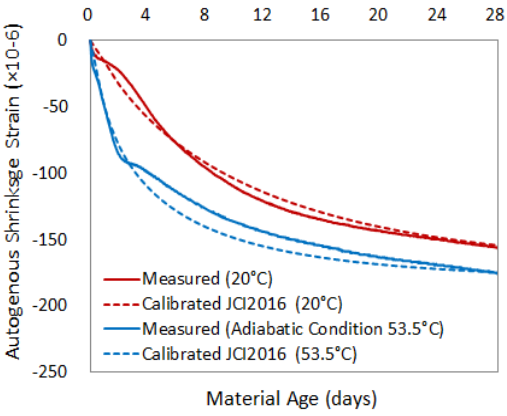

Fig.4.27(f) Calibrated JCI2016 autogenous shrinkage model according test data

Fig.4.27(g) Kosano RC slab concrete specimen measuring autogenous shrinkage and concrete temperature rise due to hydration heat under semi-adiabatic condition

4.3.4 Level 2: Member Level FEM Model Verification of Restrained Concrete Specimens

Expansion strain parameters regarding total expansion energy model[9] and reduction factors calculating effective Young's modulus to consider creep effect determined in restrained member level verifications of Shinkesen Ohashi concrete specimen models are further verified considering both JCI2016 and JSCE2007 strength development models for Kosano RC slab concrete restrained specimen models (Fig.4.28(a) to Fig.4.28(f)) as below:

(1) JIS A 6202 Restrained Expansion Strain FEM Model
(2) JCI-S-009-2012 Cylindrical Expansion Strain FEM Model
(3) Small RC Slab Specimen FEM Model

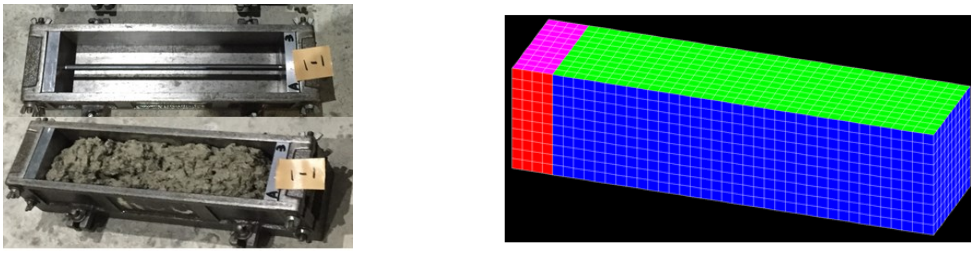

Fig.4.28(a) JIS A 6202 Restrained expansion strain specimen and FEM model for Kosano RC slab concrete

Fig.4.28(b) JCI-S-009-2012 cylindrical restrained expansion strain specimen and FEM model for Kosano RC slab concrete

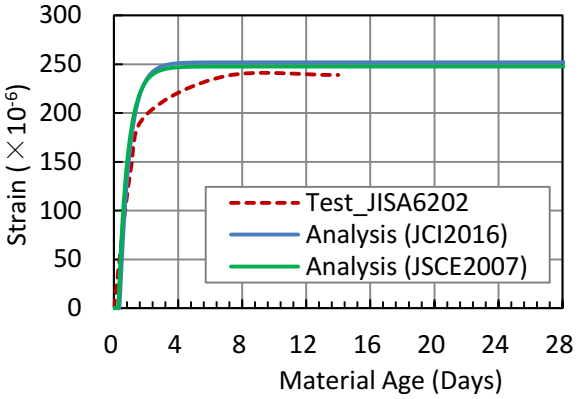

Fig.4.28(c) Verification of strain for JIS A 6202 restrained expansion strain specimen FEM model for Kosano RC slab concrete

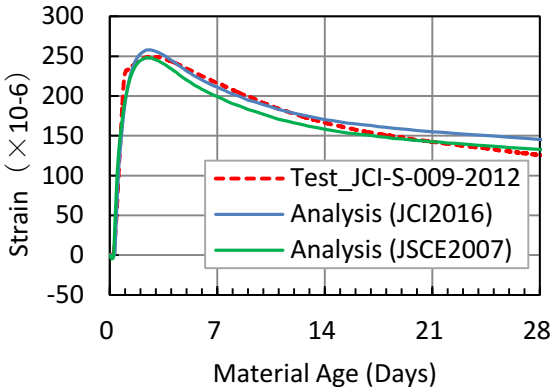

Fig.4.28(d) Verification of JCI-S-009-2012 cylindrical expansion strain specimen FEM model for Kosano RC slab concrete

Fig.4.28(e) Small RC slab specimens and FEM model regarding Kosano RC slab concrete

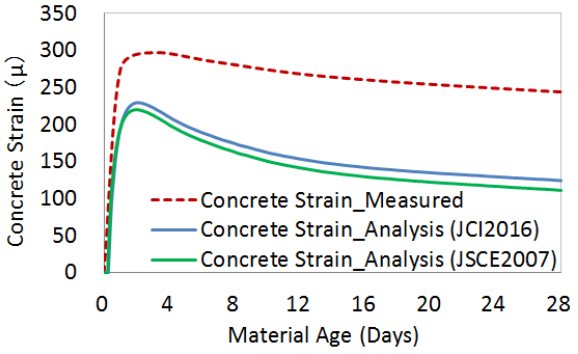

Fig.4.28(f) Simulation of concrete strain for small RC slab specimen for Kosano concrete mix

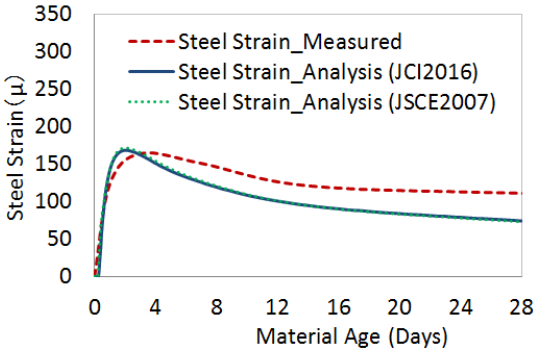

Fig.4.28(g) Simulation of steel strain for small RC slab specimen for Kosano concrete mix

Small RC slab specimens were prepared with Kosano concrete expansive additive to compare the restrained expansion behavior of concrete and steel. The top surfaces of the specimens were provided with 28 days wet curing while other surfaces were covered by plywood forms similar to the real Kosano deck slab. Simulation of concrete strain exhibited deviations from the measured value, mainly due to the input autogenous shrinkage model based on free autogenous shrinkage specimens under sealed curing. However, simulated steel strains showed

good agreement with that of measured strain. Thus the systematic FEM simulation system is further verified in restrained member level specimens for Kosano RC slab concrete.

4.3.5 Level 3: Structural Level Verification of Kosano Viaduct RC Slab FEM Model

(1) FEM modeling and Inputs for Thermal and Structural Stress Analysis

The full-scale real structural FEM model established for Shinkesen Ohashi bridge was utilized in structural level simulation of Kosano viaduct since the structural details of Kosano viaduct is quite similar to that of Shinkesen Ohashi bridge. The structural boundary conditions were kept same as Shinkesen Ohashi bridge. Structural modeling of permanent and temporary plywood forms as well as rubber bearing were also considered similar to Shinkesen Ohashi FEM model. Thermal boundaries are determined according to the ambient temperature, curing methods and exposure of the bridge components. The input ambient temperature measured at location G is shown in Fig.29.

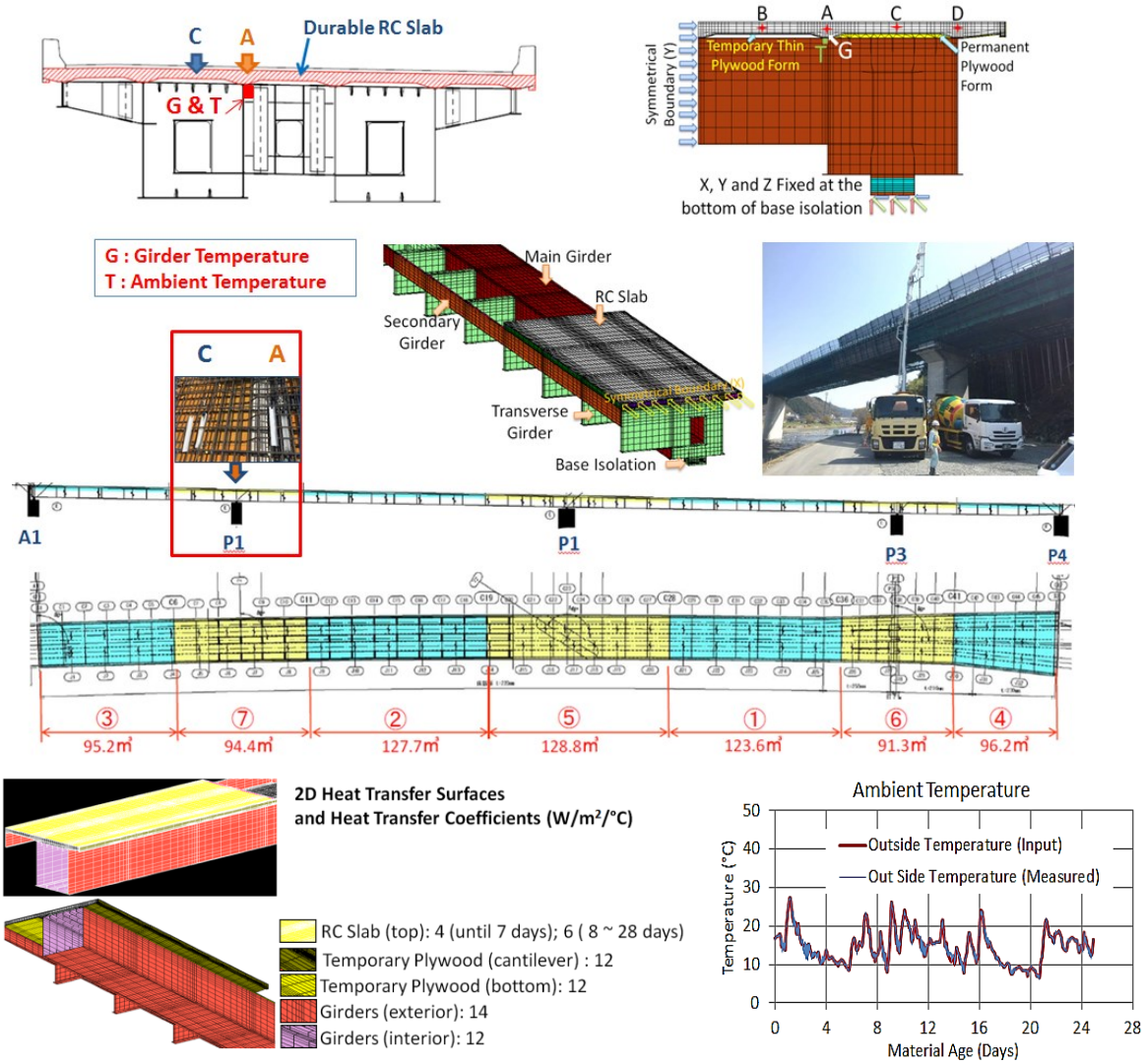

Fig.4.29 FEM full-scale structural modeling of Kosano Viaduct along structural and thermal boundary conditions

The material models established in Level 1 and parameters verified in Level 2 have been utilized in real structural simulation of Kosano Viaduct RC slab in Level 3. The thermal and mechanical properties depicted in Table 4.5 utilized in Shinkesen Ohashi Bridge model were given as inputs in Kosano Viaduct FEM model except the thermal expansion coefficient which was measured as 7.5×10^{-6} for Kosano RC slab concrete. Temperature, volumetric strains of concrete and steel as well as effective stress in concrete along the bridge axis were monitored in concrete Lot 7 upon Pier 1 (P1) in two different locations, such as in concrete upon permanent plywood (Location C) for and concrete upon steel girder (Location A).

(2) Starting Point of Thermal and Structural Stress Analysis

The hardening point of Lot 7 concrete placed upon Pier 1 of Kosano viaduct was determined as 0.42 day form the measured vertical strain with respect to temperature rise as well as concrete material age as shown in Fig.30(a) and (b). Although the thermal and structural stress analysis were started from the time of placing of concrete, the simulated strains and stresses were compared with the measured data from 0.42 days of concrete placement to avoid the unpredictable thermal behavior of concrete in very early age.

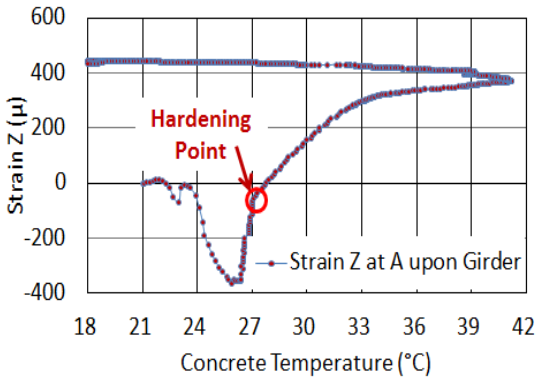

Fig.4.30(a) Vertical strain history defining hardening point with respect to concrete temperature rise due to hydration heat

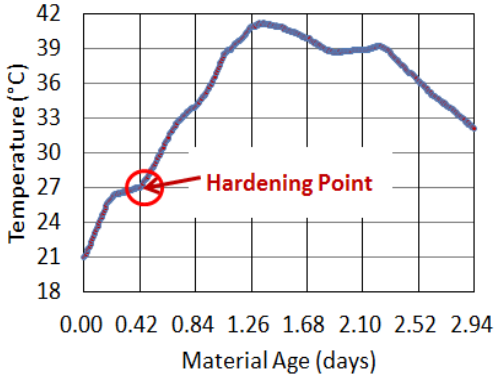

Fig.4.20(b) Temperature rise history and hardening time with respect to material age

(3) Thermal and Structural Stress Analysis Results

(a) Simulation of Temperature, Stresses and Three directional Strain regarding Kosano RC slab concrete

Fig.4.31 (a), (b) and (c) exhibit satisfactorily good agreement among the simulated and the measured temperature history at G (steel girder), A (concrete upon girder) and C (concrete upon permanent plywood form) respectively.

Fig.4.32 (a) represents the negligible effect of the stiffness of rubber bearing in simulation of longitudinal stress in Kosano RC slab.

The Kosano deck slab was wet cured until 28 days. Therefore, autogenous shrinkage in real slab is expected to be smaller than the input autogenous shrinkage model which was calibrated from the specimens under sealed curing. Fig.4.32 (b) represents the simulated longitudinal stress along bridge axis with smaller value of autogenous shrinkage (50% of the calibrated input autogenous shrinkage) showing satisfactory agreement with the measurement stress.

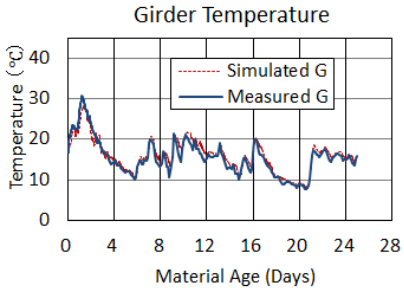

Fig.4.31(a) Simulation of girder temperature (G) of Kosano Viaduct

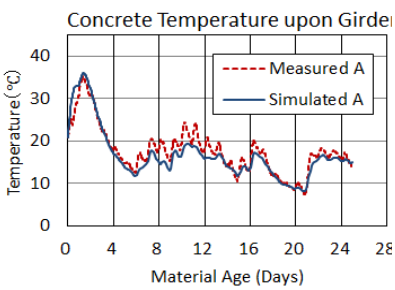

Fig.4.31(b) Simulation of concrete temperature

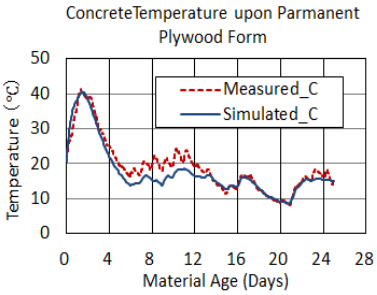

Fig.4.31(c) Simulation of concrete temperature

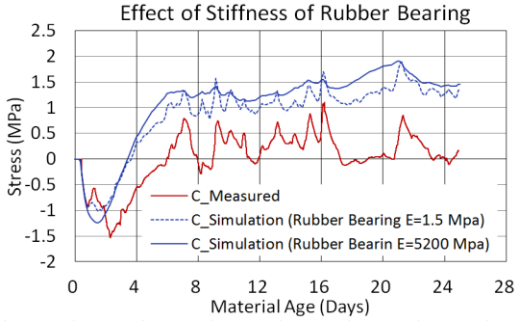

Fig.4.32(a) Effect of stiffness of rubber bearing on simulated stress along bridge axis of Kosano RC slab

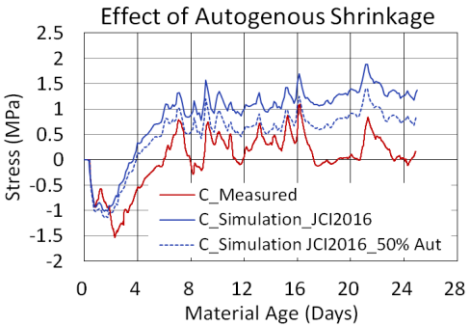

Fig.4.32(b) Effect of autogenous shrinkage on simulation of stress along bridge axis of Kosano RC slab

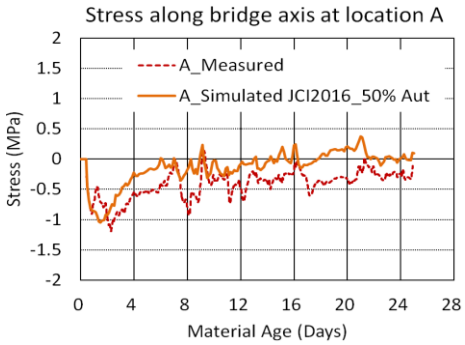

Fig.4.32(c) Simulation of concrete stress at location A along bridge axis (JCI2016)

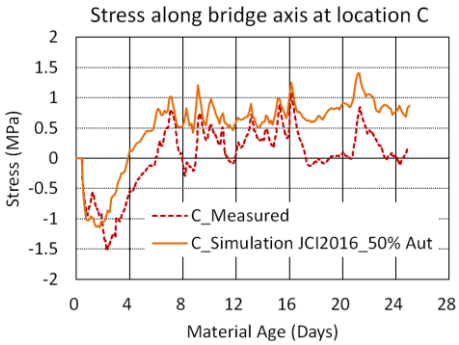

Fig.4.32(d) Simulation of concrete stress at location C along bridge axis (JCI2016)

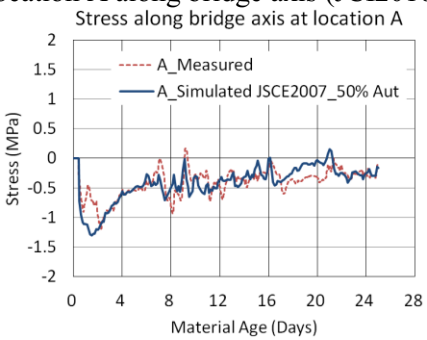

Fig.4.32(e) Simulation of concrete stress at location A along bridge axis (JSCE2007)

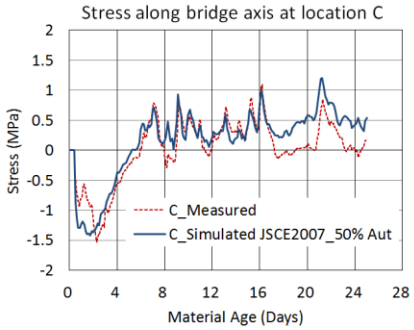

Fig.4.32(f) Simulation of concrete stress at location C along bridge axis (JSCE2007)

Fig.4.32(c), (d), (e) and (f) compare the simulated stress with low autogenous shrinkage considering both JCI2016 and JSCE2007 strength development model correspond to the reduction factors to calculate effective Young's modulus considering the effect of creep in early age. JSCR2007 showed comparatively good agreement due to the initial higher effective modulus compared to that of JCI2016. However, authors prefer JCI2016 guidelines since it can consider the temperature adjusted age of concrete in stress simulation. Finally, it can be conferred that the three levelled systematic analytical approach for FEM simulation of real structural model is successfully verified for Kosano Viaduct RC slab.

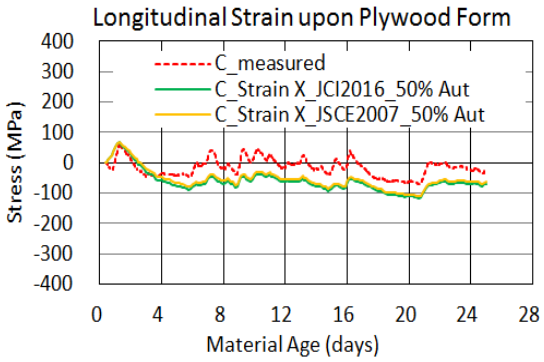

Fig.4.33(a) Simulation of longitudinal strain in concrete upon permanent plywood form

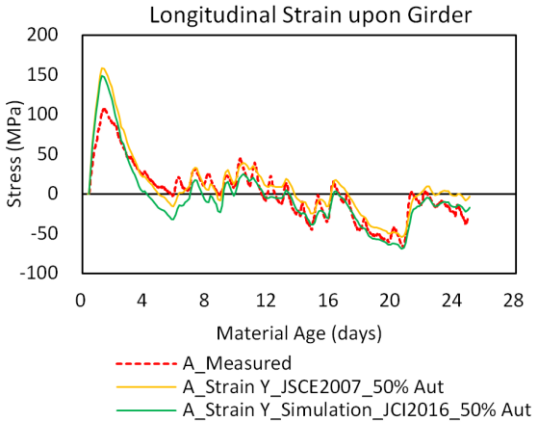

Fig.4.33(b) Simulation of transverse strain in concrete upon steel girder

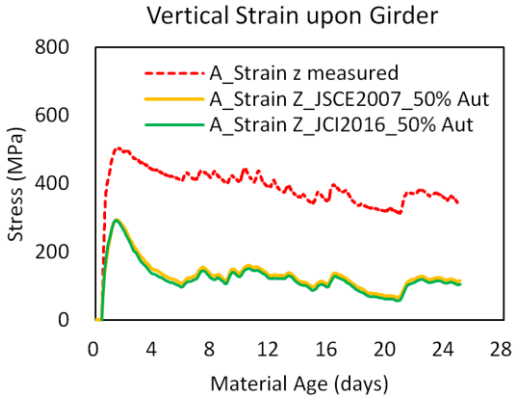

Fig.4.33(c) Simulation of vertical concrete strain upon steel girder

4.4 APPLICATION OF SYSTEMATIC FEM SIMULATION PROCEDURE IN THERMAL STRESS SIMULATION OF DURABLE RC SLAB ON PC COMPOSITE GIRDER BRIDGE (HIKOHEI BRIDGE)

Since the systematic FEM simulation procedure is successfully verified in material, member and real structural level in simulation the Shinkesen Ohashi Bridge RC slab model, the established FEM simulation procedure is applied in simulating the RC deck slab of the Hikohei Bridge. The RC deck slab for 43.7m long Hikohei bridge with post-tensioned segments PC girder bridge in Fukushima prefecture was initially planned to be constructed with concrete using ordinary Portland cement. Since, the RC bridge slabs of road infrastructures in cold regions of Japan are reported to be susceptible to severe deterioration, the multiple protection highly durable RC slab with blast furnace slag cement, expansive additive, higher air content, and low water-binder ratio (Table 4.6) was proposed in the construction of Hikohei bridge deck slab (Fig. 4.34(a)). The highly durable Hikohei bridge slab was constructed in July 2017 adopting special construction and curing methods i.e., appropriate construction steps considering setting time of concrete, providing shades for preventing solar radiation upon newly placed concrete, 28 days wet curing with double layered curing sheets etc (Fig. 4.34(b),(c),(d),and (e)). Eventually, there were no signs of early age thermal and shrinkage cracks and consecutive deterioration observed on the Hikohei bridge RC deck slab.In this context, the present section aims at simulating volumetric changes and thermal stresses in Hikohei bridge RC deck slab in FEM utilizing material properties obtained from laboratory investigations which were verified by the measurement data from the real structure following the similar systematic FEM simulation procedure established in case of the Shinkesen Ohashi Bridge RC slab simulation.

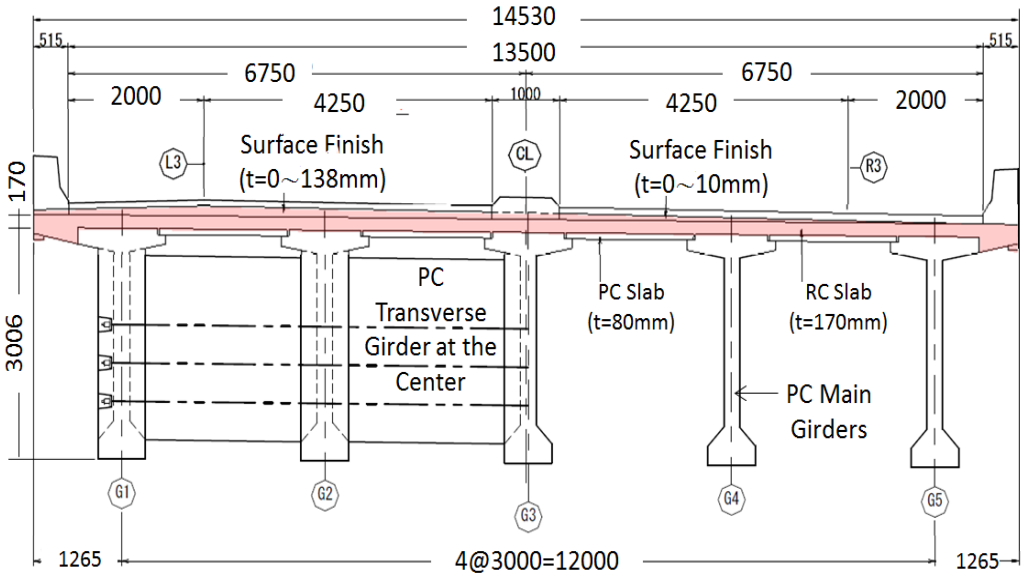

Fig.4.34(a) Colored portions indicate the application of durable concrete for deck slab on Hikohei bridge.

Fig.4.34(b) Providing shades for preventing solar radiation upon newly placed concrete.

Fig.4.34(c) Spraying water to keep the RC slab wet.

Fig.4.34(d) 28 days wet curing with double layered curing sheets.

Fig.4.34(e) RC slab was kept wet until 28 days.

Table 4.6 Concrete mix proportion for Hikohei bridge slab and test specimens

Concrete Mix	W/B %	s/a %	Air %	Unit Weight (kg/m^3)						
				W	C	Ex	S1	S2	G1	AE+Ad
Hikohei Design Value	45	44.4	5.0±1.5	173	365	20	382	376	410	3.85
BB	45	44.4	5.9	165	385	20	382	376	410	3.85
BBEX	45	44.4	6.7	172	365	20	382	376	410	3.85

4.4.1 Experimental Investigations to Determine the Material Properties of Hikohei Bridge RC Slab Concrete

The fundamental material properties such as time dependent compressive strength and Young's modulus development and free autogenous shrinkage of the proposed concrete mix were primarily evaluated by conducting material level investigations. At the same time, proctor penetration test and N-type penetration tests were performed in the site for predicting the actual setting time in advance before the construction of real Hikohei bridge deck slab. The concrete mix with and without expansive additive (BB=Blast furnace slag cement concrete without expansive additive and BBEX=Blast furnace slag cement concrete with expansive additive) were considered in the test investigations to evaluate the compressive strength and Young's modulus development and free autogenous shrinkage of the proposed concrete.

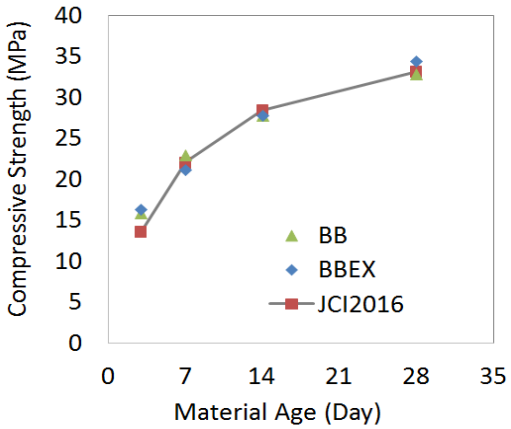

Fig.4.35(a) Compressive strength development

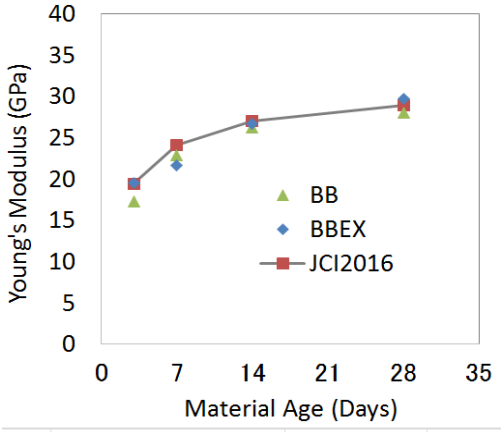

Fig.4.35(b) Young's modulus development

Fig. 4.35(c) Autogenous shrinkage specimens

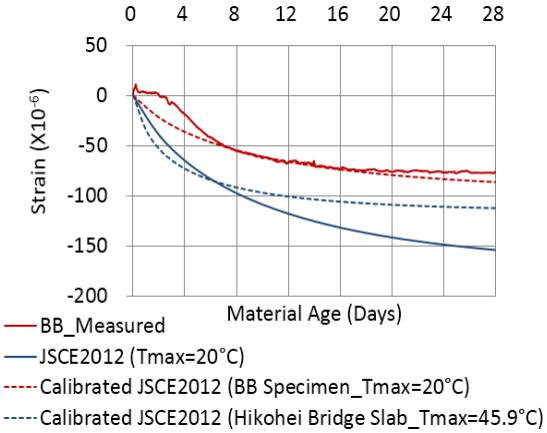

Fig. 4.35(d) Measured and calculated (modified JCI2016/JSCE2012 equation) autogenous shrinkage

(1) Compressive Strength and Young's Modulus

Time dependent compressive strength and Young's modulus development (JIS A 1108) of BBEX and BB concrete appeared to be of similar trend as shown in Fig.4.35(a) and (b). Calibrated JCI2016[7] equation for time dependent compressive strength (a=3.8 and b=0.7) and Young's modulus development (C_3=6000 and C_4=0.45) showed approximately good agreement with those of BB and BBEX, both equations(Eq.4.1(c) and Eq.4.1(e)) were applied in simulation of Hikohei bridge deck RC slab forward. Moreover, JCI2016[6] time dependent equations for development of tensile strength (Eq.4.1(d)) was also adopted in the stress analysis.

(2) Free Autogenous Shrinkage

The free autogenous shrinkage specimens were made with BB concrete in 100×100×400 mm steel molds in sealed condition at 20ºC constant curing temperature. Free shrinkage strain was measured with a low stiffness strain gauge embedded in the center of each specimen (Fig.4.35(c)). The maximum value of the measured autogenous shrinkage is around 76×10-6 whereas the autogenous shrinkage equation (Eq. 4.2(a) for blast furnace slag cement) recommended by JCI2016[7]/JSCE2012[8] considering the effect of maximum temperature produces larger value around 150×10^{-6} for BB concrete in 20°C constant curing temperature as

shown in Fig. 4.35(d). Since JCI2016 equation considering β=1 produces larger autogenous shrinkage, Eq. 4.2(a) has been scaled down by setting β=0.56 to simulate the measured autogenous shrinkage from BB concrete at 20°C temperature. Thus, calibrated JSCE2012 equation (β=0.56) considering the concrete temperature effect on autogenous shrinkage has been utilized in further simulation of Hikohei bridge deck slab instead of directly applying measured autogenous shrinkage obtained from BB concrete specimen (Fig. 4.35(d)).

(3) Setting Time Test

Both Proctor and N-type setting time test were conducted with BBEX concrete under real environmental condition at the Hikohei bridge site confirming initial setting time as 4.05 hour (0.17 day) and final setting time as 5.18 hour (0.22 day). Measurement data and simulation results were considered from 0.17 day to ignore the unpredictable thermal expansion during the very early age before initial setting of concrete which may behave as a plastic material with a large coefficient of thermal expansion having large deformation characteristics.

4.4.2 Finite Element Structural Model of Hikohei Bridge

The material properties obtained from the laboratory investigations along with some parametric assumptions were considered in simulating the model. Finally, the full-scale simulation procedure was validated by the measured concrete temperature and volume change in Hikohei bridge RC slab.

(1) Hikohei Deck Slab Construction and Field Measurement

Longitudinal (X, along bridge axis), transverse (Y) and vertical (Z) strains were measured in deck concrete upon PC girder and PC slab after concrete placement using embedded type strain gauges with thermocouples showed in Fig.4.36(a). The measured longitudinal, transverse and vertical strains along with concrete temperatures were utilized to validate the FEM model for early age (until 28th days of curing) and the simulation procedure adopted in the present research.

(2) Finite Element Model and Boundary Conditions

Hikohei post tensioned PC girder bridge consists of PC main girders, PC transverse end-girders, PC mid-span girder, PC slab (panels) and RC deck slab. As shown in Fig.4.36(b), RC deck slab was modeled with heat generating 3D solid elements whereas other components were modeled with non-heat generating 3D solid elements. The 1/4th portion of the simply supported Hikohei bridge was modeled with symmetric structural boundary conditions. Heat transfer coefficients for different heat transfer surfaces of the bridge were determined from parametric studies in thermal analysis considering the adopted curing methods (Fig.4.34(b),(c),(d) and (e)), exposure and location of the surfaces as summarized in Table 4.7. Thermal and some of mechanical properties for Hikohei slab concrete, PC girders and PC slabs are summarized in Table 4.8.

(3) Mesh Discretization in the Model

There were eight vertical finite element layers created in the RC slab (slab thickness=170mm). Thickness of the layers were increased from the heat transfer top surface to the center of the slab and again decreases from the center to the bottom heat conduction surface of the RC slab (Fig.4.36(c)). The thickness of the elements at heat transfer surface and heat conduction surface was kept small (5mm) for accurate temperature analysis considering heat transfer and heat conduction to different material. Simulation results for temperature can only be obtained from nodal points. In present simulation, the temperature results were obtained from

nodal points at the center of the RC slab along thickness direction. On the other hand, simulation results for stress and strain are acquired from the elements. Therefore, the aspect ratio of the elements at the central position along thickness direction in the RC slab was kept 1.25 to obtain satisfactory results with respect to stress analysis.

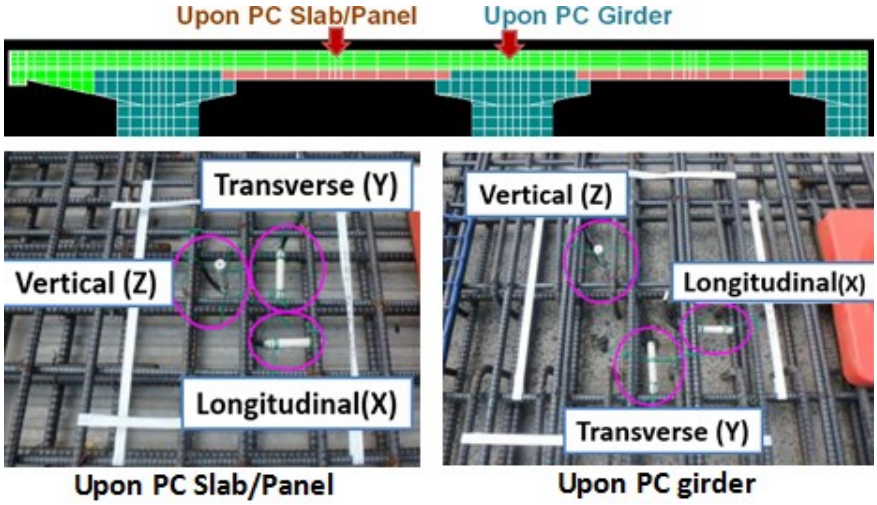

Fig.4.36(a) Locations of embedded strain gauges in slab

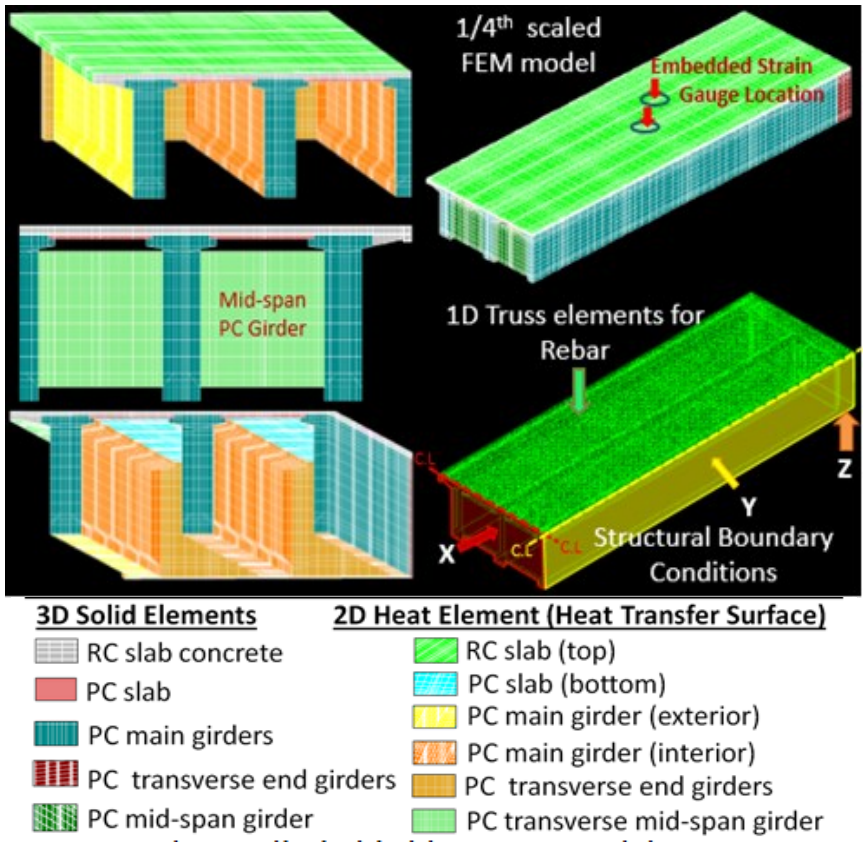

Fig.4.36(b) Hikohei bridge FEM model

Table 4.7 Input heat transfer coefficients for Hikohei bridge heat transfer surfaces

Heat Transfer Surface	Heat Transfer Coefficient (W/m^2°C)
RC slab (top)	6
PC slab (bottom)	8
PC main girder (exterior)	14
PC main girder (interior)	10
PC transvers end girder	10
PC transverse mid-span girder	8

Table 4.8 Input material properties for thermal and stress analysis for Hikohei bridge model

Properties	Deck Slab Concrete	Steel Bar	PC Girders	PC Slab
Heat Conductivity (W/m°C)	2.7	43	1.4	1.4
Specific Heat (kJ/kg°C)	1.15	0.47	1.15	1.15
Density (kg/m^3)	2300	7890	2300	2300
Initial Temperature (°C)	30.7	31	31	31
Young's Modulus (N/mm^2)	JCI2016	2x10^5	36600	36600
Poisson's Ratio	0.2	0.3	0.2	0.3
Coefficient of Thermal Expansion (X10^{-6}/°C)	9.3	10	10	10

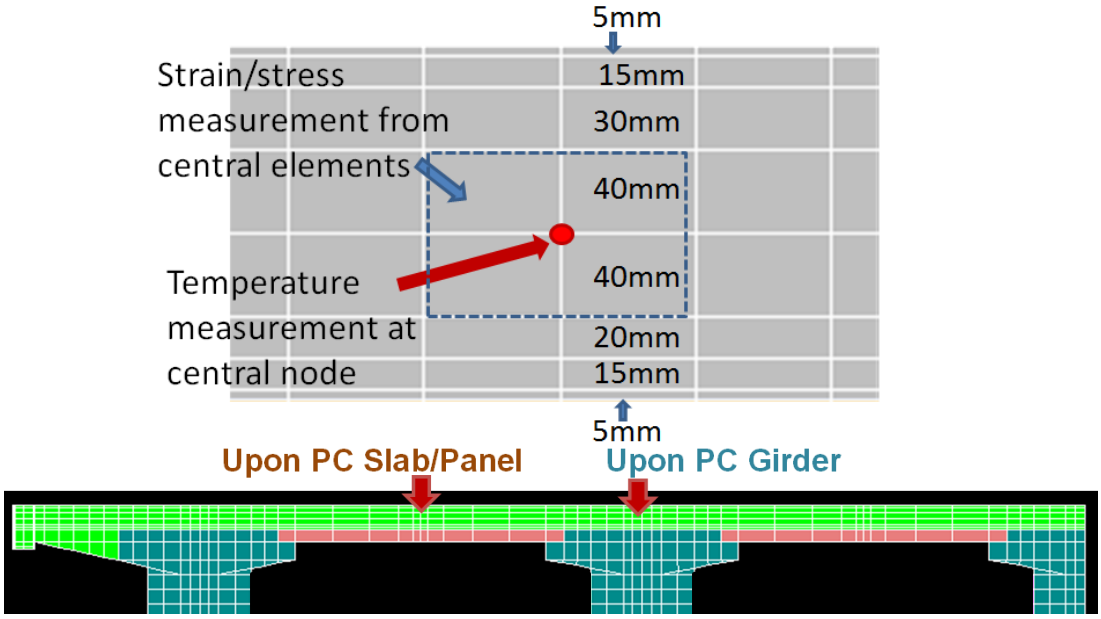

Fig.4.36(c) Mesh discretization at measurement locations

4.4.3 Input for Structural Stress Simulation

(1) Thermal Analysis Input

Calibrated JCI2016[7] Adiabatic temperature rise model was considered in thermal analysis. The ambient temperature history presented in Fig.4.36(a) recorded at the Hikohei bridge site was given as input.

(2) Compressive strength, tensile strength, Young's modulus

JSCE2016[7] time dependent equations (Eq.4.1(c), Eq.4.1(d) and Eq.4.1(e)) for compressive strength, tensile strength and Young's modulus development were adopted in the simulation.

(3) Autogenous Shrinkage Strain

Calibrated JCI2016/JSCE2012_Hikohei Bridge Slab_Tmax=45.9°C shown in Fig.4.35(d) is adopted in the simulation of Hikohei deck slab.

(4) Expansion Strain Energy model

Expansion strain model based on the total energy conservation hypothesis [9] was adopted in the present study to simulate the expansion strain due to the application of expansive additive. The expansion strain energy is obtained from the Eq.4.5. The parameters have been fixed as U_{∞}= 110x10-6, to=0.3, a=1.5 and b=1 for Hikohei bridge slab concrete conducting extensive parametric studies utilizing the strains measured along longitudinal (X), transverse (Y) and vertical (Z) axes.

(5) Creep Reduction Factors

The effect of early age creep of concrete was considered by reducing the Young's modulus of concrete at the age of temperature increasing and decreasing period as recommended in JCI2016[7].

4.4.4 Thermal and Structural Stress Analysis Results

(1) Simulation of Temperature and Strain in Hikohei Slab Concrete

Fig.4.36(b) and 4.36(c) depict the satisfactorily good agreement between the simulated and measured temperature history of deck concrete upon PC slab and PC girder respectively.Moreover, simulation of longitudinal and transverse strains exhibit substantially good agreement with the corresponding concrete strains measured upon PC slab and PC girder (Fig.4.37(a),(b) and Fig.4.38(a),(b). However, differences were observed in case of simulated vertical strains (Fig.4.23(c) and Fig.4.38(c)) seemingly caused by the larger input value of calibrated JCI2016/JSCE2012 autogenous shrinkage considering temperature effect compared to measured autogenous shrinkage in absence of vertical restraints due to reinforcing bars and underneath PC girders and slabs.

(2) Simulation of Stresses

(a) Stresses in Hikohei Bridge Deck Slab

Since the concrete temperature and volumetric strains are well simulated for Hikohei bridge deck RC slab, generation of stresses in the deck concrete upon PC slab and PC girder were evaluated to determine the cracking risk in early age. Fig.4.39(a) and (b) demonstrate the

simulated stresses generated along longitudinal (bridge axis) and transverse direction of the Hikohei deck slab. Maximum tensile stress generated along the bridge axis was 0.6 MPa whereas, there is no tensile stress generated along the transverses direction of the bride deck.

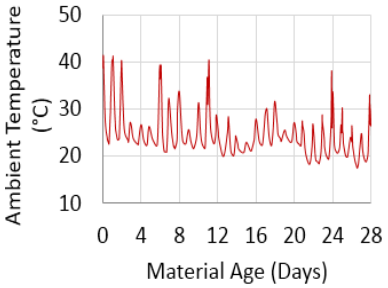

Fig.4.36(a) Recorded ambient temperature at Hikohei bridge site

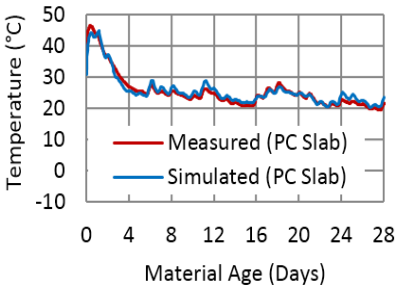

Fig.4.36(b) Simulation of concrete temperature upon PC slab

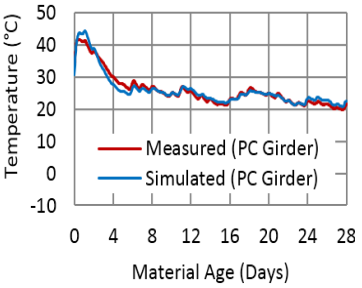

Fig.4.36(c) Simulation of concrete temperature upon PC girder

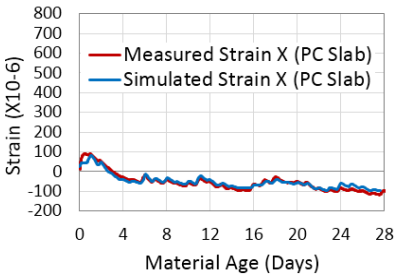

Fig. 4.37(a) Simulation of longitudinal (X) strain in concrete upon PC slab

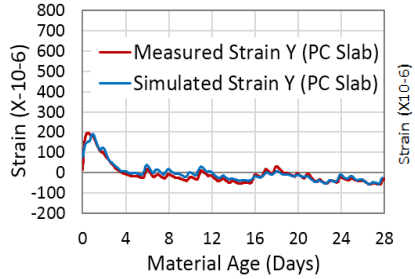

Fig. 4.37(b) Simulation of transverse (Y) strain in concrete upon PC slab

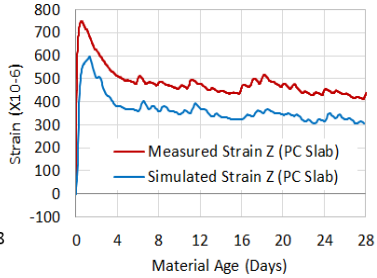

Fig. 4.37(c) Simulation of vertical (Z) strain in concrete upon PC slab

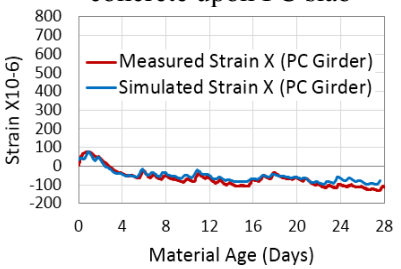

Fig. 4.38(a) Simulation of longitudinal (X) strain in concrete upon PC girder

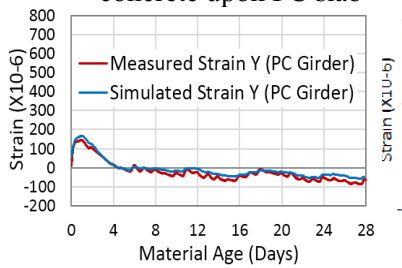

Fig. 4.38(b) Simulation of transverse (Y) strain in concrete upon PC girder

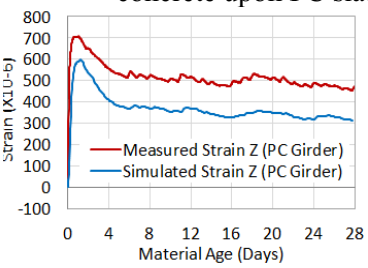

Fig. 4.38(c) Simulation of vertical (Z) strain in concrete upon PC girder

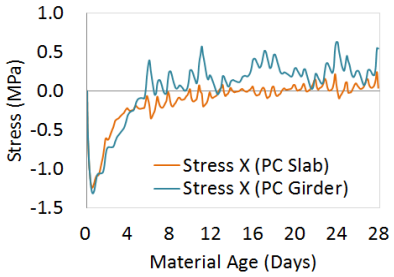

Fig.4.39(a) Simulation of longitudinal stress in concrete

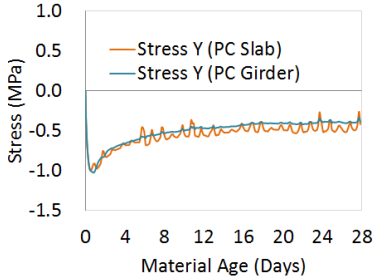

Fig. 4.39(b) Simulation of transverse stress in concrete

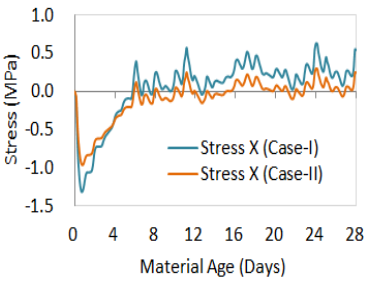

Fig.4.39(c) Effect of C.R.F on concrete stress upon PC girder

(b) Effect of Creep Reduction Factor

The effect of reduction factor on the restrained strains was confirmed by parametric study. Analysis was carried out applying increased value of R.F. i.e. 0.73 instead of 0.42 until the material age of maximum temperature (t_{max}) and 1.00 instead of 0.65 from one day after the maximum temperature (t_{max+1}) material age of concrete. Fig.9(c) demonstrates that the increase value of R.F. (Case-I) in early age has a considerable influence on reducing the simulated stresses in concrete compared to the JCI2016[7] recommendation (Case-II) adopted in the Hikohei bridge model.

4.4.5 Brief Summary of FEM Simulation of PC Composite Girder Bridge

The systematic simulation procedure for FEM analysis was successfully verified in real structural level simulation of Hikohei PC composite girder bridge in terms of concrete temperature and early age thermal and volumetric strains in RC deck slab concrete. The calibrated expansion strain energy, autogenous shrinkage, appropriate utilization of creep reduction factors and coefficients of thermal expansion of concrete were the key factors for obtaining good agreements in the simulation. Simulation of stresses in Hikohei bridge model confirmed the lower cracking risk of Hikohei deck slab concrete particularly due less structural restraint, low autogenous shrinkage and utilization of expansive additive.

4.5 SUMMARY OF CHAPTER 4

The aim of the present chapter was to evaluate the cracking risk of multiple span steel box girder Shinkesen Ohashi Bridge deck slab concrete by establishing accurate finite element models following the three leveled systematic analysis scheme for simulating thermal stress in the restrained slab. Moreover, the established three levelled systematic FEM simulation procedure was further applied and verified in simulating temperature, strains and stresses of Kosano Viaduct RC slab. Additionally, thermal and volumetric stresses in the single span PC composite girder Hikohei Bridge were also evaluated following the established FEM simulation system. The findings are summarized on the basis of three leveled simulation scheme are as follows:

(1) Level 1: Experimental Investigations for Establishing Concrete Material Models

(a) In Level-1 material models have be established for the highly durable concrete specially comprising of blast furnace slag cement and expansive additive regarding time dependent compressive strength, tensile strength and Young's modulus development based on the laboratory investigations utilizing calibrated JCI2016 Guidelines for Control of Cracking of Mass Concrete 2016.

(b) The adiabatic temperature rise and the autogenous shrinkage of the corresponding concrete were established with appropriate calibration of JCI2016 Guidelines for Control of Cracking of Mass Concrete 2016.

(c) Furthermore, initial and final setting time as well as the coefficient of thermal expansion (CTE) for the corresponding highly durable concrete were determined from the laboratory investigations.

(2) Level 2: FEM Numerical Simulation of Member Level Test Specimens

(a) The systematic FEM simulation method followed in the present study has been successfully verified in member levels in simulating the volume changes in the early age of concrete with slag cement and expansive additive utilizing the material models established in Level 1.

(b) It has been confirmed that the calibrated material parameters for total expansion strain energy model, experimentally obtained input autogenous shrinkage, appropriate utilization of creep reduction factors and confirmed time dependent compressive strength development of the concrete are the key factors for obtaining good agreements in FEM simulations for several material and member level specimens. Eventually, it can be conferred that the present simulation method followed by several material and member level verifications can be effectively applicable in real structural level simulation of FEM models for several bridges to evaluate the early age thermal and volumetric changes along with cracking risk of the RC deck slabs.

(3) Level 3: FEM Numerical Simulation of Bridges in Real Structural Level

(a) Multiple Span Steel Box Girder Bridge (Shinkesen Ohashi Bridge)

Simulation of stress in RC slab reveals the initiation of preliminary thermal cracks in concrete upon permanent plywood forms (location of maximum concrete temperature) in few segments of the RC slab where cumulative structural tensile stress was large because of stepping construction of the bridge deck.

(b) Multiple Span Steel Box Girder Bridge (Kosano Viaduct)

Field monitoring of Kosano Viaduct RC slab proved the wide range of applicability of the three leveled systematic verification system since the measured temperature and stresses in Kosano RC slab showed the same trends as simulated in case of Shinkesen RC slab. Measurement data and simulation of temperature, strains and stresses confirmed the most vulnerable section of RC slab located upon permanent plywood forms. The primary cracks tend to generate upon permanent plywood forms due to comparatively large thermal stresses coupled with structural tensile stresses due to stepping construction and propagate towards the central axis of the slab.

(c) Single Span PC Composite Girder Bridge (Hikohei Bridge)

Simulation of stresses in Hikohei bridge model confirmed the lower cracking risk of Hikohei deck slab concrete due to the low autogenous shrinkage and utilization of expansive additive. It is to be noted that concrete placement for the construction of the concerned RC deck slab was covered in a single day which reduced the risk of generating tensile stress unlike the multiple span Shinkesen bridge slab followed by stepping construction.

References

[1] Y. Tanaka, T. Ishida, I. Iwaki and K. Sato, "Multiple Protection Design for Durable Concrete Bridge Deck in Cold Regions," Journal of JSCE, vol. 5, pp. 68-77, 2017.

[2] Japan Concrete Institute, "Concrete Autogenous Shrinkage Study Group Report," 2002.

[3] Yokogawa Bridge Corporation, "Midterm Report on Highly Durable RC Slab Construction of National Highway 45 Shinkesen Bridge Slab Construction," 2015.

[4] Yokogawa Bridge Corporation, "Crack Investigation Report on Shinkesen Ohashi RC Slab," 2015.

[5] A. Hosoda, M. Morioka, M. Tanimura and T. Kanda, "Technical Committee on Performance Evaluation of High Performance Expansive Concrete and System for Crack Control," 2011.

[6] Japan Society of Civil Engineering, Standard Specifications for Design of Concrete Structures, JSCE, 2007.

[7] Japan Concrete Institute, JCI Guidelines for Control of Cracking of Mass Concrete, Tokyo, 2016.

[8] Japan Society of Civil Engineering, JSCE Standard Specifications for Concrete Structures, 2012.

[9] T. Tanabe and Y. Ishikawa, "Chemical Expansion Effect in Concrete and its Numerical Simulation Based on the Mechanical Energy Conservation Hypothesis," in JCI-RILEM International Workshop on Control of Mass Concrete and Related Issues Early Age Cracking of Structures (CONCRACK), Tokyo, 2017.

[10] http://www.oiles.co.jp/en/menshin/bridge/product/rb/, 23rd July, 2018.

[11] Alger, Mark. S. M.,: Polymer Science Dictionary (2nd ed.),Springer Publishing. ISBN 0412608707, 1997.

5

EFFECTS OF STRUCTURAL RESTRAINTS ON THE OCCURRENCE OF THERMAL STRESSES IN RC BRIDGE DECK SLABS

5.1 INTRODUCTION

The amount of volume change and the degree of restraint present in a bridge have a direct and interrelated effect on the amount of cracking that may develop in the deck slab. In this context, Chapter 5 aims at evaluating the effects of structural restraints on the occurrence of thermal stresses in RC deck slabs. In this current chapter comparative analyses were conducted in different aspects such span bridge types (single span and multiple continuous span), girder types (steel girders and PC composite girders) and support conditions (stiffness of rubber shoes) etc. The analyses results proved that cracking risk of the multiple span bridges is significantly higher than the singles span bridge since restraint against thermal movement is larger in multiple span bridges. Moreover, composite PC girder bridges exhibit better performances than the steel girder bridges as the coefficient of thermal expansion and Young's modulus for PC composite girders are similar to the supported RC slab. Therefore, PC girders provide less restraint in thermal movement of RC slab reducing the risk of cracking.

5.2 EFFECT OF RESTRAINTS DUE TO THE STEEL BOX GIRDER IN DIFFERENT SECTIONS OF THE RC SLAB

The systematic FEM simulation procedure was established for the multiple span continuous steel girder bridge (Shinkesen Ohashi Bridge) FEM model in Chapter 4. In the present chapter the effect of restraint exerted by the underneath steel box girder was evaluated on the basis of the generation of tensile stress in different location of the RC slab i.e., at middle, quarter and edge of Lot 8 (Fig.5.1(a)).

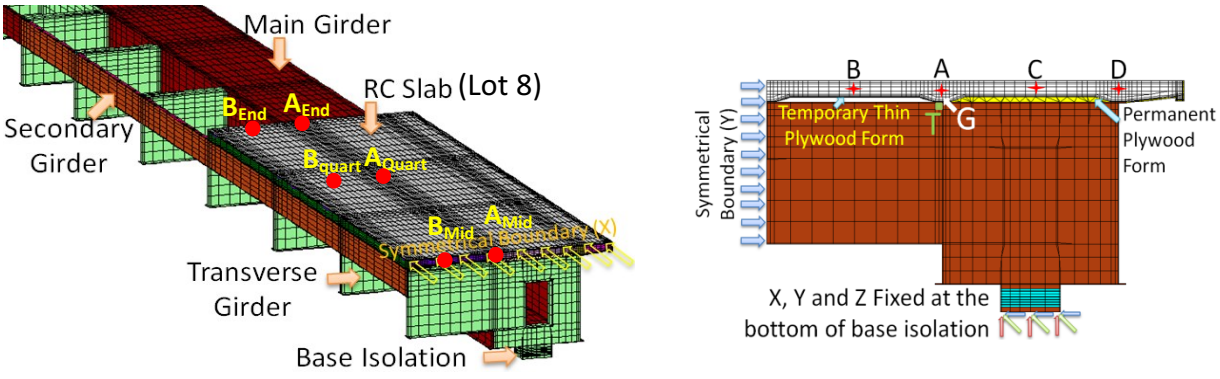

Fig.5.1(a) Position of simulated stress in concrete placement Lot 8 upon Pier 3 of Shinkesen Ohashi Bridge FEM model.

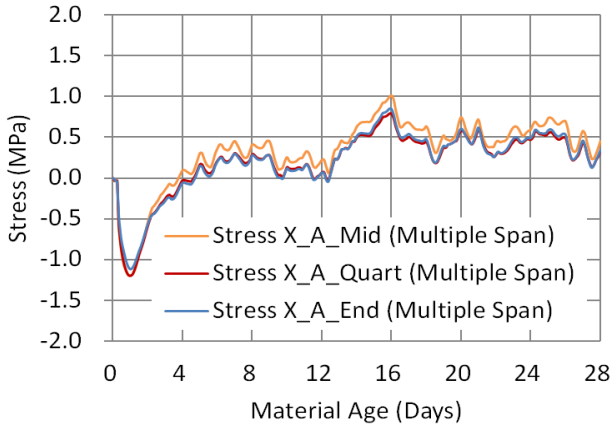

Fig.5.1(b) Simulated stresses along bridge axis at location A in the RC slab directly restrained by the girder.

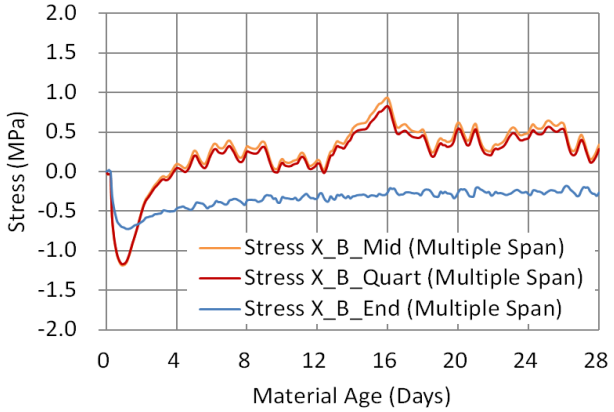

Fig.5.1(c) Simulated stresses along bridge axis at location B in the RC slab upon temporary plywood form.

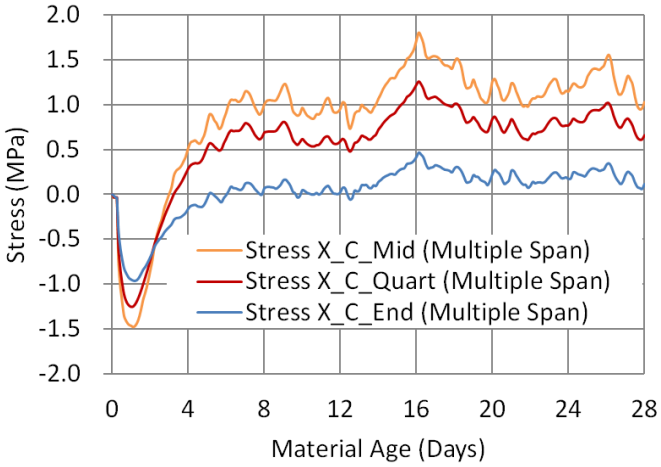

Fig.5.1(d) Simulated stresses along bridge axis at location C in the RC slab upon permanent plywood forms.

The simulated thermal stress in Fig.5.1(b) confirms that tensile stresses generated in RC slab directly restrained by the steel girder are approximately uniform in all sections of the deck slab. On the other hand, the tensile stresses generated in the slab concrete upon temporary and permanent plywood forms significantly reduce near the end of Lot 8 adjacent to the hardened concrete of Lot 1 (Fig.5.1(c) and (d)).

5.3 EFFECT OF THE STRUCTURAL TYPES OF BRIDGES: MULTIPLE SPAN CONTINUOUS STEEL GIRDER AND SINGLE SPAN STEEL GIRDER BRIDGES

The simulated tensile stresses in the RC slab on multiple span continuous steel girder bridge (Shinkesen Ohashi Bridge) FEM model was compared with the tensile stresses simulated in a single span FEM model (Fig.5.2(a)) considering the same structural components as the Shinkesen Ohashi bridge. Thermal and structural stress analysis inputs for the single span bridge model were same same as those established in the multiple span Shinkesen Ohashi Bridge model (Fig.5.2(b) and (c)). The heat transfer coefficients were also kept same as shown in Table 5.1.

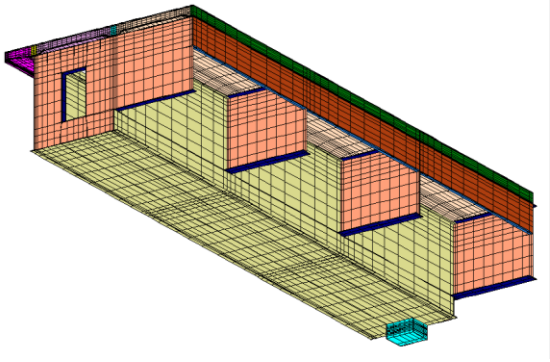

Fig.5.2(a) 1/4th single span FEM bridge model considering the same structural components of Shinkesen Ohashi Bridge.

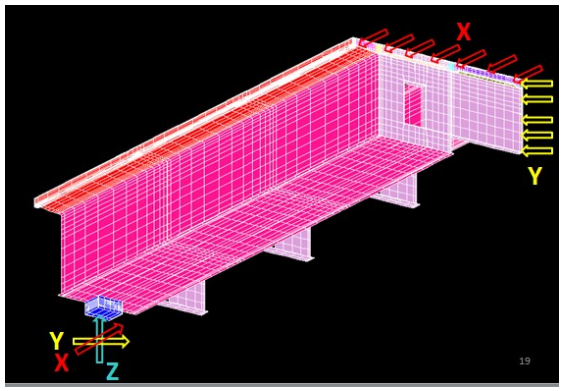

Fig.5.2(b) Structural boundary condition of the 1/4th single span FEM bridge model

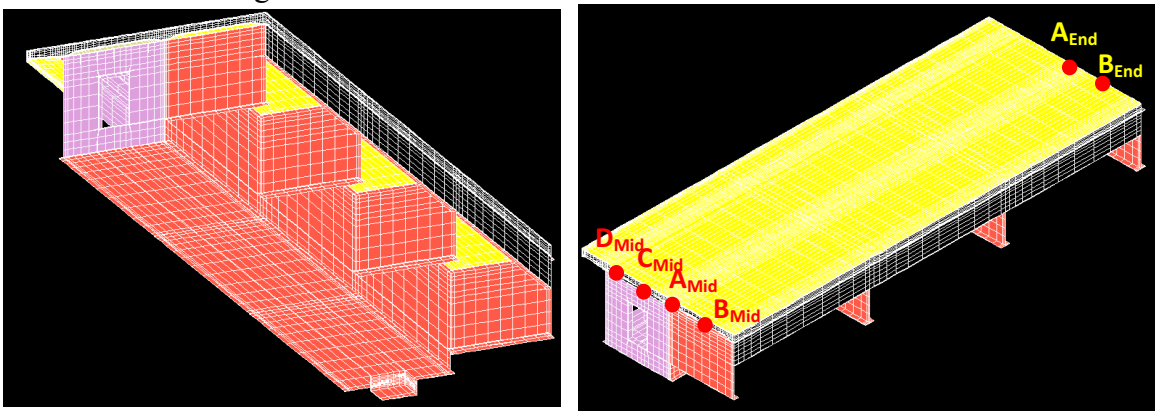

Fig.5.2(c) Heat transfer surfaces for RC slab top surface (yellow), temporary ply wood for (yellow), inner surface of the box girder (purple) and outer surface of box girder and transverse girders (orange) and the locations of simulation results.

Table 5.1 Input heat transfer coefficients for single span FEM bridge model

Heat Transfer Surface	Heat Transfer Coefficient (W/m^2°C)
RC slab (top) and cantilever	6
Temporary plywood for (bottom)	8
Main box girder (exterior)	14
Main box girder (interior)	12
Transvers girder	12
Secondary girders	12

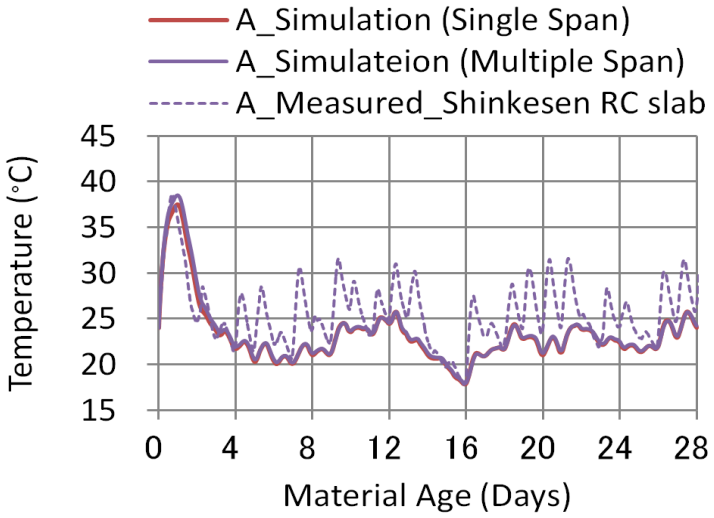

Fig.5.2(d) Simulation of temperature in RC slab at location A (mid-span) for the single span steel box girder bridge FEM model and comparison with the measured data as well as with the simulated temperature in multiple spans continuous girder Shinkesen Ohashi Bridge model.

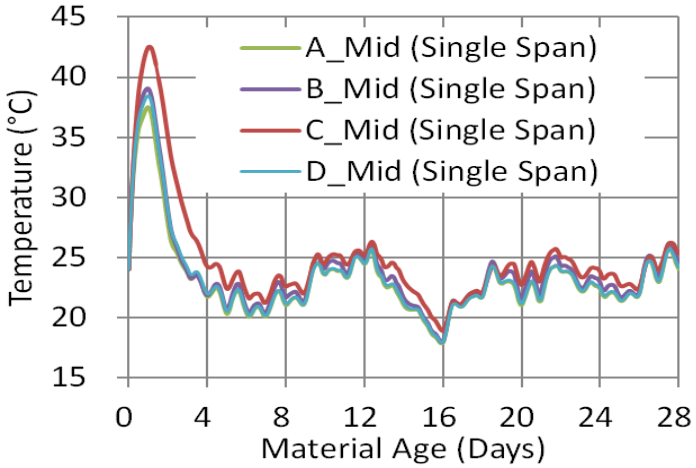

Fig.5.2(e) Simulation of temperature at mid-span in RC slab at location A, B, C and D for the single span steel box girder bridge FEM model.

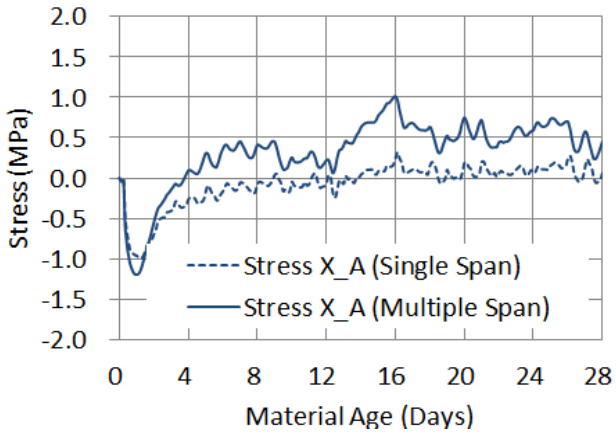

Fig.5.2(f) Comparison of simulated stresses along bridge axis at location A in RC slab directly restrained by the box girder for single span and multiple span continuous girder bridge models.

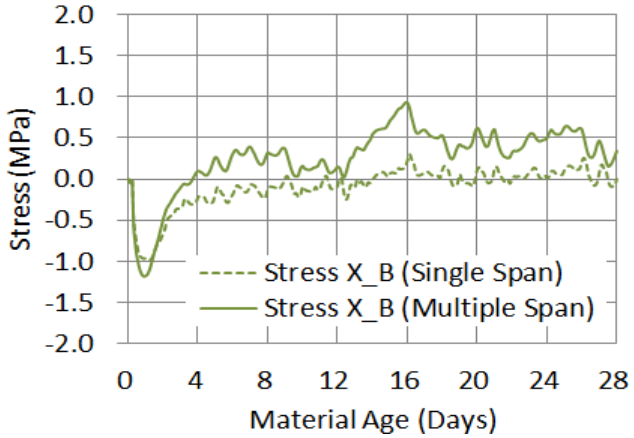

Fig.5.2(g) Comparison of simulated stresses along bridge axis at location B in RC slab upon temporary plywood form for single span and multiple span continuous girder bridge models.

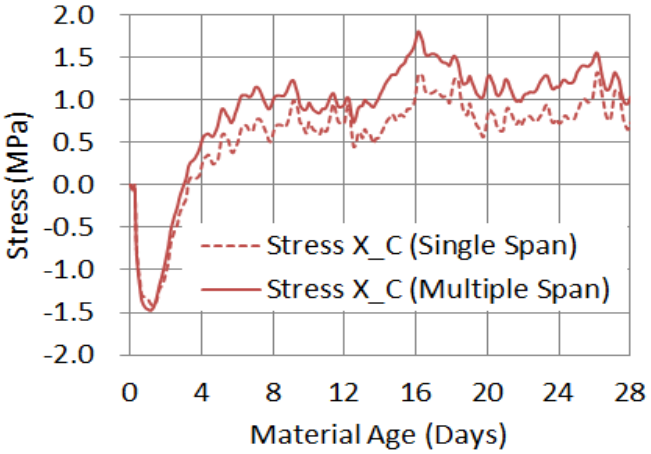

Fig.5.2(h) Comparison of simulated stresses along bridge axis at location C in RC slab upon permanent plywood form for single span and multiple span. continuous girder bridge models

5.3.1 Simulation of Temperature in Single Span FEM Steel Box Girder Bridge Model

In case of the single span steel box girder bridge model simulated temperature was approximately same as the measurement and the multiple span box girder FEM bridge model for the real Shinkesen Ohashi bridge (Fig.5.2(d)). Moreover, Fig.5.2(e) shows the simulated temperature in different location of the RC slab at mid-span. Therefore, the comparison of the simulated thermal and volumetric stresses between the the single span and the multiple span bridge models were validated.

5.3.2 Simulated Stresses in Single Span FEM Steel Box Girder Bridge Model

Fig.5.2(f),(g) and (h) illustrate the comparison of thermal and volumetric stresses developed in the RC slab for the single span steel box girder and multiple span continuous girder FEM models at locations A, B and C at the middle of the span. The simulated stresses for the single span steel box girder bridge model in each three locations are around 0.75 MPa smaller than the stresses acquired from the multiple span continuous steel box girder bridge FEM model simulation.

Therefore, it can be conferred that in case of the multiple span continuous steel girder bridges structural restraints are higher than the single span bridges.

5.4 EFFECT OF THE STIFFNESS OF THE RUBBER BEARING (SEISMIC BASE ISOLATION) ON THE SIMULATION OF THERMAL STRESS

The effect of the stiffness of the rubber bearing (base isolation) was evaluated by comparing the simulation results with the different Young's modulus of the rubber bearing model, for example, considering the Young's modulus of rubber= 1.47 MPa and Young's modulus of lead plug=13000 MPa. It is to be noted that since the existence of lead plug can reduce the lateral response of multilayer rubber bearing, Young's modulus of lead plug has been considered to confirm the effect of lead plug.

In the comparison of longitudinal strain (X, along bridge axis) and the transverse strain (Y), less restraint to thermal movement of the bridge deck was observed in case of the lower stiffness of the rubber shoe (E=1.47 MPa) in Fig.5.3(a) and (b) respectively. In this consequence, in case of simulated tensile stresses the model comprising of the larger Young's modulus of the composite rubber bearing exhibited considerable increase in tensile stresses (Fig.5.3(c) and (d)) when abrupt change of temperature was recorded .

Therefore, it has been confirmed that, appropriate modeling of rubber bearing or end restraints is indispensable for the simulation of thermal stresses.

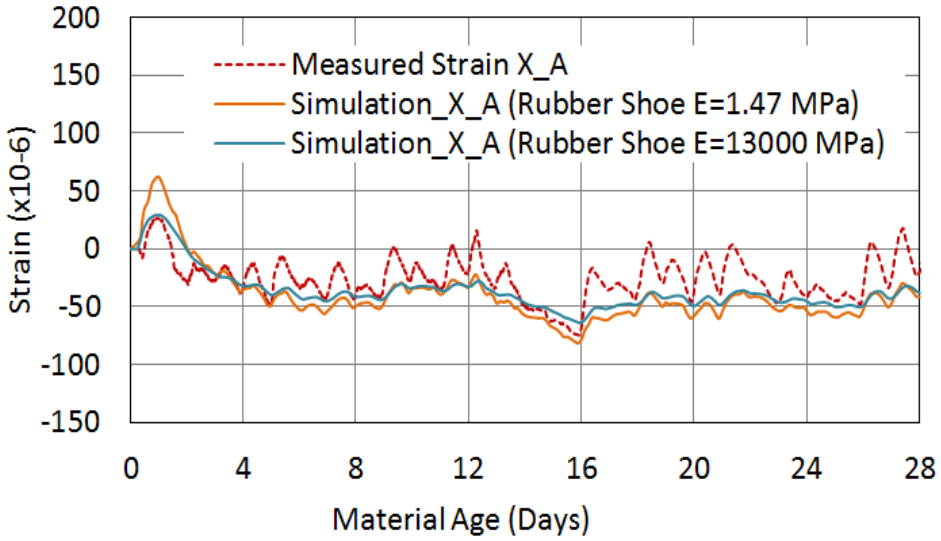

Fig.5.3(a) Longitudinal strains at location A for different Young' modulus of the rubber bearing (seismic base isolation).

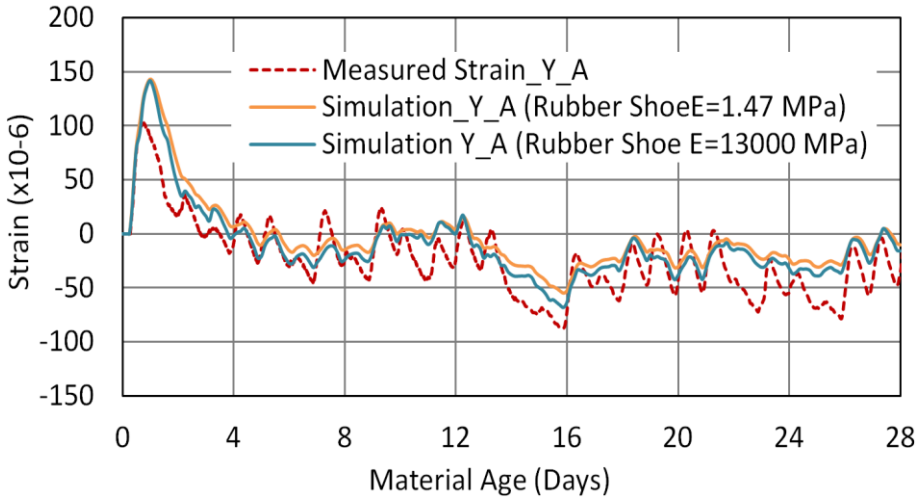

Fig.5.3(b) Transverse strains at location C for different Young' modulus of the rubber bearing (seismic base isolation).

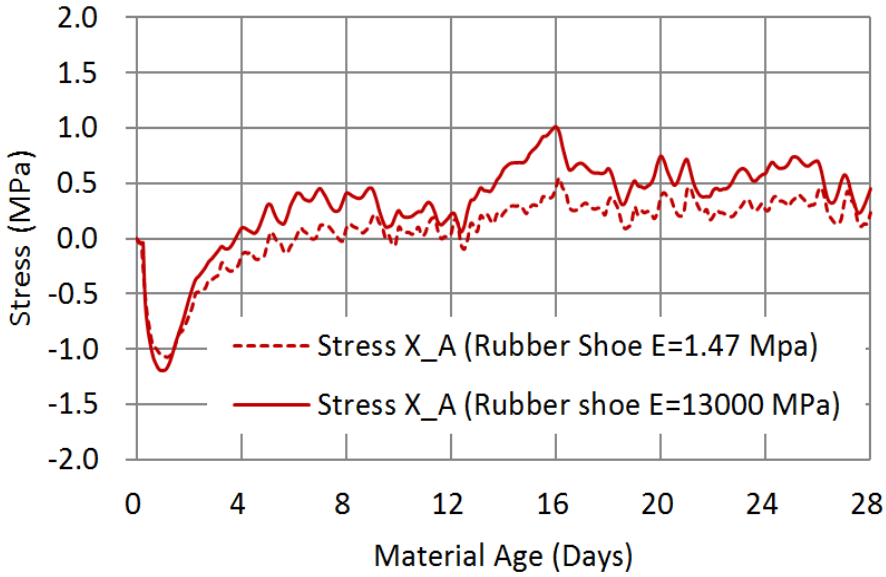

Fig.5.3(c) Simulated longitudinal stresses at location A for different Young' modulus of the rubber bearing (seismic isolation).

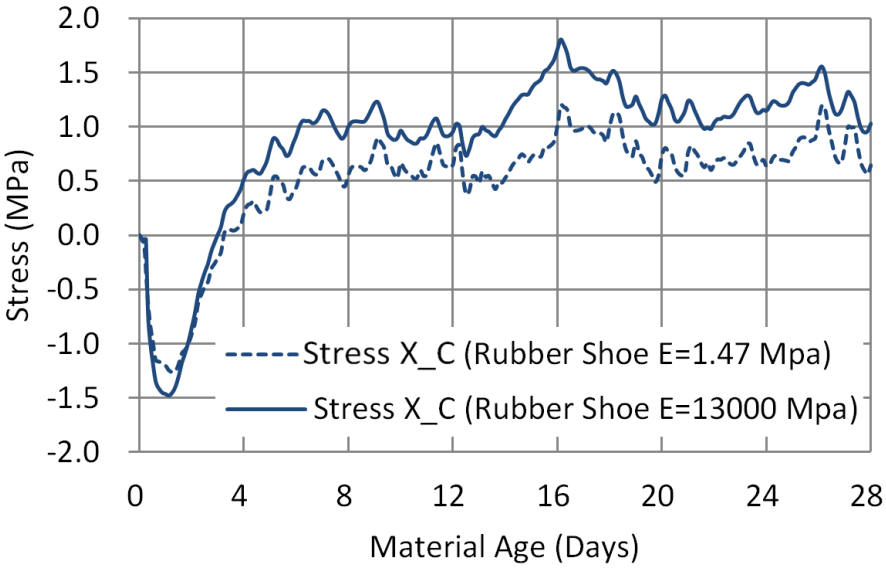

Fig.5.3(d) Simulated longitudinal stresses at location C for different Young' modulus of the rubber bearing (seismic base isolation).

5.5 COMPARISON OF THERMAL STRESS IN THE RC SLABS FOR MULTIPLE CONTINUOUS SPAN STEEL GIRDER BRIDGE AND PC COMPOSITE GIRDER SINGLE SPAN BRIDGE

Simulations of thermal and volumetric stresses (Fig.5.4 (a) and (b)) have confirmed three times higher cracking risk of Multiple Span Continuous Steel Box Girder Bridge compared to Single Span PC Composite Girder Bridge. Moreover, Tensile stresses generated due to stepping construction increase the risk of cracking in multiple span bridge deck.

It was confirmed from the simulation results that the generation of tensile stress in the RC slab due to the restraint thermal and volumetric changes are considerably less in case of PC girder bridges. Accordingly it can be conferred that the tensile stress generation is small in PC composite girder bridges with respect to the steel girder bridges because of the overall composite action of the RC slab, PC girder and stay in place (SIP) form in case of thermal movement.

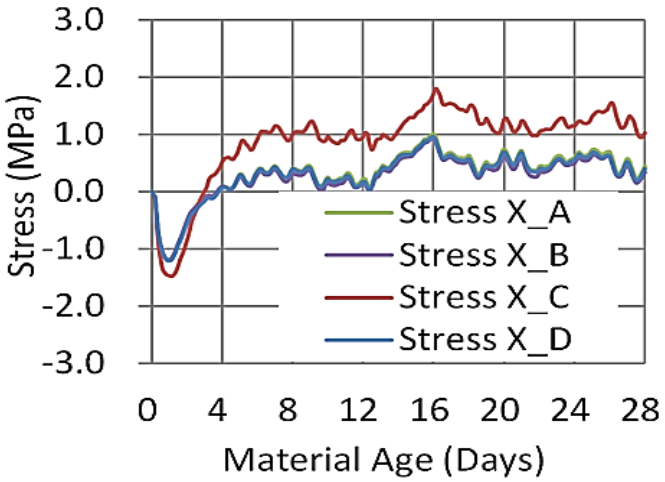

Fig.5.4(a) Simulated stresses along bridge axis in different locations of RC slab on multiple continuous span steel girder Shinkesen Ohashi bridge

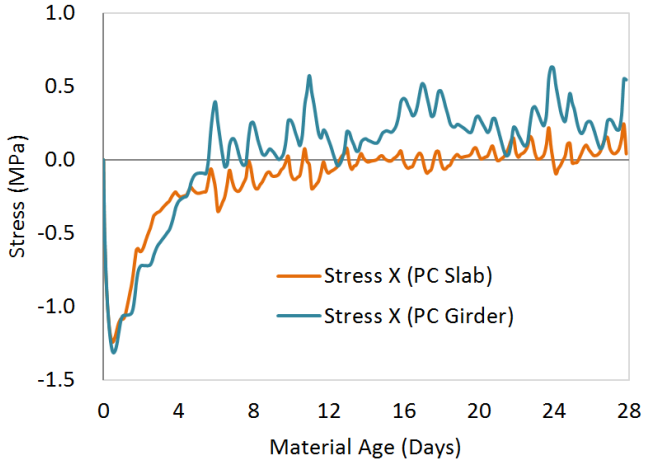

Fig.5.4(b) Simulated stresses along bridge axis in the PC composite girder Hikohei Bridge RC slab

5.6 SUMMARY OF CHAPTER 5

The comparative numerical analyses have revealed several significant effect of the structural restraints on tensile cracking stress generation in the RC deck slab are summarized as below:

(1) The tensile stresses generated in RC slab directly connected and restrained by the steel girder are approximately uniform along the length of the deck slab.

(2) The simulation of stresses in the RC slab on the single span steel box girder bridge model are smaller than the stresses acquired from the multiple span continuous steel box girder bridge FEM model. Therefore, it can be conferred that in case of the multiple span continuous steel girder bridges structural restraints are higher than the single span steel bridges.

(3) In comparison of longitudinal strain (along bridge axis) and the transverse strain, less restraint to the thermal movement of the bridge deck was observed when smaller value of the Young's modulus (E=1.47 MPa) was applied. The model comprising of the lower young's modulus of rubber exhibited considerable decrease in tensile stresses. Therefore, it has been confirmed that, appropriate utilization of the stiffness of the supports is indispensable for the simulation of thermal stresses.

(4) Simulations of thermal and volumetric stresses have confirmed three times higher cracking risk of Multiple Span Continuous Steel Box Girder Bridge compared to Single Span PC Composite Girder Bridge. Moreover, Tensile stresses generated due to stepping construction increase the risk of cracking in multiple span bridge deck.

(5) The tensile stress generation is small in PC composite girder bridges with respect to the steel girder bridges because of the overall composite action of the RC slab, PC girder and stay in place (SIP) form in case of thermal movement.

6

INFLUENTIAL FACTORS CAUSING EARLY AGE THERMAL AND SHRINKAGE CRACKS IN RC DECK SLABS

6.1 INTRODUCTION

The established FEM RC slab bridge models for multi-span steel girder bridge and single span PC composite girder bridge were utilized for parametric studies to determine the influential factors causing early age thermal and shrinkage cracks to acquire fundamental information for improving guidelines for durable RC bridge decks specially by suppressing early age cracks in RC slab. In this context, current chapter presents parametric studies based on the established FEM bridge models for multiple continuous span steel girder bridge and singles span PC composite girder bridge. Thus, the effect of significant factors influencing early age thermal and volumetric cracks in RC deck slabs on girder bridges such as coefficient of thermal expansion (CTE), concrete placing temperature, autogenous shrinkage and chemical expansion due to the application of expansive additive are quantitatively identified.

6.2 EFFECT OF COEFFICIENT OF THERMAL EXPANSION

Multiple span continuous steel girder Shinkesen Ohashi bridge and single span PC composite girder bridge FEM models are utilized to confirm the effect of coefficient of thermal expansion (CTE) of concrete on tensile stress generation in restraining RC deck slabs. Parametric studies have identified that cracking risk (Cracking Risk=Stress/Strength, Cracking Risk=100% when Stress/Strength $\geq$ 1) of Shinkesen Ohashi multiple span continuous steel girder bridge is 74% for CTE 8.4×10^{-6} of concrete (measured value) as shown in Fig.6.1(b).

It is to be noted that CTE of steel girder was defined as 9.0×10^{-6} in the simulation. Fig.6.1(a) and (b) reveal that tensile stress as well as cracking risk of RC slab might be increased when the CTE of concrete differs much from the CTE of restraining girders in case of multiple span steel girder bridge possibly due to the higher restraints caused by the significant differences of Young's modulus of concrete and steel. Therefore, it can be referred that ensuring the adjacent values of CTE of RC slab concrete and restraining steel girders may reduce the risk of cracking by 26% as shown in Fig 6.1(b).

In reverse, in case of PC composite girder bridge, cracking risk increases with the increases of CTE irrespective of the CTE of PC composite girders (Fig.6.1(c)) although the overall cracking risk is low in single span composite girder bridge.

In Fig.6.1 (d), CTEs of PC girders/PC slabs were varied keeping the CTE of RC deck slab constant (9.3×10^{-6}/°C). It reveals that lower value of CTE of restraining PC girders increase the risk of cracking by increasing the tensile stresses in RC slab concrete. On the other hand, CTEs of RC deck slab were varied keeping the CTE of PC girders/PC slabs constant (10×10^{-6}/°C) showed in Fig.6.1(b) indicating that lower value of CTE for RC deck slab has lower risk of cracking. However, Fig.6.1(a) and 616(b) indicate that there was no significant effect on stress in

compression zone (temperature increasing zone) with different coefficient of thermal expansion in case of single span PC composite girder bridge.

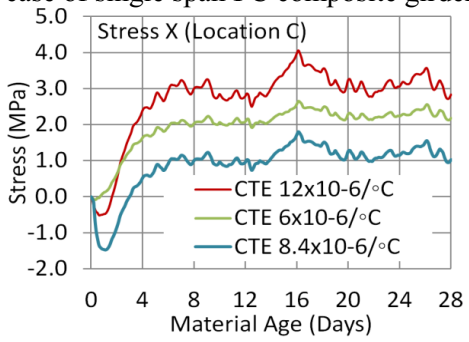

Fig.6.1(a) Effect of CTE of slab concrete on tensile stress generation in case of multiple continuous span steel girder bridge (Shinkesen Ohashi bridge)

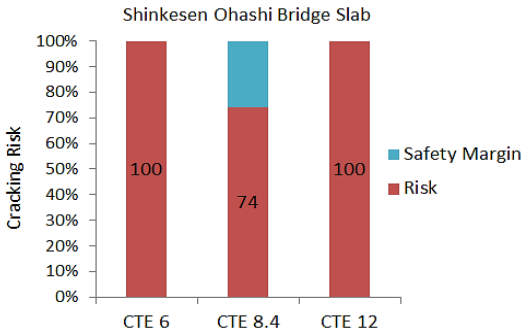

Fig.6.1(b) Cracking risk (Stress/Strength) of Shinkesen Ohashi bridge RC slab corresponding to different CTE of slab concrete

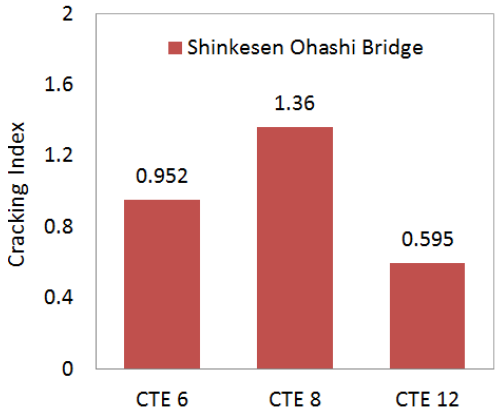

Fig.6.1(c) Effect of CTE of concrete on cracking index of the RC slab of Shinkesen Ohashi multiple span continuous steel girder bridge

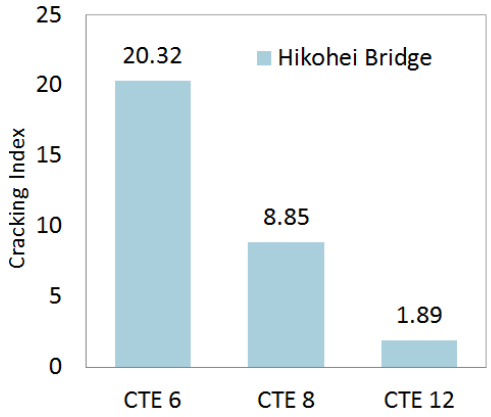

Fig.6.1(d) Effect of CTE of concrete on cracking index of the RC slab of Hikohei PC composite girder bridge

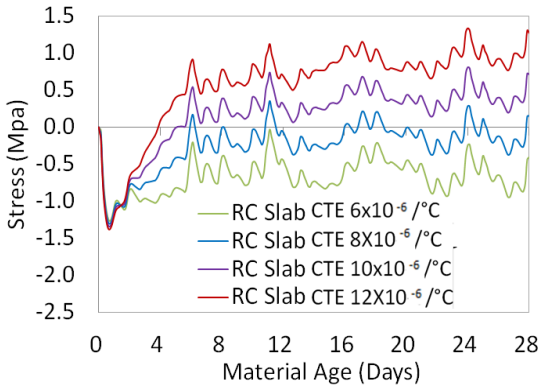

Fig.6.1(e) Effect of CTE of RC deck slab on longitudinal stresses (upon PC girder)

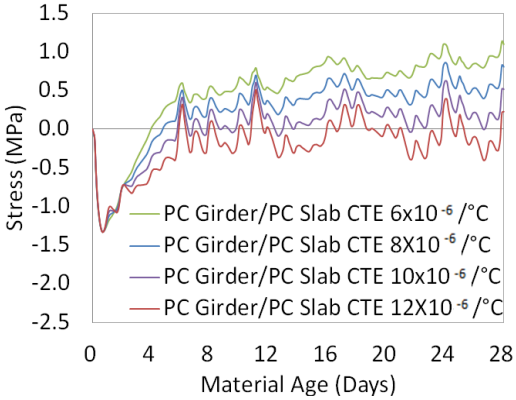

Fig.6.1(f) Effect of CTE of PC girders/PC slabs on longitudinal stresses (upon PC girder

6.3 EFFECT OF INITIAL CONCRETE PLACING TEMPERATURE

Parametric studies on initial concrete placing temperature on tensile stress generation and cracking risk of RC slab on multiple span continuous steel girder Shinkesen Ohashi bridge confirm that there is 100% cracking risk in case of initial concrete temperature rises up to 30°C. Cracking risk can be reduced by 37% when the initial concrete temperature is lowered by 15°C (Fig.6.2(a), (b) and (c)). Initial concrete temperature of concrete placement Lot 8 of Shinkesen Ohashi RC slab was 24°C exhibiting 74% cracking risk of the RC slab.

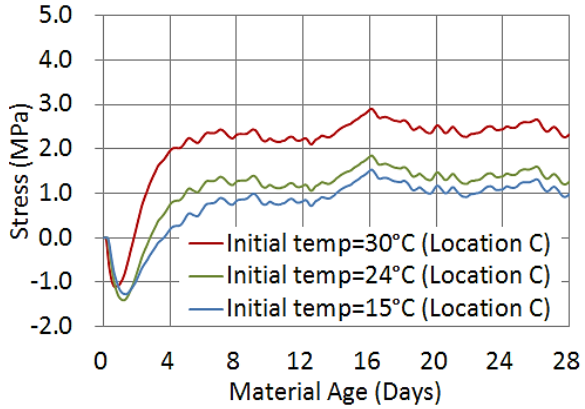

Fig.6.2(a) Effect of initial concrete temperature on tensile stress generation in case of multiple continuous span steel girder bridge (Shinkesen Ohashi bridge) RC slab

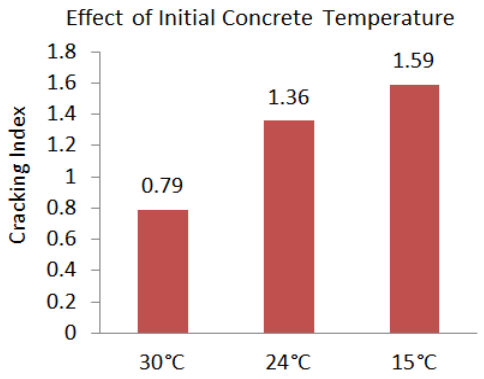

Fig.6.2(b) Effect of initial concrete temperature on cracking index of multiple continuous span steel girder bridge (Shinkesen Ohashi bridge) RC slab

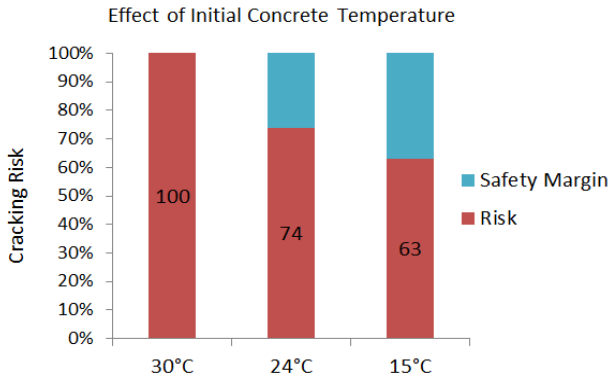

Fig.6.2(c) Effect of initial concrete temperature on cracking risk (Stress/Strength) of multiple continuous span steel girder bridge (Shinkesen Ohashi bridge) RC slab

6.4 EFFECT OF AUTOGENOUS SHRINKAGE

Parametric studies were conducted to confirm the effect of autogenous shrinkage on tensile stress generation, cracking index and cracking risk of multiple span continuous steel girder bridge slabs considering two different site conditions such as for Shinkesen Ohashi bridge and for Kosano Viaduct.

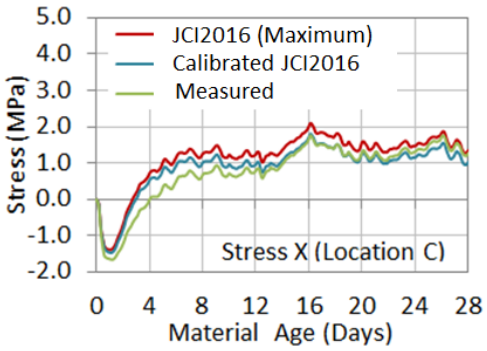

Fig.6.3(a) Effect of autogenous shrinkage on tensile stresses in Shinkesen Ohashi bridge RC slab

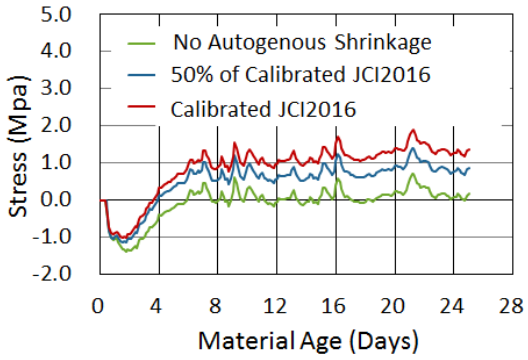

Fig.6.3(b) Effect of autogenous shrinkage on tensile stresses in Kosano viaduct RC slab

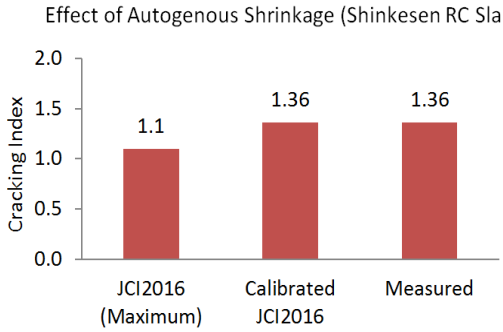

Fig.6.3(c) Effect of autogenous shrinkage on cracking index of Shinkesen Ohashi bridge RC slab

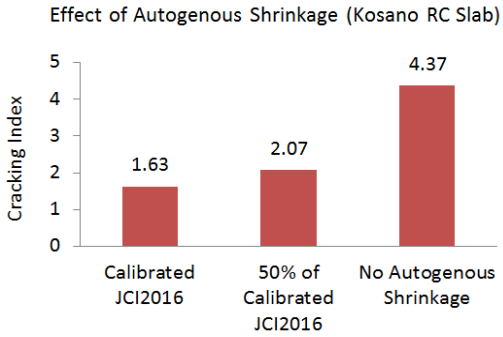

Fig.6.3(d) Effect of autogenous shrinkage on cracking index of Kosano viaduct RC slab

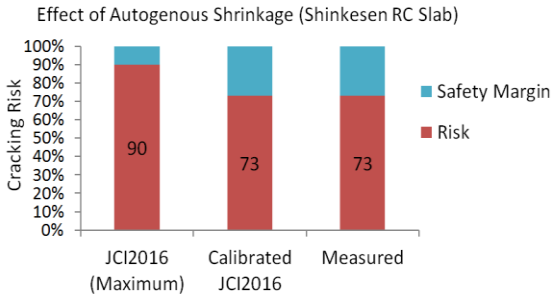

Fig.6.3(e) Cracking risk (Stress/Strength) of Shinkesen Ohashi RC slab for autogenous shrinkage

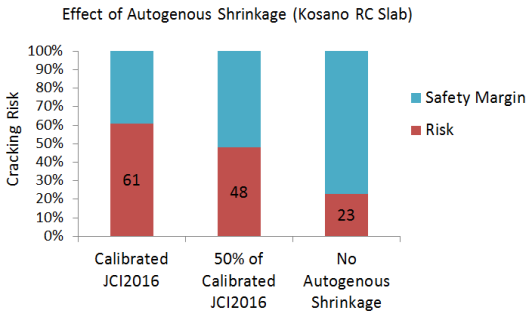

Fig.6.3(f) Cracking risk of Kosano viaduct RC slab for autogenous shrinkage

Previous researches have confirmed that large autogenous shrinkage can occur due to the blast furnace slag cement in high temperature. Since the special curing methods were adopted for both Shinkesen and Kosano viaduct RC slab constructions, the autogenous shrinkage on sites were less than the recommendations by JCI2016 autogenous shrinkage equation (Eq. 4.2(a) [2] in presented in Chapter 4) for blast furnace slag cement. In simulation of the real structures, the calibrated JCI2016 equation was applied as input autogenous shrinkage (Eq. 4.2(b) in Chapter 4). Therefore, comparative studies were carried out between the simulation results considering JCI2016 autogenous shrinkage and calibrated JCI2016 autogenous shrinkage in case of Shinkesen Ohashi RC slab (Fig.6.3(a),(c) and (e)). Fig.6.3(e) explainsa that cracking risk can be increased by 17% if the autogenous shrinkage is as large as the recommendation by JCI2016. Therefore, it can be inferred that cracking risk of Shinkesen Ohashi RC slab has been reduced by 17% by adopting special curing method.

Moreover, parametric studies on Kosano RC slab show that cracking risk of RC slab can be reduced by 13% when the autogenous shrinkage is 50% reduced (following appropriate curing methods). Additionally, If there is no autogenous shrinkage occur in RC slab, cracking risk might be reduced by 38% (Fig.6.3(b),(d) and (f)).

6.5 EFFECT OF EXPANSIVE ADDITIVE

The effect of expansive additive in reducing tensile stresses in RC slab is confirmed from the parametric studies regarding both for multiple span continuous steel girder bridge (Shinkesen Ohashi Bridge and Kosano Viaduct) and single span PC composite girder bridge (Hikohei bridge).

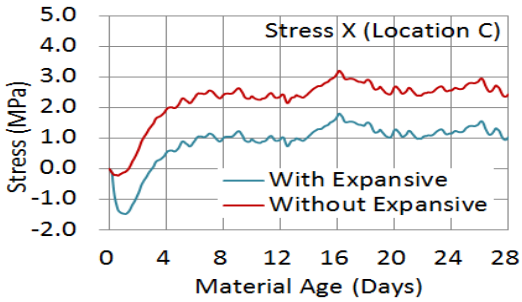

Fig.6.4(a) Effect of expansive additive in reducing tensile stresses in Shinkesen RC slab

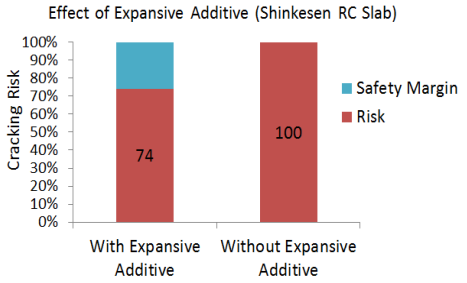

Fig.6.4(b) Effect of expansive additive in reducing tensile stresses in Shinkesen RC slab

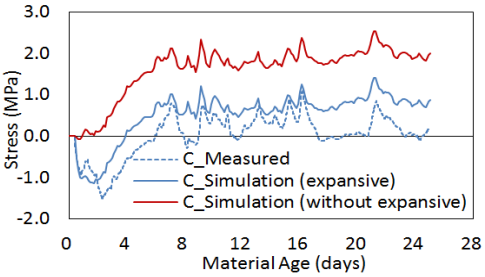

Fig.6.4(c) Effect of expansive additive in reducing tensile stresses in Kosano RC slab

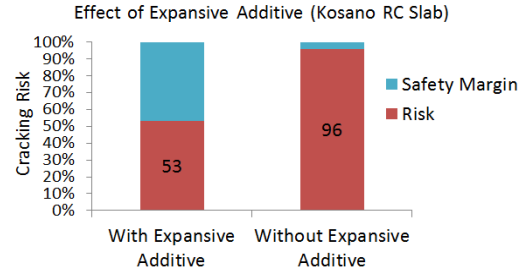

Fig.6.4(d) Effect of expansive additive in reducing tensile stresses in Kosano RC slab

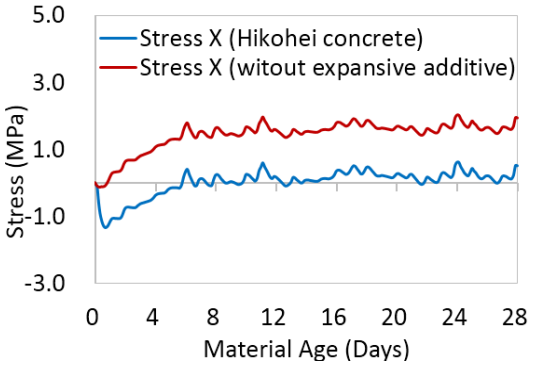

Fig.6.4(e) Effect of expansive additive in reducing tensile stresses in Hikohei RC slab

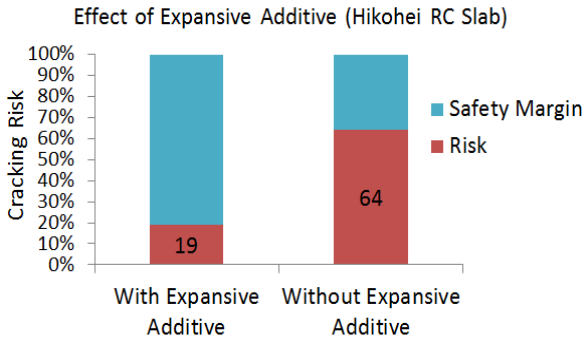

Fig.6.4(f) Effect of expansive additive in reducing tensile stresses in Hikohei RC slab

Form the parametric studies it has been revealed that the application of expansive additive have reduced the cracking risk by 26% in case of Shinkesen Ohashi RC slab, 43% in case of Kosano viaduct RC slab and 45% in case of Hikohei bridge RC slab. Finally, it can be conferred that application of 20 kg/m^3 expansive additive is capable of reducing cracking risk of RC slabs upon girder bridges by 38% on an average.

6.6 SUMMARY OF CHAPTER 6

The significant influencing factors revealed from the parametric studies causing early age cracks in girder bridges are summarized as below:

(1) Effect of CTE:

Cracking risk of RC slab may increase when the CTE of concrete differs much from the CTE of restraining girders in case of multiple span steel girder bridge possibly due to the higher restraints caused by the significant differences of Young's modulus of concrete and steel. Ensuring the adjacent values of CTE of RC slab concrete and restraining steel girders reduce the risk of cracking by 26%.

In reverse, in case of PC composite girder bridge, cracking risk increases with the increases of CTE irrespective of PC composite girders CTE since the Young's modulus of RC slab and PC composite girders are approximately same.

(2) Effect of Initial Concrete Temperature

Cracking risk can be reduced by 37% when the initial concrete temperature is lowered by 15°C from 30°C.

(3) Effect of Autogenous Shrinkage of RC slab

Parametric studies revealed that cracking risk of Shinkesen Ohashi RC slab was reduced by 17% by adopting special curing method. Moreover, parametric studies on Kosano RC slab confirmed that cracking risk of RC slab could be reduced by 13% when the autogenous shrinkage is 50% reduced applying appropriate curing methods. Additionally, in absence of autogenous shrinkage cracking risk of RC slab might be reduced by 38%.

(4) Effect of Expansive Additive

It can be conclude from the parametric studies that application of 20 kg/m^3 expansive additive is capable of reducing cracking risk of RC slabs upon girder bridges by 38% on an average.

References

[1] Japan Society of Civil Engineering, Standard Specifications for Design of Concrete Structures, JSCE, 2007.
[2] Japan Concrete Institute, JCI Guidelines for Control of Cracking of Mass Concrete, Tokyo, 2016.
[3] S. Miyazawa, R. Sato and J. Sugiyama, "Prediction Formula for Autogenous Shrinkage of Blast Furnace Cement Concrete Receiving High Temperature History," JCI Annual Convention,

7

CONCLUSIONS

7.1 GENERAL

The present research was preceded with the aim of establishing an FEM numerical simulation system based on thermal and structural stress analysis for RC deck girder bridges to simulate the volumetric changes of the deck in early age. The methodology of the numerical procedure followed three-leveled systematic analytical scheme for FEM full-scale structural simulation. Two different structural bridge types i.e., Multiple span steel box girder bridge (Shinkesen Ohashi Bridge and Kosano Viaduct in Iwate Prefecture) and Single span PC composite girder bridge (Hikohei Bridge in Fukushima Prefecture) were considered in this analysis scheme to confirm the distinctive attributes of thermal stresses in RC deck slab with respect to different structural restraints. The established FEM RC slab girder bridge models for multi-span steel girder bridge and single span PC composite girder bridge were utilized for parametric studies to determine the influential factors causing early age thermal and shrinkage cracks, finally to contribute in improving guidelines for securing highly durable RC slab specially by reducing the risk of early age cracking.

The findings of the present research connecting from the construction practice, field and laboratory investigations to the systematic three-levelled FEM numerical simulation of the real bridge structures have been illustrated in several sections as follows:

7.2 ESTABLISHING A SYSTEMATIC ANALYSIS SCHEME FOR FEM FULL SCALE STRUCTURAL SIMULATION OF RC DECK GIRDER BRIDGES

The aim of the current section was to evaluate the cracking risk of multiple span continuous steel box girder bridge deck slab by establishing accurate finite element models following a three leveled systematic analysis scheme for simulating thermal stress in the restrained RC slabs. Additionally, thermal and volumetric stresses in the single span PC composite girder Hikohei Bridge were also evaluated following the established FEM simulation system. The findings are summarized on the basis of three leveled simulation scheme as follows:

(1) Level 1: Experimental Investigations for Establishing Concrete Material Models

(a) In Level-1 material models have be established for the highly durable concrete specially comprising of blast furnace slag cement and expansive additive regarding time dependent compressive strength, tensile strength and Young's modulus development based on the laboratory investigations utilizing calibrated JCI2016 Guidelines for Control of Cracking of Mass Concrete 2016.

(b) The adiabatic temperature rise and the autogenous shrinkage of the corresponding concrete were established by calibrating recommended models by JCI2016 Guidelines for Control of Cracking of Mass Concrete 2016.

(c) Furthermore, initial and final setting time as well as the coefficient of thermal expansion (CTE) for the corresponding highly durable concrete was determined from the laboratory investigations.

(2) Level 2: FEM Numerical Simulation of Member Level Test Specimens

(a) The systematic FEM simulation method followed in the present study has been successfully verified in member levels in simulating the volume changes in the early age of concrete with slag cement and expansive additive utilizing the material models established in Level 1.

(b) It has been confirmed that the calibrated material parameters for total expansion strain energy model, experimentally obtained input autogenous shrinkage, appropriate utilization of creep reduction factors and confirmed time dependent compressive strength development of the concrete are the key factors for obtaining good agreements in FEM simulations for several material and member level specimens. Eventually, it can be conferred that the present simulation method followed by several material and member level verifications can be effectively applicable in real structural level simulation of FEM models for several bridges to evaluate the early age thermal and volumetric changes along with cracking risk of the RC deck slabs.

(3) Level 3: FEM Numerical Simulation of Bridges in Real Structural Level

(a) Multiple Span Steel Box Girder Bridge (Shinkesen Ohashi Bridge)

Simulation of stress in RC slab reveals the initiation of preliminary thermal cracks in concrete upon permanent plywood forms (location of maximum concrete temperature) in few segments of the RC slab where cumulative structural tensile stress was large because of stepping construction of the bridge deck.

(b) Multiple Span Steel Box Girder Bridge (Kosano Viaduct)

Field monitoring of Kosano Viaduct RC slab proved the wide range of applicability of the three leveled systematic verification system since the measured temperature and stresses in Kosano RC slab showed the same trends as simulated in case of Shinkesen RC slab. Measurement data and simulation of temperature, strains and stresses confirmed the most vulnerable section of RC slab located upon permanent plywood forms. The primary cracks tend to generate upon permanent plywood forms due to comparatively large thermal stresses coupled with structural tensile stresses generated due to the stepping construction and propagate towards the central axis of the slab.

(c) Single Span PC Composite Girder Bridge (Hikohei Bridge)

Simulation of stresses in Hikohei bridge model confirmed the lower cracking risk of Hikohei deck slab concrete due to the low autogenous shrinkage and utilization of expansive additive. It is to be noted that concrete placement for the construction of the concerned RC deck slab was covered in a single day which reduced the risk of generating tensile stress unlike the multiple span Shinkesen bridge slab followed by stepping construction.

7.3 EFFECTS OF STRUCTURAL RESTRAINTS ON THE OCCURRENCE OF THERMAL STRESSES IN RC BRIDGE DECK SLABS

The amount of volume change and the degree of restraint present in a bridge have a direct and interrelated effect on the amount of cracking that may develop in the deck slab. In this context, present study aims at evaluating the effects of structural restraints on the occurrence of thermal stresses in RC deck slabs. Comparative analyses were conducted in different aspects such span bridge types (single span and multiple continuous span), girder types (steel girders and PC composite girders) and support conditions (stiffness of rubber bearing) etc. The comparative numerical analyses have revealed several significant effect of the structural restraints on tensile cracking stress generation in the RC deck slab are summarized as below:

(1) The tensile stresses generated in RC slab directly connected and restrained by the steel girder are approximately uniform along the length of the deck slab.

(2) The simulation of stresses in the RC slab on the single span steel box girder bridge model are smaller than the stresses acquired from the multiple span continuous steel box girder bridge FEM model. Therefore, it can be conferred that in case of the multiple span continuous steel girder bridges structural restraints are higher than the single span steel bridges.

(3) In comparison of longitudinal strain (along bridge axis) and the transverse strain, less restraint to the thermal movement of the bridge deck was observed when smaller value of the Young's modulus was applied. The model comprising of the lower young's modulus of rubber exhibited considerable decrease in tensile stresses. Therefore, it has been confirmed that, appropriate utilization of the stiffness of the supports is indispensable for the simulation of thermal stresses.

(4) Simulations of thermal and volumetric stresses have confirmed three times higher cracking risk of Multiple Span Continuous Steel Box Girder Bridge compared to Single Span PC Composite Girder Bridge. Moreover, Tensile stresses generated due to stepping construction increase the risk of cracking in multiple span bridge deck.

(5) The tensile stress generation is small in PC composite girder bridges with respect to the steel girder bridges because of the overall composite action of the RC slab, PC girder and stay in place (SIP) form in case of thermal movement.

7.4 INFLUENCING FACTORS FOR GENERATION OF EARLY AGE THERMAL AND SHRINKAGE CRACKS IN RC DECK SLABS

The established FEM RC slab bridge models for multi-span steel girder bridge and single span PC composite girder bridge were utilized for parametric studies to determine the influential factors for generating early age thermal and shrinkage cracks to contribute in upgrading guidelines ensuring highly durable RC slab specially by suppressing early age cracks. In this context present study conducted parametric studies based on the established FEM bridge models for Shinkesen Ohashi Bridge, Kosano Viaduct and Hikohei Bridge to uncover the significant influential factors such as the effect of coefficient of thermal expansion (CTE), initial concrete temperature, autogenous shrinkage and chemical expansion on cracking risks in the early age of the RC deck slab.

The findings of the present chapter are summarized as below:

(1) Effect of CTE: Cracking risk of RC slab may increase when the CTE of concrete differs much from the CTE of restraining girders in case of multiple span steel girder bridge possibly due to the higher restraints caused by the significant differences of Young's modulus of concrete and steel. Ensuring the adjacent values of CTE of RC slab concrete and restraining steel girders reduce the risk of cracking by 26%. In reverse, in case of PC composite girder bridge, cracking risk increases with the increases of CTE irrespective of PC composite girders CTE since the Young's modulus of RC slab and PC composite girders are approximately same.

(2) Effect of Initial Concrete Temperature: Cracking risk can be reduced by 37% when the initial concrete temperature is lowered by 15°C from 30°C.

(3) Effect of Autogenous Shrinkage of RC slab: Parametric studies revealed that cracking risk of Shinkesen Ohashi RC slab was reduced by 17% by adopting special curing method. Moreover, parametric studies on Kosano RC slab confirmed that cracking risk of RC slab could be reduced by 13% when the autogenous shrinkage is 50% reduced applying appropriate curing methods. Additionally, in absence of autogenous shrinkage cracking risk of RC slab might be reduced by 38%.

(4) Effect of Expansive Additive: It can be conclude from the parametric studies that application of 20 kg/m3 expansive additive is capable of reducing cracking risk of RC slabs upon girder bridges by 38% on an average.

7.5 FUTURE TASKS

(1) Recent field investigations have revealed that the early age transverse cracks generated in few segments of the RC deck slab of the Shinkesen Ohashi multiple span continuous steel box girder bridge is widening. It is anticipated that drying shrinkage is one of the main factors for increasing the width of the minor early age cracks. Therefore, the systematic FEM simulation procedure established in the present study should include the sophisticated simulation of long-term shrinkage and creep of the RC slab concrete.

(2) Further, extensive parametric studies need to be conducted to confirm the effect of hydration heat of cement, initial temperature, ambient temperature, summer and winter season construction, coefficient of thermal expansion of concrete, thermal effect on expansion and shrinkage of concrete, appropriate curing methods, construction steps, structural systems and restraint conditions etc. utilizing the established FEM bridge models.

(3) Finally, the obtained knowledge will be contributed in improving guidelines for securing the highly durable RC deck slab constructions of the bridges in cold and severe environments in Japan controlling cracks due to restraint volume changes.